SOIL SUCTION RESPONSE OF GRANULAR RAILWAY FORMATION MATERIALS UNDER CYCLIC LOADING

by

Mario Vincent Schulz-Poblete

Submitted in partial fulfillment of the requirements for the degree
Master of Engineering (Geotechnical Engineering)

in the

Department of Civil Engineering
Faculty of Engineering, Built Environment and Information Technology

UNIVERSITY OF PRETORIA

July 2018

SUMMARY

SOIL SUCTION RESPONSE OF GRANULAR RAILWAY FORMATION MATERIALS UNDER CYCLIC LOADING

by

Mario Vincent Schulz-Poblete

Supervisor(s):	Professor P.J. Gräbe Professor S.W. Jacobsz
Department:	Civil Engineering
University:	University of Pretoria
Degree:	Master of Engineering (Geotechnical Engineering)
Keywords:	Soil suction, cyclic loading, railway geotechnics, railway formation, tensiometer, granular, moisture content

Changing climatic conditions worldwide are causing a change in moisture conditions of railway formations and slopes, thereby either strengthening or weakening them. Current railway formation design methods do not take into account the changing moisture conditions over the predicted life of a railway formation. These changes in soil strength are due to the influence of soil suctions. The basic principles of unsaturated soil mechanics have been well established in the field of geotechnics, and this study joins an international body of work that seeks to apply unsaturated soil theory to the field of railway and pavement formation materials.

This study comprised of box testing of subgrade and subballast formation materials at different moisture contents. These formation models were instrumented with tensiometers to monitor the effect of cyclic loading on soil suctions under typical heavy haul loading magnitudes (26 tonne/axle). The materials were tested under a number of different loading frequencies subjected to the same cyclic heavy haul load magnitude. The study investigated the suctions present in railway formation materials, as well as the application of suction instrumentation in railway conditions.

Initial testing of the tensiometers showed evidence of interference caused by the stress imposed by the soil skeleton on the tensiometer housing. This prompted a development program that resulted in an improved tensiometer model that was isolated from the effects of external loading and could therefore successfully measure the suctions present in the formation material. Suctions were successfully measured in both the subgrade and subballast material under various moisture contents demonstrating the different suction magnitudes generated by the materials under expected formation conditions. The subballast material was found to generate suctions of between 1 and 15 kPa over a wide range of degrees of saturation (S_r: 0.32 – 0.96), while the subgrade material was found to generate a greater range of suctions between 1 and 95 kPa with a smaller variation in degree of saturation (S_r: 0.61 – 0.88).

The deformability of both the subgrade and subballast materials were affected to different degrees as a function of the soil suctions. The subgrade material was found to be dependent on the moisture state and soil suctions to a greater degree than the subballast material. A deformation of 141 % of the failure criterion was observed at low suctions (1 – 5 kPa) in the subgrade material at loads similar to those experienced by South African heavy haul railway formations. In contrast, the deformation significantly reduced to 55 % of the failure criterion when the suctions increased by a relatively small amount ($\backsim$10 kPa). Further desaturation of the subgrade material resulted in higher suctions (40 – 95 kPa) strengthening the formation further to a final deformation of 47 % of the failure criterion. It was found that subballast deformation was significantly affected by the loading frequency and less by moisture state. Due to the low suctions present in the subballast material, the maximum deformation observed was 61 % of the failure criterion under effectively saturated conditions with suctions $\leq$1 kPa. Under the highest suctions present in the subballast material ($\backsim$14 kPa), the material only strengthened to the point where 47 % of the failure criterion was observed.

The application of geotechnical testing methods to granular formation materials are also investigated and discussed, in terms of the effectiveness of tensiometers and filter paper methods in determining suction, as well as considerations when sampling granular soil for moisture content. The study therefore provides important information for laboratory testing of formation materials, the techniques required to successfully measure suctions in railway formations and the implications of cyclic loading on formations at various degrees of saturation.

ACKNOWLEDGEMENTS

Throughout the time it took to write this dissertation I was supported by a great many special people, whom I would like to acknowledge as follows:

To my supervisors **Prof. Hannes Gräbe** and **Prof. SW Jacobsz**, who always steered my dissertation in the right direction and taught me the hallmarks of good research. I hope those lessons are faithfully reflected in the work presented. Special thanks is given for the times I came to them with only half an idea and they were patient with me.

To the **Transnet Chair in Railway Engineering** and **Prof. Gräbe** as its head. The financial support of the chair is the only reason I was able to pursue full time postgraduate studies at the University and experience one of the most stimulating and enjoyable periods of my life.

To **Johan Scholtz** in the Civil Laboratory, who taught me to operate the MTS machine and was always available to give some advice on practical matters. Thank you also to **Jurie van Staden**, who allowed me to scrounge around his geotechnical laboratory and use his equipment.

To my friend **Rick Vandoorne** who was always willing to discuss a good idea and at least entertain the bad ones. The time he took out of his always busy schedule to give me pointers in Matlab and correct my chapters was invaluable, and I think the dissertation would have been poorer without him.

To my best friend and close partner in crime **Horacio Mones Ruiz**, whose entire list of names I don't mention for fear of overwhelming the reader too early in the dissertation. He has provided me with one of the most fulfilling friendships I have ever had through our years at the University. It is not at all hyperbole to say I would not be where I am now without him.

To my family: **Alfredo**, **Joey** and **Bianca Schulz**. Your unending support through my undergraduate and postgraduate courses have gotten me this far and I am frightened of how far exactly they might take me. To the top I imagine. Their love and care have made me the man I am today, and I hope that I have made them all proud. My thanks also go out to my two sweet little dachshunds **Lexie** and **Robin**

who were always a welcome diversion when I needed a break, and have given me endless hours of enjoyment.

To my girlfriend **Carissa Naidoo**, who really shouldn't be this far down the list but can console herself knowing she is at the top of my heart and first in my mind. Her sometimes ferocious support has given me strength in times when I really wasn't sure if there was any left, and has cared for me throughout.

To my flatmate and oldest friend **Gavin Jones**, as an engineer and an accountant we do not pretend to know what the other does and why, but his friendship has meant the world to me even longer than we have stayed together. I have always marvelled at his wit and turn of phrase, and I am lucky to have stayed with such a good person all this time.

To the team of postgraduates in the Civil Department of the University of Pretoria. They are too numerous to mention here individually, but many of them have contributed to this in your own way. Thank you for making the work environment at the University so enjoyable, and making sure I look forward to it everyday.

Lastly to the **University of Pretoria** itself. It has through the last 6 years always been a place full of wonderful and interesting people and places, I have enjoyed my time there tremendously and it has changed me in many ways for the better. I will cherish the memories it has given me forever.

TABLE OF CONTENTS

CHAPTER 1 INTRODUCTION **1**

1.1 Background 1

1.2 Objectives of Study 2

1.3 Scope of Study 2

1.4 Methodology 3

1.5 Organisation of Report 3

CHAPTER 2 LITERATURE STUDY **5**

2.1 Formation 5

2.1.1 Subballast 5

2.1.2 Subgrade 7

2.1.3 South African Specifications 9

2.2 Unsaturated Soil Mechanics 11

2.2.1 Soil Suctions 11

2.2.2 Soil Water Retention Curve 16

2.2.3 Soil Stress 21

2.2.4 Deformation Characteristics 24

2.3 Suction Measurement 28

2.3.1 Discrete Suction Measurement 28

2.3.2 Continuous Suction Measurement 29

2.4 Summary 33

CHAPTER 3 EXPERIMENTAL PROCEDURE **35**

3.1 Model Setup 35

3.1.1 Strongbox Setup 36

3.1.2 Formation Material Construction 37

3.1.3 Hydraulic Load Frame . . . 38
3.1.4 Loading Block . . . 40
3.1.5 Instrumentation . . . 40
3.2 Testing Schedule . . . 45
3.2.1 Pre-Test Preparation Phase . . . 45
3.2.2 Primary Testing Phase . . . 46
3.2.3 Post-Test Testing Phase . . . 48
3.3 Material Characterisation . . . 49
3.3.1 Soil Parameters . . . 49
3.3.2 Soil Water Retention Curve . . . 52
3.4 Tensiometer Development . . . 56
3.5 Data Processing . . . 59
3.5.1 Deformation Data Processing . . . 59
3.5.2 Tensiometer Data Processing . . . 61
3.6 Summary . . . 63

CHAPTER 4 ANALYSIS . . . 65
4.1 Deformation Behaviour . . . 66
4.1.1 Material Deformation Overview . . . 67
4.1.2 Material Failure Mode . . . 72
4.1.3 Material Stage Deformation Behaviour . . . 75
4.2 Suction Behaviour . . . 84
4.2.1 Material Suction Overview . . . 85
4.2.2 Suction Equalisation and Agreement with the Soil-Water Retention Curve . . . 90
4.2.3 Filter Paper Results . . . 92
4.2.4 Suction and Moisture Content Comparison . . . 95
4.3 Discussion . . . 103

CHAPTER 5 CONCLUSIONS AND RECOMMENDATIONS . . . 108
5.1 Conclusions . . . 108
5.1.1 Deformation Behaviour . . . 109
5.1.2 Suction Behaviour and Measurement . . . 109
5.1.3 Effect of Suction on Deformation . . . 110
5.2 Recommendations . . . 111

LIST OF FIGURES

2.1 Pavement layers for a 26 tonne axle loading (Transnet, 2006) 9
2.2 Systematic increase of pore pressures in a subgrade material (Cary and Zapata, 2016) 13
2.3 Pore pressure response under drained and undrained cyclic loading in a 7 % clay sample (Mamou et al., 2017) 14
2.4 Axial strain (top) and excess pore water pressure (bottom) response of drained and undrained cyclic loadings in a 14 % clay sample (Mamou et al., 2017) 15
2.5 Schematic of suction regimes in a typical SWRC 16
2.6 Example of a soil water retention curve (Huat et al., 2012) 17
2.7 Extended Mohr-Coulomb failure envelope (Huat et al., 2012) 22
2.8 Development of resilient modulus from cyclic loading (Li et al., 2016) 26
2.9 Cross-section of Durham University-Wykeham Farrance tensiometer (Lourenço et al., 2008) 30
2.10 Stepwise calibration of tensiometer at 0.51 degree of saturation (top) and 0.97 degree of saturation (bottom) (Take and Bolton, 2003) 31

3.1 Schematic of the box test setup 36
3.2 Strongbox orthographic representation 37
3.3 Placement of material before (left) and after (right) compaction 38
3.4 MTS hydraulic load frame 39
3.5 Layout of instrumentation and equipment for testing 40
3.6 Cross-sectional schematic of unshielded and shielded tensiometers 42
3.7 Side by side comparison of unshielded and shielded tensiometer designs 42
3.8 Cross-sectional schematic of modified shielded tensiometer 43
3.9 Tensiometer saturation cell during saturation 44
3.10 Tensiometer installation with cable protection 45

3.11 Moisture sample locations, numbered from left to right 48
3.12 Particle size distribution for SB and AB materials 50
3.13 Saturated SB sample with tensiometers installed (left) and dried sample with tensiometers uncovered (right) 53
3.14 Piecewise filter paper calibration graph adapted from Hamblin (1981) 54
3.15 SWRCs of **(a)** subgrade (AB) and **(b)** subballast (SB) materials in terms of S_r and MC 55
3.16 Total stress dependency test on tensiometers 57
3.17 Deformation data processing example 60
3.18 Representative points taken from deformation measurements 61
3.19 Detail of data envelope for raw tensiometer data 62
3.20 Tensiometer mean suction line example 63

4.1 Subgrade (AB) material deformation during testing 68
4.2 Permanent deformation of subgrade (AB) material as a function of moisture content (MC) for the different testing stages 69
4.3 Subballast (SB) material deformation during testing 70
4.4 Permanent deformation of subballast (SB) material as a function of moisture content (MC) for the different testing stages 71
4.5 Comparison of total deformation of the subgrade (AB) and subballast (SB) materials against degree of saturation (S_r) 72
4.6 Subgrade (AB) material deformation 50 mm from loading block (LVDT Position B) . 73
4.7 Subballast (SB) material deformation 50 mm from loading block (LVDT Position B) 74
4.8 Subgrade (AB) **(a)** permanent deformation behaviour and **(b)** cumulative permanent deformation during loading stages 76
4.9 Subballast (SB) **(a)** permanent deformation behaviour and **(b)** cumulative permanent deformation during loading stages 78
4.10 Summary of total deformations of tested materials at different moisture contents . . . 79
4.11 Distribution of deformation proportions across loading stages for **(a)** subgrade (AB) and **(b)** subballast (SB) materials 81
4.12 Rate of deformation of subgrade (AB) across all loading stages as a function of **(a)** loading cycles and **(b)** time 83
4.13 Suballast (SB) suctions at Position 1 with tensiometer locations in formation (inset) with symbols showing start and end of stages 85

4.14 Subgrade (AB) suctions at Positions 3,4 and 5 with tensiometer locations in formation (inset) 87
4.15 Pore pressure build-up in subgrade (AB) for test AB 13 % MC 88
4.16 Summary of soil suctions in subgrade (AB) and subballast (SB) materials as a function of degree of saturation (S_r) 89
4.17 Change in negative pore pressures from the start of the test (•) to the end of the test and overnight monitoring (▲) for **(a)** subgrade (AB) and **(b)** subballast (SB) materials 91
4.18 Difference in final tensiometer (•) and filter paper (▲) suction values for **(a)** subgrade (AB) and **(b)** subballast (SB) materials 93
4.19 Moisture content contours and sampling locations (•) for subballast (SB) materials **(a)** SB 2 % MC, **(b)** SB 4 % MC, **(c)** SB 6 % MC after testing 96
4.20 Moisture content contours and sampling locations (•) for subgrade (AB) materials **(a)** AB 9 % MC, **(b)** AB 11 % MC, **(c)** AB 13 % MC after testing 97
4.21 Overnight suctions in relation to the **(a)** targeted and **(b)** measured moisture contents (MC) in the subgrade (AB) material 100
4.22 Overnight suctions in relation to the **(a)** targeted and **(b)** measured moisture contents (MC) in the and subballast (SB) material 102
4.23 Comparison of **(a)** total deformations with **(b)** soil suctions of tested materials 105

LIST OF TABLES

2.1 Typical subballast properties (Li et al., 2016) 6
2.2 Common subgrade failure modes (Li et al., 2016) 8
2.3 Earthworks material specification (Transnet, 2006) 10
2.4 Range of suctions from literature 12

3.1 Testing frequencies and their associated line speeds 47
3.2 Primary loading schedule 47
3.3 Material Atterberg limits, maximum dry density (MDD) and optimum moisture content (OMC) 50
3.4 Material grading parameters 51
3.5 Material CBR properties 51
3.6 Average response of tensiometer models to loading on the casing 58
3.7 Average noise in tensiometers 58
3.8 LVDT sampling frequency by test stage 59
3.9 Tensiometer sampling frequency by test stage 61

4.1 Summary of tests 66
4.2 Summary of testing procedure for each test 66
4.3 Deformation in each loading stage as a percentage of cumulative material deformation 80
4.4 Comparison of target versus average moisture contents after testing 98

CHAPTER 1 INTRODUCTION

This chapter presents the background to the study, followed by the objectives, scope, methodology and layout of the study. The purpose of this chapter is to contextualise the reason for the study, and its place in the future of railway and geotechnical engineering.

1.1 BACKGROUND

The design of railway formations both internationally and in South Africa has traditionally relied on empirical design methods that yield a required formation type. This formation type may be defined in terms of the number of layers required and types of materials used. There is however no consideration given to the effect of in-situ conditions in these methods, particularly the effect of moisture content. Given the changing climatic conditions worldwide, it is therefore important that the effect of moisture change over the life of a railway formation is considered.

Studies that have been undertaken internationally to apply soil suction theory to railway formation materials. Work has been done on quantifying the effect of soil suction on formation stiffness (Cary and Zapata, 2011, Azam et al., 2013, Otter et al., 2016, Han and Vanapalli, 2016), as well as modelling the effect of moisture conditions on the strength of the soil (Saad, 2014, Mamou et al., 2017). There have also been laboratory studies on the response of soil suctions to cyclic loading (Cary and Zapata, 2016, Hosseini et al., 2017).

The studies mentioned have been either numerical modelling or carefully instrumented small-scale laboratory tests. There however exists a gap between the successful laboratory testing of material and the implementation of suction instrumentation in-situ. Railway formations in the field present a much more hostile environment to suction measurement methods and instrumentation than those encountered

in the field. It is therefore necessary for work to be carried out in the laboratory that closely models the conditions and challenges of measuring suctions in granular formations undergoing cyclic loading to establish the correct testing methods.

1.2 OBJECTIVES OF STUDY

The main objective of the study may be described as follows:

- To evaluate the effect of soil suctions on the strength of typical South African railway formation materials, as well as find the ranges of typical soil suctions in these materials.

The following were considered secondary objectives in the study:

- To evaluate the effect of different loading frequencies on soil suctions and material deformations.
- To provide guidelines on the measurement of soil suction and associated parameters in granular formation materials.

The initial objectives of the study focused on exploring the deficiencies in current instrumentation and methods when applied to granular formation materials, and then the development of techniques and methods that overcame these deficiencies. These developments were in turn applied to establishing the relative magnitudes of soil suction and relative changes in soil suction as a function of different factors. Based on the findings of previous studies it was thought that the loading frequency would have an effect on both the soil suctions and the deformation. It was important to test the soil response to loading frequencies that may be encountered during both regular and speed restricted railway operations. A further objective of this was to explore the applicability of 'accelerated testing' on unsaturated soils as used in ballast testing.

1.3 SCOPE OF STUDY

The study was focused on applying soil suction testing measurements techniques to railway formations under transient conditions, as well as to provide information on the behaviour of formation materials in box testing. Deformation and suction behaviour of the soils, as well as measurement of suctions, were considered the primary topics that required investigation.

For deformation analysis the permanent deformation of the soil was measured, but soil stiffness was not considered. This parameter has been studied by other authors as listed in Section 1.1. Additionally, geotechnical parameters as commonly investigated in triaxial testing and other small-scale laboratory tests were not included in the scope of this investigation. This includes factors such as volumetric strain, dilatancy and coefficients of friction.

1.4 METHODOLOGY

To meet the objectives described in Section 1.2, a literature review was conducted to summarise the findings in relevant fields and to establish best practises. Following this, preliminary testing was undertaken on fully instrumented formation models to identify behaviour of the models, water retention capacities and tensiometer behaviour. Soil water retention curves (SWRCs) were constructed using a testing regime to quantify the range of soil suctions in the materials at different moisture states. Further development in tensiometer design was undertaken as a result of deficiencies identified during preliminary testing. This development project sought to overcome the total stress influence on the tensiometer readings. Verification tests were then carried out to establish whether the tensiometer readings had been successfully isolated from the effect of total stress from the soil skeleton.

A test schedule was planned incorporating static and cyclic loading at different frequencies. This test schedule was then used to test 2 different railway formation materials, a subballast (SB) and a subgrade (AB). Each material was tested at 3 different moisture contents (MC), comprising a total of 6 tests. These tests made use of linear variable differential transformers (LVDTs) to measure deformation and tensiometers and the filter paper method to measure the soil suction behaviour.

Analysis was then conducted on the test results in terms of suction changes during the test, rates of deformation, and deformation due to loading frequency The results of the analysis are discussed in relation to the stated objective, and conclusions were presented.

1.5 ORGANISATION OF REPORT

The report consists of the following chapters:

- Chapter 1 consists of the introduction and background to the report. This chapter describes the objectives, scope and methodology of the study.
- Chapter 2 consists of a literature review on all topics considered important as a background to the study.
- Chapter 3 consists of the experimental procedure. This chapter presents the testing methods and procedures.
- Chapter 4 consists of the analysis and discussion of experimental data.
- Chapter 5 consists of the conclusions drawn from the study, as well as recommendation on further areas for study.

CHAPTER 2 LITERATURE STUDY

This chapter aims to investigate relevant literature regarding the previous work done in the field of cyclic loading of railway soils and characterisation of their response. This seeks to compile research done in the field of railway geotechnics, as well as relevant research from other geotechnical disciplines to provide an overview of the state of the art regarding the measurement and effect of pore pressures in soils.

2.1 FORMATION

Railway tracks use pavement layers consisting of granular layers to distribute the dynamic forces applied to the weaker underground layers. The railway formation is constructed with the subgrade as a base layer, and the subballast placed above that. The ballast is placed atop the subballast to complete the formation structure. The subballist and subgrade will be discussed in further detail below.

2.1.1 Subballast

The subballast is a stiff granular layer underlying the ballast that contains coarse particles mixed with angular aggregate to provide interlock and drainage. Li et al. (2016) lists the primary functions of subballast as:

1. Drainage in track substructure
2. Reduction of stresses to subgrade
3. Separation of the coarse ballast and finer subgrade materials, and prevent interpenetration
4. Frost protection to the subgrade in colder climates

While frost protection is not of great importance in a South African context, the subballast is crucial for the other 3 functions. There are conflicting priorities at play between the 3 important points, as the grading of the subballast affects its functionality. To create a free-draining layer, a subballast material must have a fines content of 2–3% (Tandon et al., 1996), to prevent water retention by clayey fines. Additionally, a subballast with fines in excess of 10% (Li et al., 2016) is more likely to deform excessively under cyclic loading and lose stiffness. However, if one limits the percentage of fines in the subgrade, it loses its separation capability. Therefore, these considerations must be balanced when designing a subballast layer for a specific environment and its expected conditions. Typical subballast properties are given by Table 2.1.

Table 2.1: Typical subballast properties (Li et al., 2016)

Property	Value
Friction angle, ϕ	25°–40°
K_0	0.4–1
Resilient modulus, M_R	55–105 MPa
Poisson's ratio	0.3–0.4
Minimum Permeability	0.001 m/s

A saturated subballast is prone to degrading because of softening of the soil matrix. This softened material loses stiffness, and therefore it has an impaired ability to pick up and distribute loads. Additionally the cyclic loading imposed by the train passing overhead will cause a fluctuation in pore pressures. These increased pore pressures cause a loss of formation strength and may lead to excessive deformations. For this reason the subballast is limited to a layer thickness of 300 mm, and a reduction in fines content is encouraged to allow free drainage of water.

Thom and Brown (1987) investigated formation materials of varying gradations and found that the compacted unit weight of a soil is the dominant factor in determining the strength of the soil regardless of gradation (excluding fines-dominated gradations). However, the drainage retentions of a material were found to be dominated by gradation rather than density. This investigation therefore demonstrated the conflicting requirements for drainage and strength.

2.1.2 Subgrade

The subgrade is an underlying layer of soil that acts as a foundation for the entire track structure, it is however potentially the weakest of all the formation layers, and therefore requires the stiffer overlying layers to spread load (Li et al., 2016). It is usually made of natural or in-situ soil that is excavated and re-compacted to the correct density. Therefore, it is inherently variable, and may contain granular material and a significant amount of fines, but seldom large aggregates.

A granular subgrade is preferred for the stiffness provided by particle interlock. These materials only need to be compacted to ensure their stiffness, and the best performing materials typically have <5 % clay. While a free draining material is preferable, the focus for the subgrade is often simply to maintain a specific moisture condition. Clayey soils are especially vulnerable to weakening the layer with shrink-swell cycles, and all the alignment problems that go with soil volume change. Therefore, an emphasis is usually put on preventing the in-situ moisture content and preventing excessive environmental outside moisture from penetrating into the formation (Li et al., 2016). Table 2.2 shows the possible subgrade failure modes.

Table 2.2 shows that dead load (i.e. a static load) will cause a different failure mode to manifest than a live load (i.e. a cyclic or transient load). This points to the fact that the modes of deformation are fundamentally different. This concept is explored further in Section 2.2.4. Furthermore, the failure types are also influenced by the soil structure. The presence of coarse or fine particles affect the type of deformation undergone: granular materials like sands and gravels are more suceptible to collapse settlement (Knappett and Craig, 2012) and vibratory compaction (Franki, 1995). Soils with high fines contents may under different conditions and compositions show evidence of heave/swell behaviour or progressive shear failure, where fine clay particle facilitate the movement of grains past each other (Knappett and Craig, 2012, Li et al., 2016).

Table 2.2: Common subgrade failure modes (Li et al., 2016)

Common Soil Type	Cause	Type	Factor	Features
Coarse	Dead Load/Environment	Collapse settlement	Saturation of poorly compacted (loose) sands	Non-recoverable settlement
	Live Load	Cyclic mobilty / Liquefaction	Cyclic loading, saturated silt, fine sands	Large displacement, more pronounced with vibration, occurs in subballast or subgrade
Fine	Dead Load	Massive shear failure	Weight of track, inadequate soil strength	Embankment, triggered by sudden water content increase
		Consolidation settlement	Saturated soil, formation/embankment weight	Increased static soil stress compared to before construction
	Environment	Swelling/Shrinkage	Highly plastic soils, change in moisture content	Rough track surface
	Live Load	Subgrade attrition	Subgrade not protected from ballast, water, hard clay-rich soils	No subballast
		Progressive shear failure	Repeated over-stressing, high water content	Subgrade squeezing, crib/shoulder heave, depression under sleeper

2.1.3 South African Specifications

In South Africa, the Transnet technical specification S410 (Transnet, 2006) contains the allowable parameters for layerworks and earthworks for railway lines. Pavement layers are divided into the special subballast (SSB), subballast (SB), and the subgrade layers A and B. The formation design for a 26 tonne axle load consists of a 900 mm formation as shown in Figure 2.1.

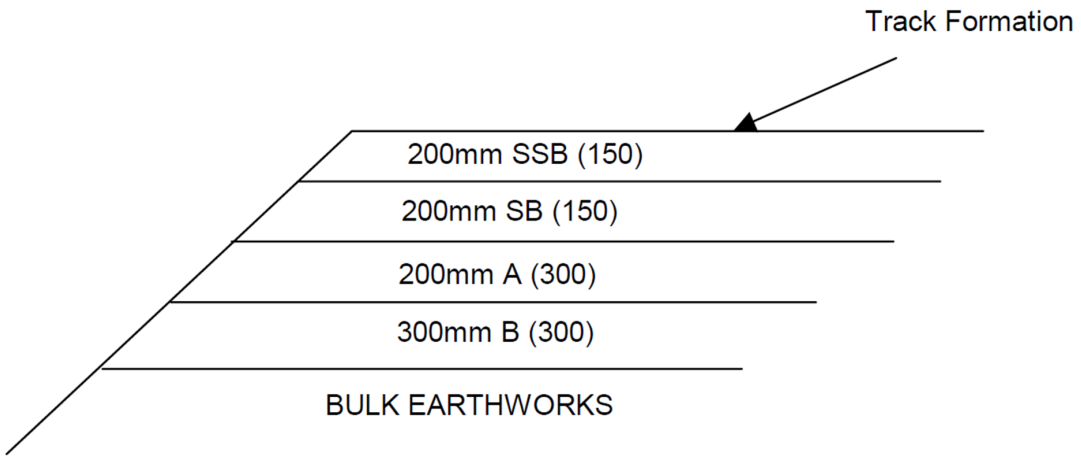

Figure 2.1: Pavement layers for a 26 tonne axle loading (Transnet, 2006)

The layer properties required in South African railway lines are specified in Table 2.3 for subballast, subgrade, and fill material. This table contains the allowable grading envelope, allowable Atterberg limits, and strength related parameters such as the California Bearing Ratio (CBR).

Table 2.3: Earthworks material specification (Transnet, 2006)

LAYER		MATERIAL PROPERTIES									Min. compaction % of Mod AASHTO Density	Min strength after compaction CBR
		SAR Index	Minimum Grading	% BY MASS PASSING SIEVE (sieve in mm)					PI	Max. CBR Swell		
				75	13.2	2.0	0.425	0.075				
SUB	SSB	<50	2	100	60-85	20-50	10-30	5-15	3-10	0.5	98	60 **(o)** (1.5-3 MPa)
LAYERS	SB	<80	1.8	100	70-100	20-60	10-40	5-20	3-10	0.5	95	30 **(o)** (1.5-3 MPa) **+**
A		<110	1					<40	<12		95 (100*)	20
B		<155	0.5					<70	<17		93 (98*)	10
Bulk Earthworks									<25	2	90 (95*)	5
*	These densities apply to non-cohesive soils											
(o)	Strengths in brackets apply in place if CBR values where sub-ballast is stabilised											
+	Increase to 45 in the absence of Layer SSB unless otherwise specified (Increase not normally required for dry area)											

2.2 UNSATURATED SOIL MECHANICS

Unsaturated soil mechanics is the study of soil behaviour under conditions where there is not sufficient water contained in the soil matrix to fill the pores. This leads to behaviour that is different to saturated soil mechanics, which is better understood and often simpler. As described earlier, strength and stiffness of pavement formations are affected by their moisture state, and therefore this field of soil mechanics is of great interest to a pavement engineer.

2.2.1 Soil Suctions

When a soil is saturated, all of the pores are occupied by pore water. This leads to fairly predictable behaviour in terms of a well quantified effective stress where the total stress (σ) is the difference of the effective stress (σ') and pore water pressure (μ_w). When the soil begins to dry out, water starts leaving the pores, starting with the pores of largest diameter first, and leaving successively smaller pores as drying continues.

There are 2 types of soil suction, *matric* and *osmotic* suction. Matric suction is the suction caused by the surface tension forces of the menisci in the soil fabric, while osmotic suction is due to the concentration of soluble salts suspended in the pore water (Huat et al., 2012). The term $\mu_a - \mu_w$ is taken as matric suction, where $\mu_a = 0$ under atmospheric conditions and the value of μ_w is negative in the suction range. A soil has a maximum sustainable suction due to the fact that a meniscus cannot be larger than the pore itself. So when the meniscus diameter is equivalent to the pore diameter, that pore has reached its highest possible value of suction (Huat et al., 2012). Jones and Kohnke (1952) tested the veracity of the capillary model of maximum possible suction and found that it under-predicted the suction that could be produced by a pore of a specific diameter, due to the imperfect geometry of pores.

Work has been done to establish the magnitude of suctions in unbound granular materials used in road formations (base and subbase). Table 2.4 summarises the suctions found in different granular materials including recycled crushed concrete (RCA), reclaimed asphalt pavement (RAP), recycled crushed masonry (RCM) and various railway formation materials.

Table 2.4: Range of suctions from literature

Material	Suction range (kPa)	Air-entry range (kPa)	Test method	Reference
Basalt aggregate	0 - 45	-	Filter paper	Walker (1997)
Sandstone aggregate	0 - 3500	-		
RCA	0 - 90	0 - 22	Hanging water column and Tempe cell	Rahardjo (2010) & Nokkaew et al. (2012)
RAP	0 - 60	0 - 1.1		
RCA/RCM blend 1	0 - 88	0 - 9	Filter paper and hanging water column	Azam et al. (2014)
RCA/RCM blend 2	0 - 240	0 - 18		
Virgin aggregate	0 - 19	0 - 8		

From Table 2.4 it can be deduced that high suctions are possible in granular materials. The limited suction ranges of some of the materials are likely due to limitations of the test method. While the filter paper method can theoretically determine the entire range of low and very high suctions, other methods such as the pressure plate apparatus have a limited range of effective suction measurement. The suctions in recycled materials correspond with similarly graded virgin aggregates (Gupta et al. (2009)), this is due to similar pore sizes occurring with similar gradings, while the chemical composition of the aggregates is of little importance to the magnitude of suctions.

Work was done by Cary and Zapata (2016) to establish the systematic increase of matric suction in a railway subgrade material (Unified SC classification) as cyclic loading takes place. This study was done with a unsaturated triaxial apparatus with 16 000 to 96 000 cycles applied in their tests, depending on the sample. The rate of systematic increase of excess pore pressure in a sample was found to be a function of the loading rate, rest period, and stress state of the soil, given the same initial matric suctions for each sample. This behaviour is presented by Figure 2.2, containing the systematic increase in pore pressure as a function of cycles for 2 saturated and 4 unsaturated samples. It should be noted

that the excess pore water pressures presented in Figure 2.2 occurred in undrained conditions (saturated samples) and constant water content conditions (unsaturated samples).

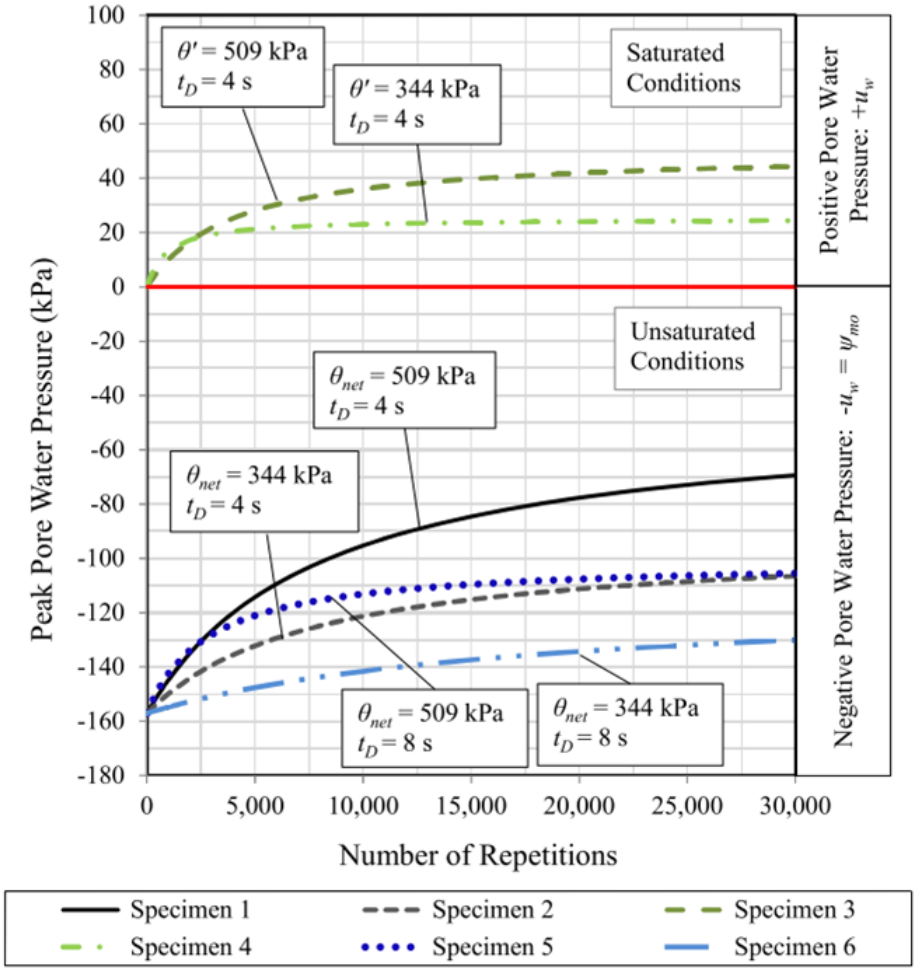

Figure 2.2: Systematic increase of pore pressures in a subgrade material (Cary and Zapata, 2016)

An investigation by Mamou et al. (2017) monitored the pore pressure change in unsaturated samples of subgrade materials while undergoing cyclic loading in a hollow cylinder test. Tests were done on both undrained and drained samples. Figure 2.3 shows that under drained conditions, no excess pore water pressure build up was detected.

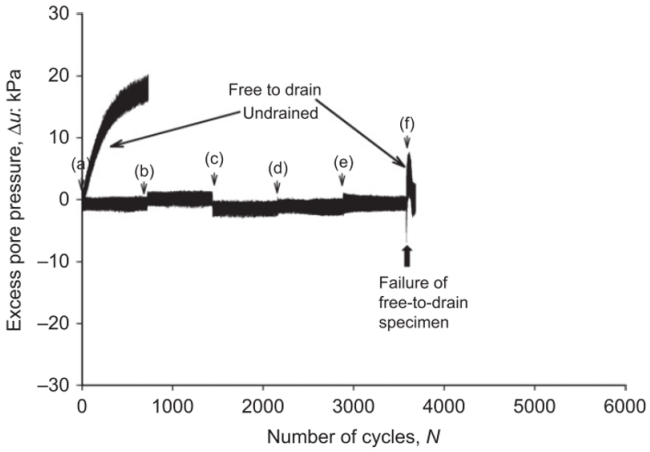

Figure 2.3: Pore pressure response under drained and undrained cyclic loading in a 7 % clay sample (Mamou et al., 2017)

The investigation by Mamou et al. (2017) was primarily concerned with the role of drainage conditions in the deformation behaviour of formation material undergoing cyclic loading and principle stress rotation. Previous work by Brown and Selig (1991) has shown that there exists a cyclic shear stress threshold beneath which a sample will remain stable under cyclic loading. Once this threshold is exceeded, the sample rapidly deforms. At this point failure is deemed to have occurred. It is also at the point that the threshold is passed that the excess pore pressures will begin to build up in undrained conditions. It is interesting to note that in the investigation by Mamou et al. (2017) the build up of excess pore water pressures was always coincident with the shear stress threshold being passed, regardless of the drainage condition. This behaviour can be seen to an extent in Figure 2.3, but is demonstrated more clearly in Figure 2.4.

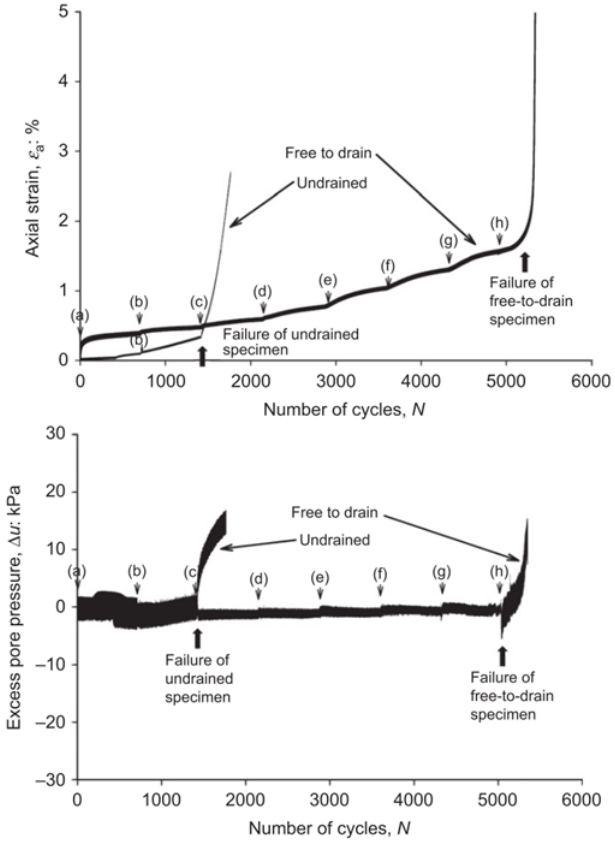

Figure 2.4: Axial strain (top) and excess pore water pressure (bottom) response of drained and undrained cyclic loadings in a 14 % clay sample (Mamou et al., 2017)

At each step in Figure 2.4 marked (a)-(h), the shear stress in the sample was increased in steps up to failure. Mamou et al. (2017) clearly showed that the stress threshold is dependent on the drainage of a sample, as well as the clay content of a sample. Higher clay contents were associated with higher stress thresholds. The fact that higher clay contents would lead to lower excess pore pressures seems counter-intuitive, however, it was found that in drained tests the build up of excess pore pressures were associated with rapid increases in volumetric strain. It was theorised that increasing the clay content in the granular samples produced a more well-graded sample. These well-graded samples showed higher stiffness's, and therefore, greater resistance to volumetric strain.

2.2.2 Soil Water Retention Curve

Every soil has a specific suction response to drying or wetting. Since these responses vary from material to material, each soil must be characterised separately. This is achieved by determining the Soil Water Retention Curve (SWRC). It is useful to characterise the material in terms of suction versus volumetric water content (θ) or degree of saturation (S_r). Figure 2.5 shows a typical SWRC shape, along with the 3 moisture 'regimes' at different values of S_r. These regimes delineate 3 different states of behaviour in the soil mass as a result of the different interactions of the soil, water and gas phases.

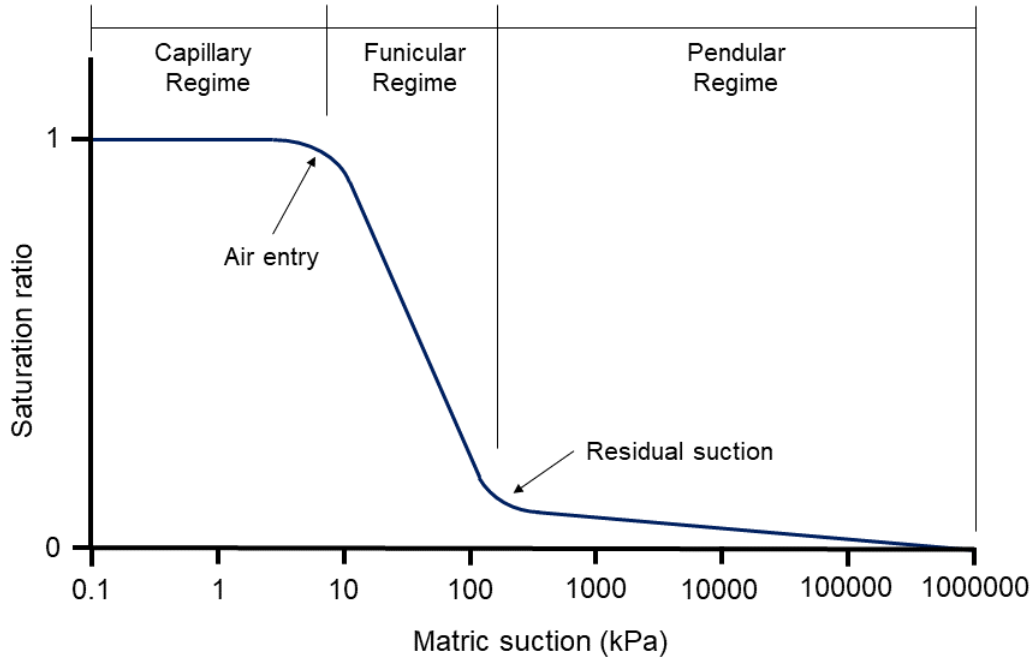

Figure 2.5: Schematic of suction regimes in a typical SWRC

Lu and Likos (2004) describes the *capillary* and *pendular* regimes in terms of the dominant pore water retention mechanism. In the pendular regime, thin films of water are held in place by short range adsorption effects. While in the capillary regime, capillarity causes an increase in matric suction as the water content stays the same due to tension forces generated in the pore water. The *funicular* regime

acts as a transition zone between the capillary and pendular regimes, but it continues to be dominated by capillary effects. The difference between the the capillary and funicular is that the capillary regime occurs at – or close to – saturation, while the funicular occurs after air entry into the saturated sample. As the funicular regime progresses, further desaturation of the sample will occur until pore water occurs in films around the soil, thin enough for adsorption to play a dominant role. At this point (residual suction) the gradient of the SWRC change, and the pendular regime has been entered. Figure 2.6 shows a parameter known as residual water content (θ_r). The residual water is adsorbed water retained by clay particles (McQueen and Miller, 1974), and it therefore follows that a more clayey material will have a higher residual water content due to the increased number of clay particles.

Figure 2.6 presents 2 SWRCs for a specific soil to demonstrate wetting and drying hysteresis. The upper curve is followed when the soil is undergoing drying from a wet condition, and the lower curve is followed when a soil is undergoing wetting up from dry conditions. These 2 curves are known as the *Primary Drying Curve* and *Primary Wetting Curve* respectively (Huat et al., 2012).

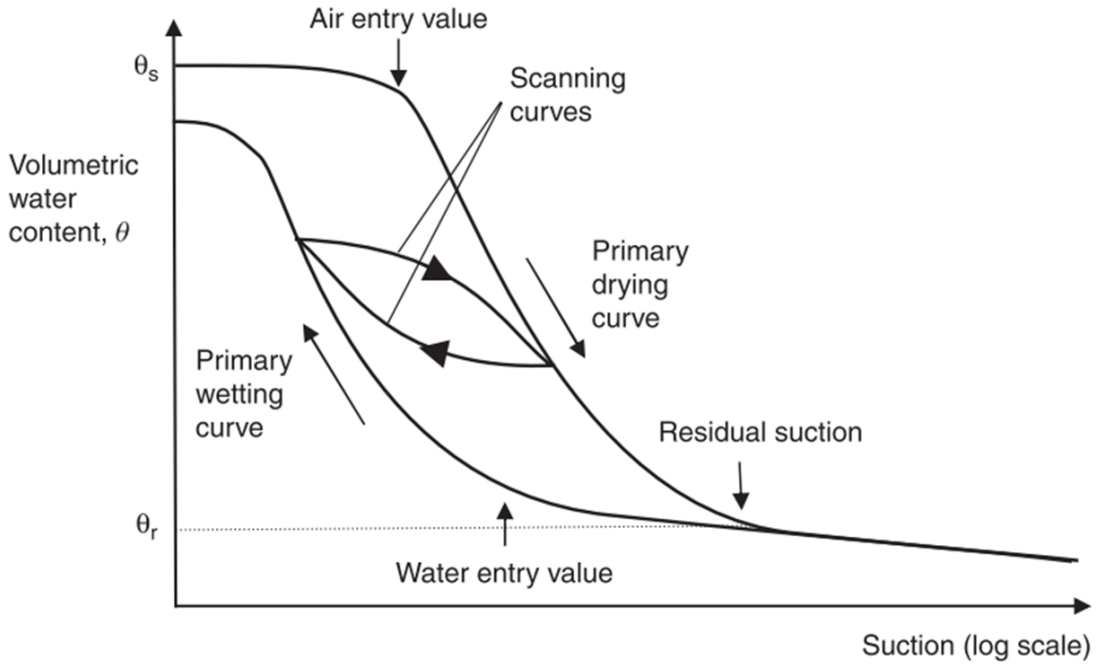

Figure 2.6: Example of a soil water retention curve (Huat et al., 2012)

Assuming the soil is perfectly saturated before the primary drying curve is determined, the saturated water content (θ_s) will remain constant for a range of decreasing suctions, until air-entry occurs in

the largest pores. This causes the inflection shown on Figure 2.6 known as the air entry value. Upon following the primary wetting curve to completion, the water content may not return to the value of θ_s, but rather some lower value, as some air bubbles may still be trapped in the soil water (Huat et al., 2012).

The area bounded by the primary drying and wetting curves describe all the possible moisture-suction states that a soil can attain. If either a wetting or drying process is stopped at some intermediate saturation, and the opposite process is begun, the moisture state will follow a *scanning curve* as it traverses between the boundaries. When a boundary is encountered, the state will follow that boundary as long as the process is continued (Huat et al., 2012).

In the study on suctions in RCA and virgin aggregate base materials, Azam et al. (2014) found that the equations proposed by van Genuchten (1980) and Fredlund and Xing (1994) can be used to reliably fit a SWRC through discrete suction points measured by the filter paper method in a granular material. These methods were shown to be simpler to apply than other competing methods. The Fredlund and Xing method has been expanded upon by Fredlund et al. (2011) to include a practical method of estimating the wetting curve from the drying curve by changing the a parameter. Changing the a parameter shifts the drying curve to smaller suction by a certain factor that is determined based on the material. The van Genuchten and Fredlund and Xing equations are presented by Equations 2.1 and 2.2 respectively as summarised in Fredlund et al. (2011).

$$w(\psi) = \frac{\theta_s}{[1 + (a\psi)^n]^m} \tag{2.1}$$

$$w(\psi) = C(\psi)\frac{\theta_s}{\{ln[e + (\psi/a)^n]\}^m} \tag{2.2}$$

Where:

- θ = Volumetric water content (%)
- θ_s = Saturated volumetric water content (%)
- ψ = Matric suction (kPa)

- a = Fitting parameter related to air-entry value
- m = Fitting parameter to fit data
- n = Fitting parameter related to rate of desaturation of soil after air-entry
- C = Correction factor for Fredlund and Xing equation

The correction factor for the Fredlund and Xing equation (C) extends the range of the model from the residual water state to the completely dry state. The correction factor can be discarded if only the suctions in the range of air-entry to residual moisture content are of interest. Equation 2.3 presents the equation for the correction factor.

$$C(\psi) = 1 - \frac{ln(1 + \psi/\psi_r)}{ln[1 + (1000000/\psi_r)]} \tag{2.3}$$

Where:

- ψ_r = Residual matric suction (kPa)

The fitting parameters a, m and n require calculation, and are based on the shape of the funicular regime. They may be calculated as shown in Equations 2.4, 2.5 and 2.6 respectively (Fredlund and Xing, 1994):

$$a = \psi_i \tag{2.4}$$

$$m = 3.67ln\left[\frac{\theta_s C(\psi_i)}{\theta_i}\right] \tag{2.5}$$

$$n = 3.72s^* \frac{1.31^{m+1}}{mC(\psi_i)} \tag{2.6}$$

Where:

- ψ_i = Inflection point suction (kPa)
- θ_s = Saturated volumetric moisture content (%)
- θ_i = Inflection point volumetric moisture content (%)
- s^* = Fitting parameter related to slope of funicular regime

The equations for the fitting parameters require the parameter s^*, which in turn requires the slope of the tangent line s. Both parameters may be calculated by Equations 2.7 and 2.8 respectively.

$$s^* = \frac{s}{\theta_s} - \frac{\psi_i}{1.31^m(\psi_i+\psi_r)ln[1+(1000000/\psi_r)]} \tag{2.7}$$

$$s = \frac{\theta_i}{ln(\psi_p/\psi_i)} \tag{2.8}$$

Where:

- s = Slope of funicular tangent line
- ψ_p = Intercept of slope tangent line with semilog suction axis (kPa)

Fredlund et al. (2011) also provides a rational method to estimate the wetting curve from a measured drying curve. When both curves are measured, the wetting curve will be to the left of the drying curve (in a lower range of suctions) and will be approximately parallel to the drying curve in the different moisture regimes. Estimating the wetting curve requires taking the expression for the drying curve and changing the a parameter. This will shift the drying curve by a value expressed as a percentage. The percentage value of lateral shift is based on taking 100 % as the one step in the log scale. For example, a shift from 10 kPa to 1 kPa will be a shift of 100 %, but so will as shift of 1 000 kPa to 100 kPa. The expression to estimate the log-shift of the a parameter for the wetting curve is presented in Equation 2.9.

$$\xi = 100[log(\psi_{ad}) - log(\psi_{aw})] \tag{2.9}$$

Where:

- ξ = Lateral shift (%)
- ψ_{ad} = Suction value on drying curve for specific water content/saturation ratio
- ψ_{aw} = Suction value on wetting curve for specific water content/saturation ratio

2.2.3 Soil Stress

Unsaturated soils have greater shear strength than their saturated soil counterparts. This is due to the increased contact stresses between particles in the presence of negative pore water pressure. In addition to this, the surface tension on the meniscus inside a pore produces a further stabilising effect between particles (Huat et al., 2012).

A popular approach in saturated soil mechanics, the Mohr-Coulomb failure criterion was extended to unsaturated soil by Fredlund et al. (1978). The traditional Mohr-Coulomb failure criterion for saturated soils is presented in Equation 2.10:

$$\tau_f = c' + \sigma' tan\phi' \tag{2.10}$$

Where:

- τ_f = Shear stress at failure (kPa)
- c' = Cohesion intercept (kPa)
- σ' = Effective normal stress (kPa)
- ϕ' = Angle of friction (°)

The suggested extended Mohr-Coulomb failure envelope is described by Equation 2.11.

$$\tau_f = c' + (\sigma - \mu_a) tan\phi^a + (\mu_a - \mu_w) tan\phi^b \tag{2.11}$$

Where:

- τ_f = Shear stress at failure (kPa)
- c' = Cohesion intercept (kPa)
- $(\sigma - \mu_a)$ = Net stress (kPa)
- ϕ^a = Angle of friction for changes in net stress (°)
- $(\mu_a - \mu_w)$ = Matric suction (kPa)
- ϕ^b = Angle of friction for changes in matric suction (°)

Figure 2.7 shows a 3 dimensional visualisation of the extended Mohr-Coulomb failure envelope, showing the strength gain as matric suction increases. This strength gain due to suctions is represented by the increased value of c', and ϕ^b represents the rate of strength gain as the suction increases.

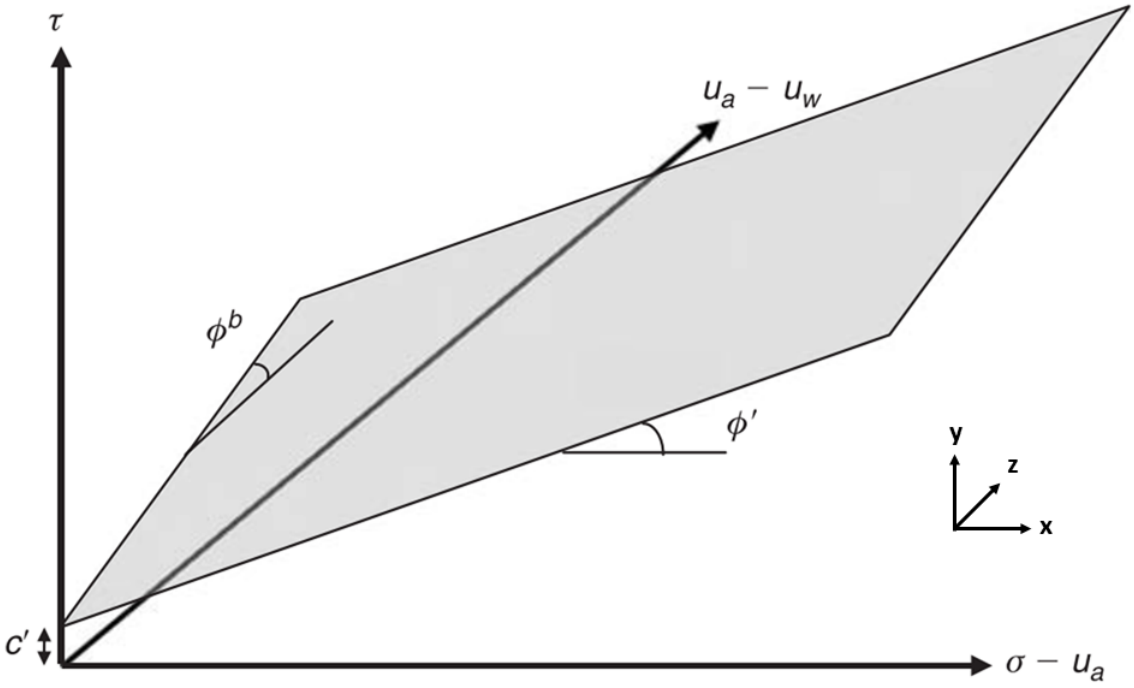

Figure 2.7: Extended Mohr-Coulomb failure envelope (Huat et al., 2012)

It should be noted that the geometry of the failure surface is not quite as simple as Figure 2.7 may seem

to show. Fredlund (1987) found that ϕ^b changes with matric suction. While ϕ^b starts initially at a value that is approximately equal to ϕ', it will generally decrease to a residual value of total cohesion beyond where it is not really affected by an increase in matric suction. In addition to this, Toll et al. (2008) (among others) has found that the value of ϕ^a also changes with changes in matric suction. While it starts off at a value equal to ϕ', it will increase with an increase in matric suction, therefore it cannot be assumed to maintain that value for the entire range of matric suctions experienced. The increased value of ϕ^a is due to adjacent particles being drawn together by matric suctions into aggregates of particles, and behaving like coarser materials, hence the larger angle of friction.

The effective stress equation first proposed by Terzaghi (1943) has long been a cornerstone of saturated soil mechanics as it defines effective stress as the governing force of soil behaviour. Bishop (1959) attempted to extend the effective stress principle to unsaturated soil mechanics by introducing the coefficient of effective stress (χ). This coefficient varied between 0 and 1, depending on the saturation state of the soil, and allowed an estimation of the stress due to matric suction present in the soil. Equation 2.12 presents the Bishop effective stress function for unsaturated soil.

$$\sigma' = \sigma - \mu_a + \chi(\mu_a - \mu_w) \tag{2.12}$$

Where:

- σ' = Effective stress (kPa)
- σ = Total stress (kPa)
- μ_a = Pore air pressure (kPa)
- χ = Coefficient of effective stress
- $\mu_a - \mu_w$ = Matric suction (kPa)

A different approach was followed by Lu et al. (2010) in formulating a closed form equation for effective stress in unsaturated conditions. This method required the determination of the Suction-Stress Characteristic Curve (SSCC) as described in Lu and Likos (2006). The SSCC directly relates the soil matric suction (as measured by tensiometers or filter paper) to the suction stress (σ^s) experienced by

the soil. Suction stress is defined as the stress in the soil skeleton generated by the present soil suction. Equation 2.13 presents the closed-form solution for σ^s.

$$\sigma^s = -\frac{S_e}{a}(S_e{}^{n/(1-n)} - 1)^{1/n} \tag{2.13}$$

Where:

- σ^s = Suction stress (kPa)
- S_e = Effective degree of saturation (kPa)
- n = Fitting parameter related to rate of desaturation of soil after air-entry

The explicit calculation of σ^s allowed the simplification of the Bishop effective stress concept (Bishop, 1959) by eliminating the need for the χ coefficient. This simplifies the Terzaghi effective stress equation for unsaturated soils as shown in Equation 2.14.

$$\sigma' = \sigma - \mu_a - \sigma^s \tag{2.14}$$

A comparison of the functions for the SSCC (Equation 2.13) and the van Genuchten SWRC (Equation 2.1) shows that the functions shares parameter n and a. Lu et al. (2014) confirmed that a and n were common parameters shared by the SSCC, SWRC and the hydraulic conductivity functions (HCF). It was experimentally proven that the parameters could be found by a single function, and the other functions could be established using the common parameters.

2.2.4 Deformation Characteristics

A railway line is subjected to variable cyclic loads within its lifespan. Although railway lines are designed for a resilient deformation response against the imposed loading, permanent deformation does take place and will accumulate over its lifespan (Li et al., 2016).

Resilient Response

The resilient modulus (M_r) of a pavement layer is defined as the modulus of a well compacted soil after repeated loadings. After a sufficient number of loading cycles, continued cyclic loading will cause a recoverable deformation after every cycle (Li et al., 2016). The resilient modulus is defined by Equation 2.15.

$$M_r = \frac{\sigma_d}{\varepsilon_r} \tag{2.15}$$

Where:

- M_r = Resilient modulus (MPa)
- σ_d = Applied repeating deviator stress (kPa)
- ε_r = Recoverable strain in direction of axial stress

The value of M_r is not constant and is a function of the following factors (Lekarp et al., 2000):

1. Stress state under load, including magnitude of deviator and confining stresses
2. Soil type and structure, dependent on compactive effort
3. Physical state of soil, including moisture content and dry density

Of the 3 factors influencing M_r, the physical state is often focused on, as it is the one that is most easily changed by human intervention or the environment. Figure 2.8 shows the development of the M_r during cyclic loading as well as the plastic strains that precede it.

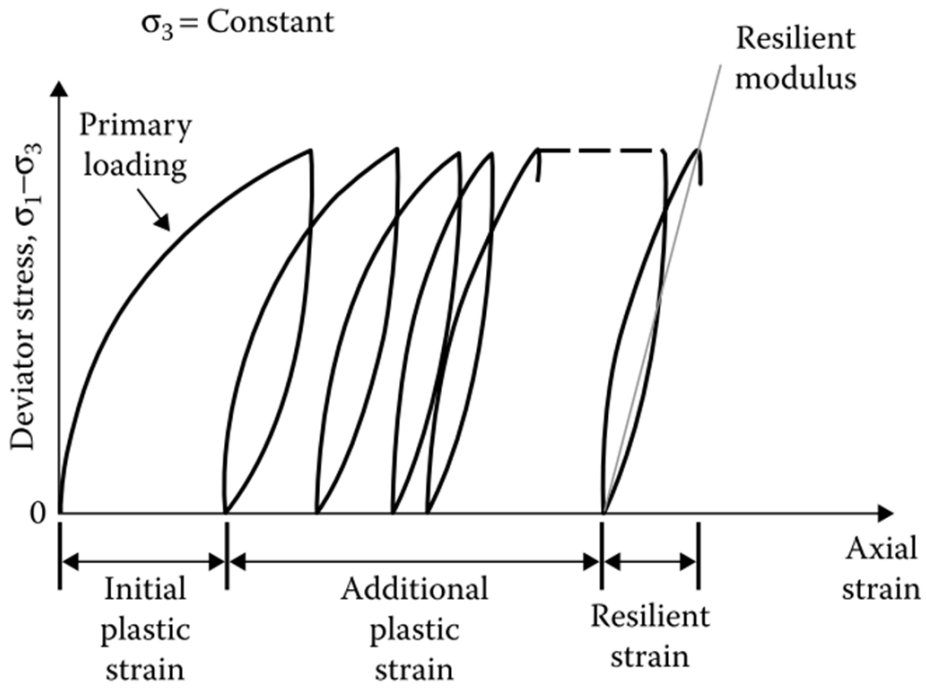

Figure 2.8: Development of resilient modulus from cyclic loading (Li et al., 2016)

M_r tends to remain at a constant residual value after a number of cycles, assuming there is a negligible change in the physical state of the soil, often associated with environmental conditions. Since the magnitude of σ_d is most important in the final value of M_r, most models for soils are based on a relationship between these 2 parameters (Li et al., 2016).

Rorke (2016) performed a comprehensive study on factors affecting railway formation M_r. It was found that the following factors affect the magnitude of the M_r in order of decreasing importance:

1. Matric suction
2. Cyclic deviator stress
3. Confining stress
4. Principal stress rotation (PSR)

The matric suction (and by extension the moisture state) was therefore found to be the most important factor governing M_r. Rorke (2016) reported a sixfold increase in M_r with an increase of matric suction.

Permanent Deformation

When cyclic loading is applied to a railway formation, plastic strains will start to accumulate. Some of these occur during the early life of the line as in Figure 2.8, as the formation compacts itself to a degree necessary to develop a consistent resilient modulus.

For a subgrade material, there exists a critical level of deviator stress that can induce rapid plastic deformation. This critical value of deviator stress produces high plastic deformations that are not attainable by a static load of the same magnitude (Li et al., 2016). An increased moisture content in the subgrade layer can also cause large permanent deformations. In a study on clayey railway embankment material, Vorster (2016) demonstrated that slight increases in moisture content can mean the difference between a stable embankment and a large amount of permanent deformation, culminating in a slip failure. This investigation emphasised the importance of cyclic loading when generating the failures at a higher moisture content. A material that was stable for both static and cyclic loading at 22 % moisture content, was stable at 23 % moisture content for static loading conditions, but failed under cyclic loading. Rorke (2016) reiterated the importance of moisture content (MC) on permanent deformation. This study reported strain of 0.17 % at MC = 7 % and 0.002 % strain at MC = 4 %. This comparative loss of strength points to the importance of the matric suction and by extension σ^s as described in Section 2.2.3

When testing formation materials in the laboratory, it is important to consider the difference in permanent deformation behaviour between static loading, cyclic loading and cyclic loading with principal stress rotation (PSR). Vorster (2016) showed that cyclic loading caused more deformation than static loading at the same applied stress. However, to best model the effect of axle loading on a formation, the effect of PSR must be considered. Studies have shown that the formations will suffer greater deformation when undergoing cyclic loading with PSR than without. This is true for both permanent (Gräbe and Clayton, 2009) and resilient deformation (Gräbe and Clayton, 2014). Furthermore, good agreement was found between lab testing using PSR and in-situ deformation measurements as described in Gräbe et al. (2005). Therefore cyclic loading with PSR is considered the most representative form of deformation testing, when available.

Pavement formations typically have some clayey particles in them which can trap moisture. With the moisture trapped, cyclic loads will cause the build-up of pore pressures as excess pore water

pressure is unable to equalise before the next load is applied (Wilson and Greenwood, 1974). While this trend applies to both normally consolidated (NC) and over-consolidated (OC) soils, the behaviour of each is somewhat different. OC soils would typically dilate in the initial cycles, causing a negative pore pressure. This negative pore pressure would eventually become positive after continued loading. However, it should be noted that while both NC and OC soils exhibited this behaviour, a correlation was found between an increase in over-consolidation ratio (OCR) and a decrease in excess pore water pressure. This suggests the logical conclusion that OC soils are more resistant to cyclic loading.

2.3 SUCTION MEASUREMENT

Many methods have been proposed to measure soil suctions, some of which measure discrete values of suction, while others are able to take continuous measurements of suction with time.

2.3.1 Discrete Suction Measurement

Specially calibrated filter papers may be used to measure the suction in a soil sample between 1 - 100 000 kPa (Huat et al., 2012). These filter papers provide a high quality suction measurement, albeit of a discrete point on the SWRC. Therefore, it is necesarry to use a SWRC fitting equation such as van Genuchten (1980) or Fredlund et al. (2011) as described in Section 2.2.2. ASTM (2003) provides a standardised method for performing a filter paper test. While the filter paper can measure both total and matric suction, only the method to determine matric suction is described here. In this method, 3 filter papers are dried out in an oven at 105° for a period of 16 hours. The mass of the dry filter papers must be measured on a laboratory balance with a resolution of 0.0001 g. The sample should consist of a cylinder of material that has been divided into 2 pieces. The 3 filter papers are placed between the 2 pieces, and the sample is sealed in an airtight container to prevent moisture loss.

The filter papers and soil are then left in the airtight container for 7 days to equilibrate. Once this time has passed, the mass of the filter paper must be taken immediately after removal from sample. ASTM (2003) recommends that the time from removal to measurement be kept under 5 seconds, as a 5 % change in mass has been observed if left for 5 - 10 seconds. Once the moisture content of the filter paper is established, a calibration curve from literature must be used to relate moisture content and suction. Marinho and Oliveira (2006) found that the suction equilibration time generally increases with suction, as higher suctions (and less available pore water) inhibited the flow of pore

water between soil and filter paper necessary for accurate suction measurement. Marinho and da Silva Gomes (2011) further argued that decreased contact between the soil and the filter paper also requires longer equilibration times, with 14 days being the recommended time given for equilibration.

Work done by Marinho and da Silva Gomes (2011) quantified the effect of material grading and filter paper contact on suctions measured by the filter paper method. This experiment considered clay (kaolin), fine sand and coarse sand material types. It was found that suctions measured by the filter paper method would increase as a result of the lack of contact between the soil and the filter paper. The increase in measured suction was found to be due to the measurement of a degree of osmotic suction in addition to the required matric suction. In this way the lack of contact between soil and filter paper partially mirrors the test standards set out by ASTM (2003), whereby full contact is required when measuring matric suction, and no contact is required when measuring total suction (matric + osmotic). While the observation of increased measured suction held true for all materials tested, it was found to manifest most commonly in coarse grained materials. The reason given for this behaviour was that the surface roughness of the coarse material created an uneven contact surface for the filter paper to rest on. This effectively reduced the contact area to the coarse grains protruding from the surface of the sample.

2.3.2 Continuous Suction Measurement

Negative pore water pressures can often be measured by the application of tensiometers. Tensiometers consist of an assembly of a high air entry (HAE) ceramic against a diaphragm that has a strain transducer attached. A cross section of a typical assembly is shown in Figure 2.9. The HAE ceramic contains microscopic pores of a controlled size that are used to retain de-aired water. When the ceramic filter has been saturated, an interface is established between the water in the ceramic pores and the air-water mixture in the soil adjacent. A tensiometer may only measure matric suction, as the water in the tensiometer is allowed to mix and exchange dissolved solutes with the soil water. This means that a tensiometer cannot measure osmotic suction (Lu and Likos, 2004). Any matric suction in the soil adjacent to the ceramic will result in a tensile force applied to the water in the ceramic. Saturation is important for the tensiometer, as a ceramic with poor saturation will have a slow response time, as well as a pressure hysteresis with fluctuation of suctions (Take and Bolton, 2003).

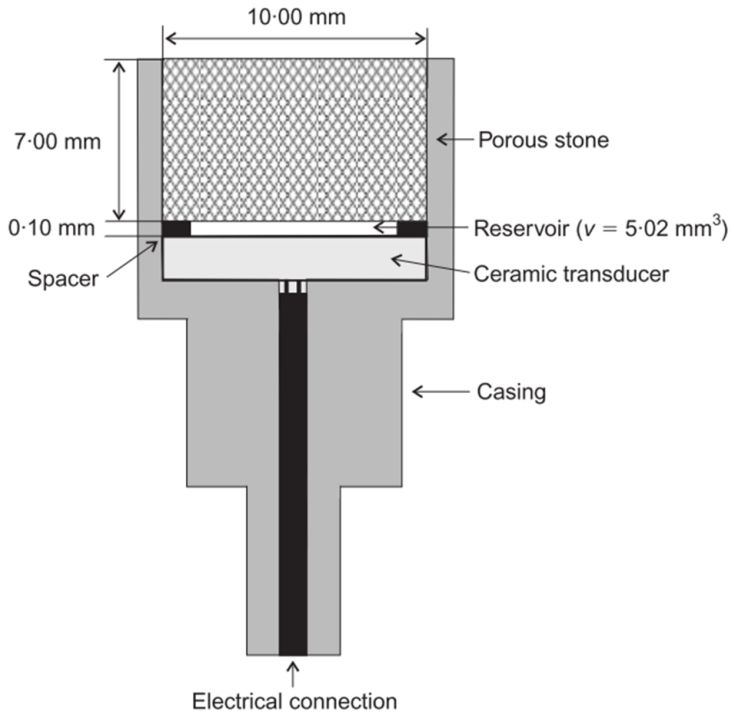

Figure 2.9: Cross-section of Durham University-Wykeham Farrance tensiometer (Lourenço et al., 2008)

Tensiometers are commonly saturated by the method laid out by Take and Bolton (2003), whereby ceramic filters should go through a two-stage filter saturation process. In the initial saturation phase, the ceramic must be oven-dried and placed into a low-moisture, enclosed vessel.

Once in the vessel, the de-aired water is introduced under vacuum and saturation is allowed to occur under pressure. The vacuum ensures that the low pressure environment inside the ceramic pores encourages the ingress of higher pressure water. However this initial saturation is often unsatisfactory. Take and Bolton (2003) showed that in a tensiometer that was allowed to saturate for 20 minutes under less than 1 kPa of water pressure, negative water pressures are not correctly read. Figure 2.10 demonstrates the difference in response between a poorly saturated tensiometer ($B = 0.51$) and a well saturated tensiometer ($B = 0.97$) in the negative pressure range. Clearly, a well saturated tensiometer can be calibrated in the positive pressure range and used in the negative pressure range, while that is not true for poorly saturated tensiometers.

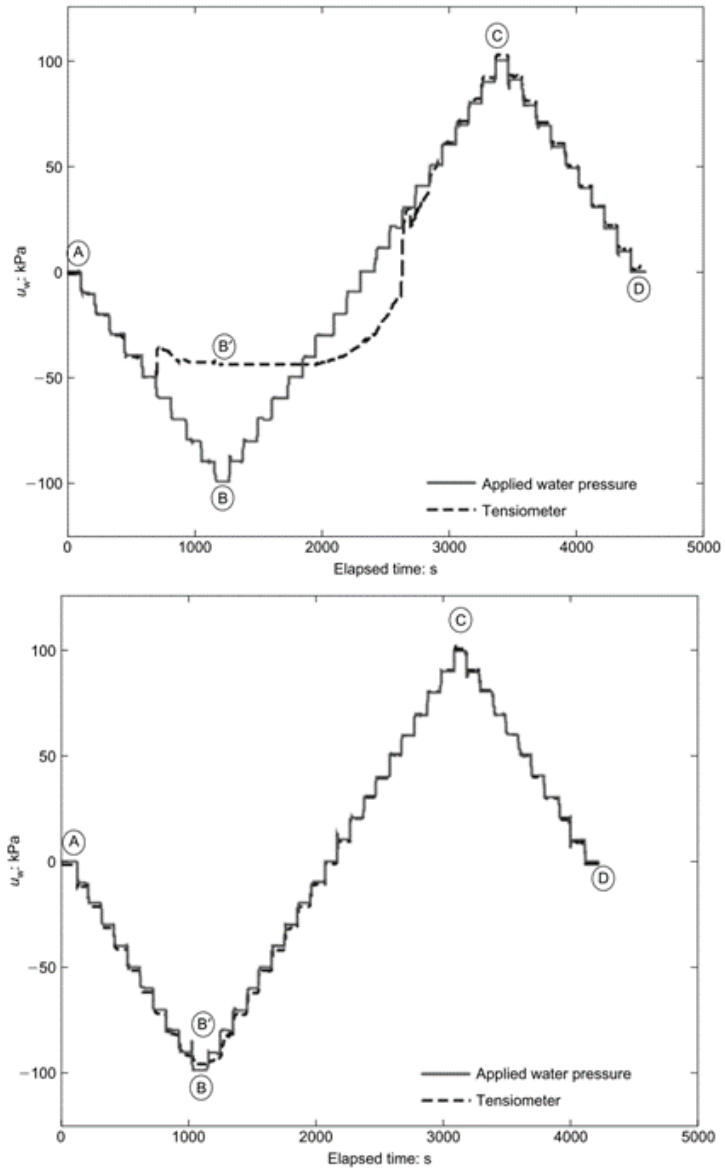

Figure 2.10: Stepwise calibration of tensiometer at 0.51 degree of saturation (top) and 0.97 degree of saturation (bottom) (Take and Bolton, 2003)

Further research by Lourenço et al. (2008) showed that tensiometers can indeed be calibrated by extrapolating the response to positive pore pressures to the the response at negative pore pressures, if a calibration coefficient is used. This calibration coefficient must be found individually for each tensiometer.

When instrumenting a material with tensiometers, it is important to be mindful of factors that affect

the response time of the tensiometer. The response time (or equalisation time) of the tensiometer refers to the length of time required for the tensiometer suction to equalise with the suction in the soil sample. Factors that affect the response time of the tensiometer include:

- Degree of saturation (S_r) of the soil sample
- Conditions between tensiometer face and soil
- Soil structure

The response time of tensiometers is inhibited at lower values of S_r due to the decreasing hydraulic conductivity with increases of matric suction (Guan and Fredlund, 1997, Oliveira and Marinho, 2008). In physical terms, the response time is then the time required for moisture to travel from the soil to the tensiometer (or vice-versa), thereby reaching suction equilibrium. The conditions present between tensiometer face and soil, and the soil structure are somewhat interrelated as the soil-tensiometer interface dictates the type of response a tensiometer will give. Cracks in the soil at the tensiometer face will lengthen the response time of the soil, but will not change the eventual value of matric suction measured (Guan and Fredlund, 1997). This behaviour is due to lack of contact between the tensiometer and soil. To overcome this lack of contact, soil pastes have been used to ensure a continuous path for pore water between the soil and the tensiometer face. A study was conducted by Oliveira and Marinho (2008) to establish the effect of different soil pastes on the response time and suctions measured by the tensiometer. The following pastes were tested:

- Fines of parent soil (< 2 mm)
- Fines of parent soil (< 0.425 mm)
- Kaolin

No significant differences in response time or suction measured were found between the 3 types of soil pastes. Rather, response time tended to increase both when the soil paste was too dry or too wet. It was found that the soil paste should be wetted to between its plastic and liquid limits to minimise response time. Along with fines from parent materials and kaolin clay, silica flour is also commonly used as a soil paste (Tandon et al., 1996).

Accurate measurements of soil suction or pore pressure are therefore only possible if the tensiometer response time is shorter than the change in pore pressure. If this criterion is not met, the suctions

measured will not reflect the suctions in-situ. This has implications for dynamic testing, where there may be rapid small-scale fluctuations in pore pressure while loading takes place. These changes may occur in too short a timeframe for the tensiometers to equilibrate and measure the fluctuations. Additionally, Lourenço et al. (2009) found that suction measurement during dynamic testing may be complicated by the movement of soil across the tensiometer ceramic face. It is thought that excessive movement of soil across the tensiometer face may disturb the hydraulic connection formed between soil and tensiometer, causing fluctuations in the suction reading. This disturbance may be brief in a wet sample, as the hydraulic connection may be rapidly re-established as a function of the short response time in wet samples. However, disturbances in drier materials may lead to longer periods of fluctuating suction readings due to the longer equalisation times.

2.4 SUMMARY

The literature review presented a large body of work relevant to the subject being investigated. The background of railway formation design and behaviour was discussed in terms of South African and international practice. Factors important to the proper functioning of the railway formation were identified and discussed individually, with special attention given to the effect of soil moisture on the formation life.

The theory behind unsaturated soil mechanics and its relationship to saturated soil mechanics was explored, as well as prevailing theoretical models that describe the interrelations between parameters such as soil suction, soil stress and hydraulic conductivity. After theoretical unsaturated soil mechanics had been explored, the implications of soil suctions on permanent and resilient deformation of railway formations were discussed.

Modelling unsaturated soil behaviour in practice requires accurate measurement of soil suctions. The successful measurement of suctions in granular formation materials, particularly during cyclic testing, were found to be dependent on a number of factors. It is therefore important to identify these factors to ensure good suction measurement practices in the final test. These factors were primarily related to the hydraulic connection between soil and the measurement instrument (be it tensiometer or filter paper) and the response time of the tensiometer in different conditions.

The theoretical advances in unsaturated soil mechanics have created an environment where the practical application of those theories have become a possibility. The applications of unsaturated soil theory are therefore being explored in pavement and railway formations to quantify the contribution of suctions to the strength and stiffness of railway formations to provide better design and analysis methods for the future.

CHAPTER 3 EXPERIMENTAL PROCEDURE

This chapter describes the equipment, tests performed, and instrumentation for the experiments. The rationale behind the design and testing decisions as well as setup and procedures are discussed. The purpose of this section is to describe a practical testing framework in all its detail. This should take into account the best practices identified in the literature review.

3.1 MODEL SETUP

The physical model used in the experiment consisted of a 500 x 500 mm strongbox filled with compacted soil to a depth of 200 mm. This model was instrumented to monitor pore pressures/suctions using tensiometers and surface deflection using linear variable differential transformers (LVDTs). These instruments are discussed in greater detail in Section 3.1.5. Figure 3.1 shows a schematic cross-section of the fully instrumented strongbox as used in the tests.

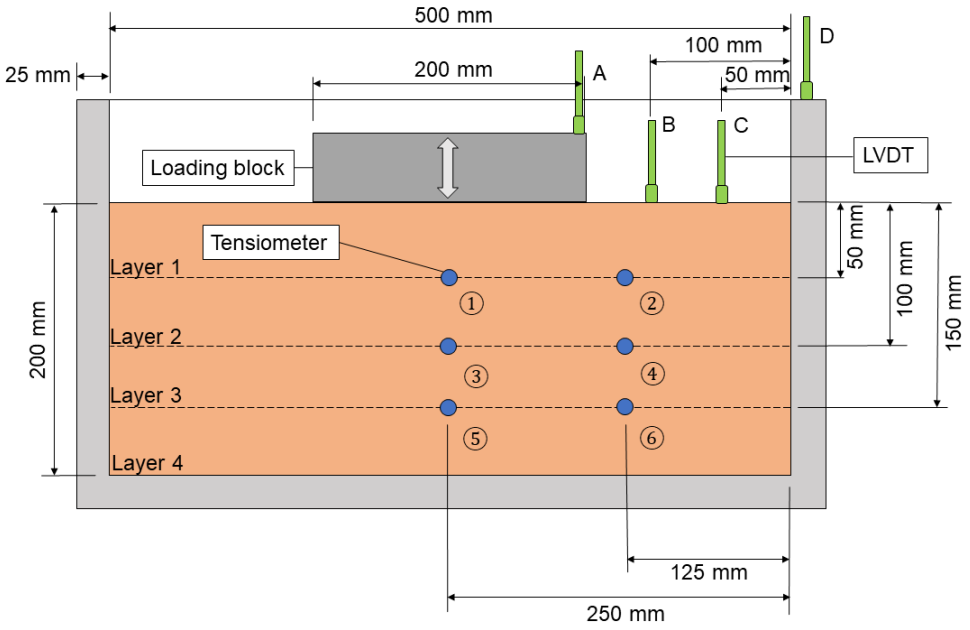

Figure 3.1: Schematic of the box test setup

3.1.1 Strongbox Setup

A steel strongbox with 500 x 500 x 350 mm internal dimensions was used throughout testing. A new 3 mm base plate was welded to the strongbox. Figure 3.2 shows an orthographic representation of the box.

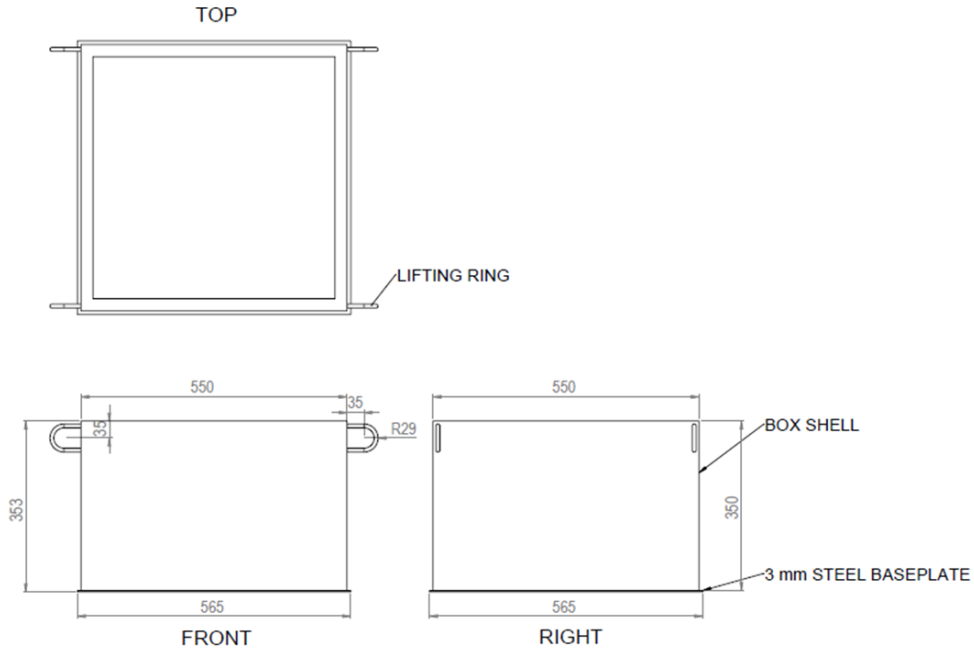

Figure 3.2: Strongbox orthographic representation

3.1.2 Formation Material Construction

The formation was constructed in 4 layers of 50 mm to a formation depth of 200 mm. Material was weighed out for each layer based on the maximum dry density (MDD). Given that the MDD was known, the 95 % Mod AASHTO density was determined from the MDD. Since the volume of each 50 mm layer was known, the dry mass of material required for every layer could be determined. The material for each layer was sorted into individual containers. The required amount of water was added. The samples were left in the container for a minimum of 24 hours to equilibrate. To construct the formation in layers, the material for a single layer was added to the strongbox and compacted. The amount of material per layer was determined by calculating the required mass of material for the volume of one layer at 95% Mod AASHTO. Compaction was carried out by hand using a 150 mm section of 100 x 55 I-beam welded to a steel rod. Compaction density was regulated by ensuring that the allotted mass of soil fitted within the boundaries of the layer. Figure 3.3 shows a subballast layer before and after compaction.

Figure 3.3: Placement of material before (left) and after (right) compaction

Once all 4 layers had been placed and compacted, the material on the top was levelled by hand to allow seating of the loading block. An approximately level surface could be made by hand, but the seating had to be completed with a 10 kN load prior to testing.

3.1.3 Hydraulic Load Frame

Testing was done on a hydraulic loading frame with a capacity of 500 kN at 30 Hz. This loading frame was designed by the MTS company and shall be referred to as the MTS machine henceforth. The MTS machine consists of a steel bench with a suspended hydraulic piston over it. This piston functions by way of 3 hydraulic pumps that maintain operating temperatures with chilled oil. Figure 3.4 presents a photograph of the machine and loading bench.

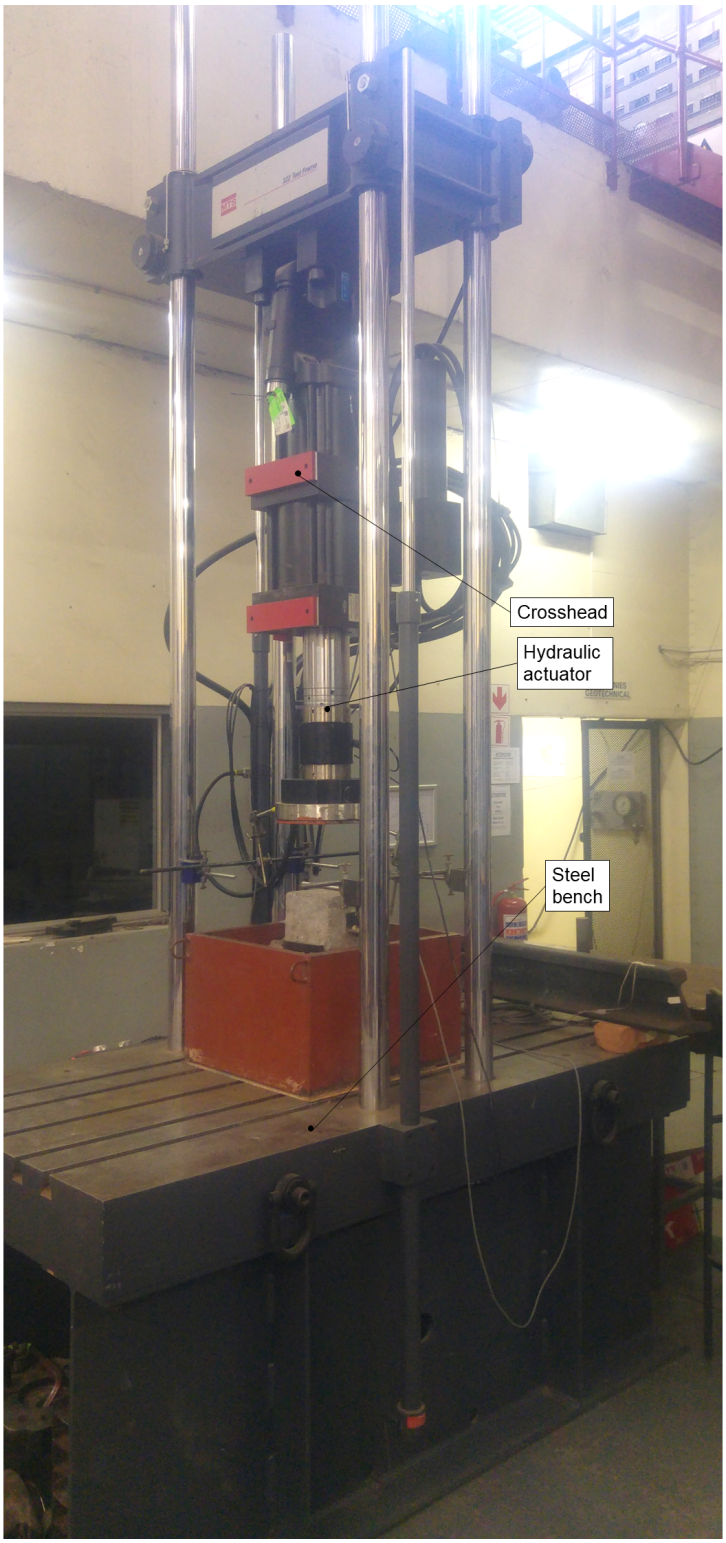

Figure 3.4: MTS hydraulic load frame

3.1.4 Loading Block

A loading block was fabricated using 500 mm sections of 100 x 55 I-beam to produce a 200 x 500 mm block used for all testing. The sections were joined by welds along their edges. Pieces of flange at the bottom of the block were trimmed away to produce a width of 200 mm. After welding, the welds were ground to create a flat and level surface at the top and bottom.

When loaded into the strongbox, a steel cylinder was placed on the loading block to provide spacing between the loading block and piston. This was done to prevent damage to the LVDTs, which were placed in the way of the piston at a level above the loading block. Combined, the 200 mm loading block and steel cylinder weighed 39 kg and exerted a pressure of 7.7 kPa at the surface of the soil. An annotated photo of the layout of the instruments and loading block is shown in Figure 3.5.

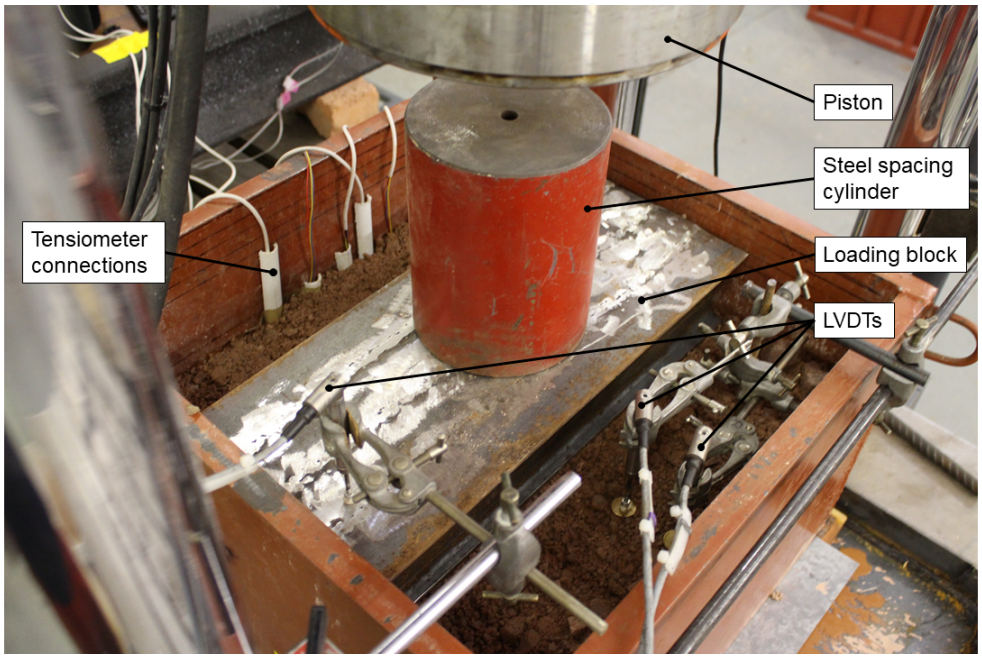

Figure 3.5: Layout of instrumentation and equipment for testing

3.1.5 Instrumentation

This section describes the installation and use of instrumentation in the experimental setup. Both deformation and suction measurement instrumentation and methods are discussed.

Linear Variable Differential Transformers

LVDTs were installed to measure deflection of representative portions of the formation. Figure 3.1 shows the placement of LVDTs A, B, and C along the centreline of the strongbox. LVDT A was installed to measure the deflection of the loading block as it deforms the formation, while LVDT B was placed to monitor the corresponding heave. LVDT C was placed 50 mm from the edge to monitor possible movement at the edge of the sample as a result of confinement effects. Confinement was expected to play a role in the stress state of the soil at the furthest edges of the sample. At these positions, stress would be applied by the wall of the strongbox on the adjacent soil and superimpose on the existing stresses, to create a zone of higher stress. This confining effect was as a result of having a large loading block in relation to the strongbox width. However, the loading block was sized to allow for higher forces to result in the correct 100 kPa surface stress.

Tensiometers

Tensiometers where built using sensors rated to a positive pressure of 700 kPa and ceramics with an air entry value of 300 kPa. Three types of tensiometers were built and used during the project. The initial design had the sensor, ceramic and soldering sealed in a protective casing of UV hardening glue, with only the face of the ceramic exposed. This design was found to perform adequately in tests with no surcharge load present, such as in a soil water retention test. However, once a surcharge load was applied, the measured values of pressure would fluctuate with the increased load and then return to normal. This was found to be a problem particularly under cyclic loading. Under cyclic loading these tensiometers fluctuated in response to imposed loads, with the loading frequency being too high to allow the tensiometers to return to their initial values during continuous loading. This fluctuation was found to be due to the flexible nature of the hardened UV glue. A force imposed on the tensiometer casing would result in a deflection of the casing and a corresponding change in the pressure in the water body inside the ceramic. Therefore, it was necessary to design an improved tensiometer that could measure the change in water pressure while remaining insensitive to the total stress imposed on it by the soil skeleton. For this purpose a new design was created whereby the tensiometer components (sensor, ceramic and cable) were placed inside a section of aluminium tubing and sealed inside with epoxy to provide insulation from water. Cross-sectional schematics of these tensiometers are presented in Figure 3.6, while Figure 3.7 shows the 2 designs side by side.

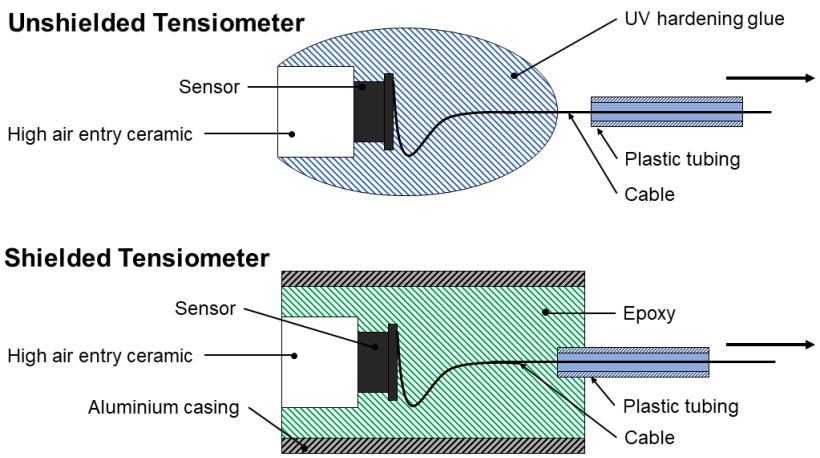

Figure 3.6: Cross-sectional schematic of unshielded and shielded tensiometers

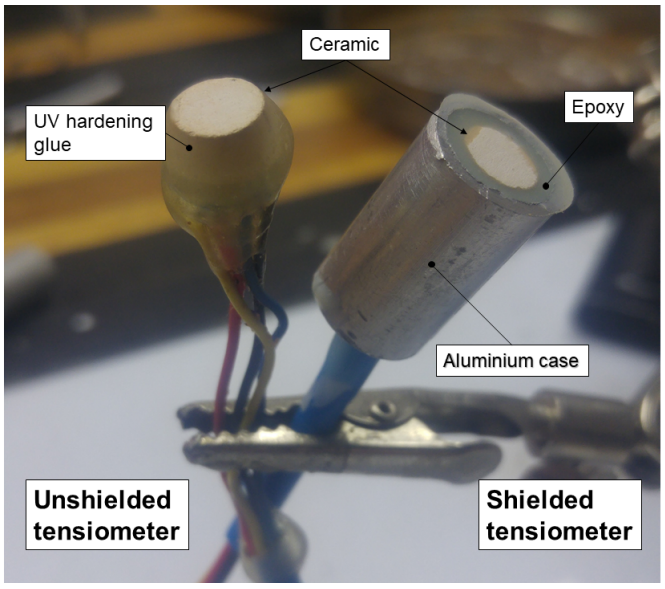

Figure 3.7: Side by side comparison of unshielded and shielded tensiometer designs

The aluminium casing tensiometer was found to dampen the effect of total stress, but not eliminate it. Further improvements were made and it was found that seating the shielded tensiometer inside a section of steel tubing with a layer of foam prevented any force applied to the steel casing affecting the tensiometer readings. A schematic of this design is shown in Figure 3.8.

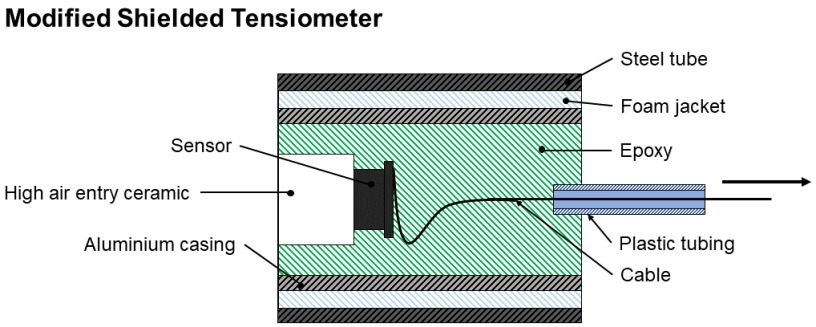

Figure 3.8: Cross-sectional schematic of modified shielded tensiometer

Three days prior to the testing day, the tensiometers were placed in a drying oven at 60 °C for a minimum of 4 hours to ensure that they do not have any entrapped water, which would compromise saturation. Two days prior to the testing day, tensiometers were saturated in a modified triaxial cell that could accommodate 6 tensiometers at a time (Figure 3.9). A vacuum was imposed on the trixial cell before de-aired water was intruduced. This vacuum was maintained until the ceramic faces of the tensiometers were submerged, upon which the vacuum was released. When the tensiometers were first introduced to de-aired water in the cell, there was a lag period before water started to enter the pores and cause a change in the sensor reading. Once this had happened, the sensor would register changes in cell pressure, albeit not necessarily with the correct magnitude and with a lagged response. This was due to the presence of air and water in the ceramic pores. To shorten the time required for saturation, the method recommended by Take and Bolton (2003) was applied, whereby a number of stepped load cycles were applied to force air out of the ceramic. Three full load cycles were applied during saturation, from 0 to 300 kPa in steps of 50 kPa. Once the tensiometer response had improved, the pressure was increased to 300 kPa and left as such for a minimum of 6 hours to complete saturation. After the saturation period was complete, the tensiometer readings were logged while the pressure was increased from 0 to 300 kPa in increments of 50 kPa to calibrate each tensiometer's unique response to pressure changes.

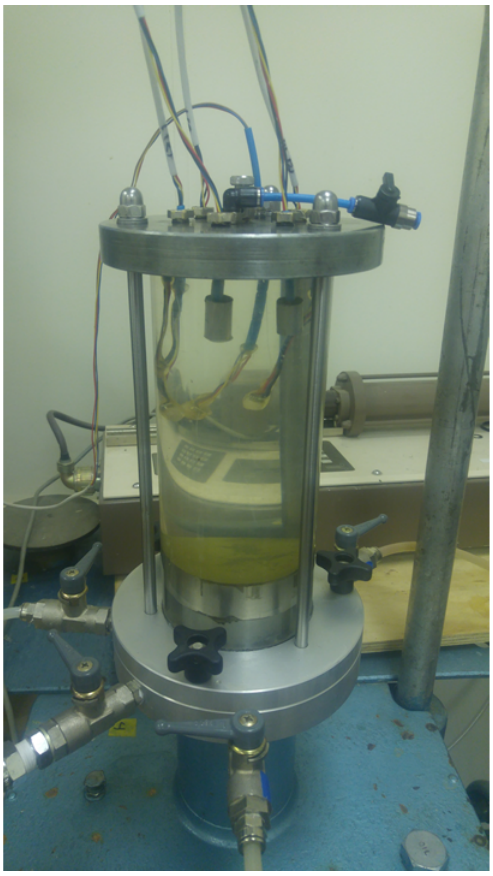

Figure 3.9: Tensiometer saturation cell during saturation

Tensiometers were kept overnight in vessels of de-aired water to retain their saturation. To install a tensiometer, a shallow hole was made in the formation at the required position by removing material. The tensiometer was then placed in the hole and was covered with the selected material. This selected material was composed of the <2 mm fraction of the formation soil. Once the selected material was placed in a small mound on the tensiometer, it was carefully compacted by hand to seat the tensiometer in the soil and protect it from pieces of aggregate in the natural material. The cable was protected by sections of cut PVC pipe to prevent aggregate severing the connection. Figure 3.10 provides an example of tensiometer installation.

Figure 3.10: Tensiometer installation with cable protection

3.2 TESTING SCHEDULE

A robust testing schedule was developed to test all relevant aspects of the soil. This testing schedule was kept consistent during all tests so that different samples would be directly comparable in terms of energy applied to the formation. Testing was divided into the following stages:

- Pre-test preparation phase
- Primary testing phase
- Post-test testing phase

Each stage of testing is described in the following subsections.

3.2.1 Pre-Test Preparation Phase

Preparation for a test began 2 days prior to the day of the test. This time was required to prepare both the soil and tensiometers for each test.

Each test required approximately 105 kg of material. Two days prior to the test, 120 kg of material was dried overnight at 105 °C. The following day the soil was sorted into 4 sealed containers, each containing the required amount of dry soil for 1 layer of the formation. These containers were then individually wetted to the correct moisture content and left overnight for the water to equilibrate throughout the sample.

Two days before the start of the test, the tensiometers had to be saturated. After being dried at 60 °C for a minimum of 4 hours. Once in the saturation cell, a normal saturation typically took 12 hours from setup to completion.

Once the model was set up, the formation was loaded monotonically to a vertical load of 10 kN for 10 minutes to ensure correct seating of the loading block and some further compaction of the formation.

3.2.2 Primary Testing Phase

During the primary testing phase, the loading frequencies were varied with rest periods in between, while the force was kept constant. The maximum force of 10 kN (approximately 100 kPa exerted by the loading block on soil) was specified based on pressure values found by Gräbe et al. (2005). These pressure values were recorded by pressure plates installed at different depths in a newly constructed railway formation during the passage of heavy haul trains. Values of vertical pressure were observed between 70 – 130 kPa between the depths of 200 – 600 mm (with higher pressures being associated with shallower depths) in trains comprised of Transnet Freight Rail CCR – 11 wagons. Using the range of possible pressures would have introduced an additional factor into the testing, and therefore 100 kPa was selected as a practical compromise to be applied to both the SB and AB formations. The loading was applied with a sinusoidal loading pattern, where one complete sinusoidal cycle was equivalent to the leading and trailing bogies respectively of two adjacent wagons (totalling 4 axles). Cyclic loading frequencies were therefore calculated based on the dimensions and likely speeds of the CCR – 11 wagons. Table 3.1 shows the different testing frequencies used and their corresponding line speeds.

Table 3.1: Testing frequencies and their associated line speeds

Frequency (Hz)	Equivalent speed (km/h)
0.25	10
1	42
2	84
10	420

The first 3 speeds in Table 3.1 are all speeds that could be encountered on the line under operational conditions. Conventional operating speed is 80 km/h whereas speeds of 10 and 40 km/h may be expected during times when speed restrictions are imposes on the line. The speed of 420 km/h (10 Hz loading) is unrealistic in the field. However it was included to allow the observation of any pore pressure or deformation reactions resulting from accelerated testing on soils. This was intended to show the change in soil suctions in response to loading rate. Table 3.2 shows the primary loading schedule.

Table 3.2: Primary loading schedule

Max. Practical Load (kN)	Frequency (Hz)	Cycles	Time (min)	Time (h)
10	0.25	2000	133	2.22
Rest	-	-	5	0.08
10	1	3000	50	0.83
Rest	-	-	5	0.08
10	2	3000	25	0.42
Rest	-	-	5	0.08
10	10	10000	17	0.28
Rest	-	-	5	0.08
Total			**245**	**4.07**

To ensure that different loading phases were comparable, a certain constant number of cycles (eg. 2000 cycles) could be compared on the basis of the same amount of energy being applied to the sample during this time. However, more cycles were allowed for in the higher loading frequency ranges

because it was found that the MTS machine required increasing cycles to establish a constant loading pattern at increasing frequencies. The machine was found to meet the required 10 kN load almost immediately at frequencies of 0.25 Hz and 1 Hz. However, the 2 Hz stage was found to reach stable cycling amplitude of 0 – 10 kN after 300 cycles. For the 10 Hz loading stage, 1300 cycles were required for the cyclic loading amplitude to reach a stable condition.

The 5 minute resting periods were inserted between each loading stage to allow pore pressures to normalise in the event of a systematic change in suctions as a result of continual cyclic loading.

3.2.3 Post-Test Testing Phase

Once the primary phase had been completed, it was important to quantify the moisture state of the formation. Approximately 250 g of material was removed at each of the 20 representative locations in the formation. These included the locations of the tensiometer as well as the spaces inbetween the tensiometer locations. The sampling locations are shown in Figure 3.11.

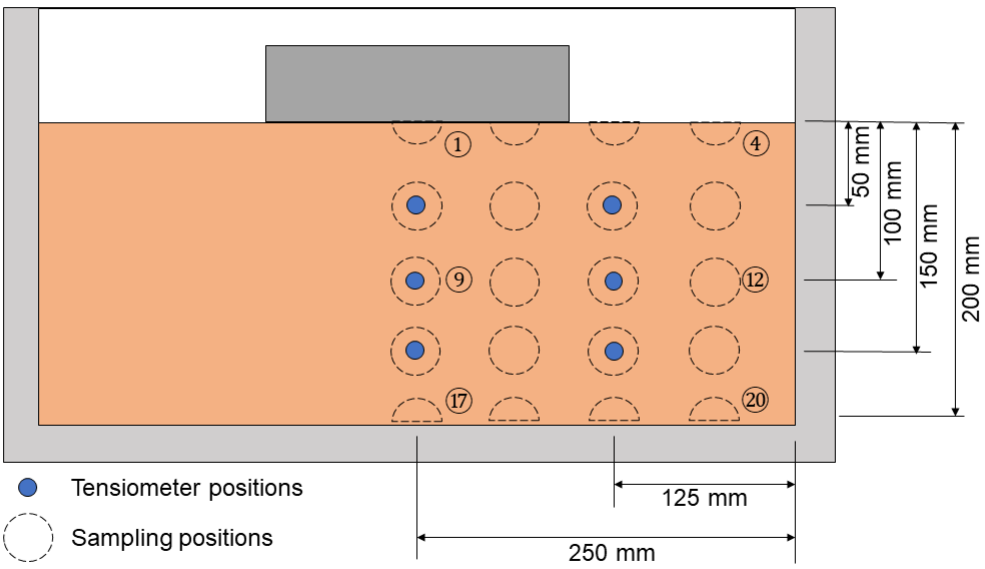

Figure 3.11: Moisture sample locations, numbered from left to right

These samples were dried out at 105 °C as in a conventional moisture content test. The results of the moisture content tests were then used in a contour plot to establish the moisture distribution in the sample after the test had been completed.

3.3 MATERIAL CHARACTERISATION

This section describes testing done in addition to the MTS testing. These tests were done to identify and solve problems, prove concepts and characterise the material used for testing.

3.3.1 Soil Parameters

To characterise the soils being used, approximately 100 kg of the subballast (SB) and subgrade (AB) materials were sent to a commercial geotechnical laboratory for testing. The SB material was designed to be stiff and free draining and therefore consisted of a high proportion of gravel and sand. The AB material was also granular, albeit with an increased proportion of fines when compared to the SB material. Laboratory testing consisted of the following tests:

- Foundation indicators
- Maximum dry density (MDD) & optimum moisture content (OMC)
- California bearing ratio (CBR)

Figure 3.12 presents the particle size distribution for both soils and Tables 3.3, 3.4 and 3.5 provide a summary of the laboratory results for both materials.

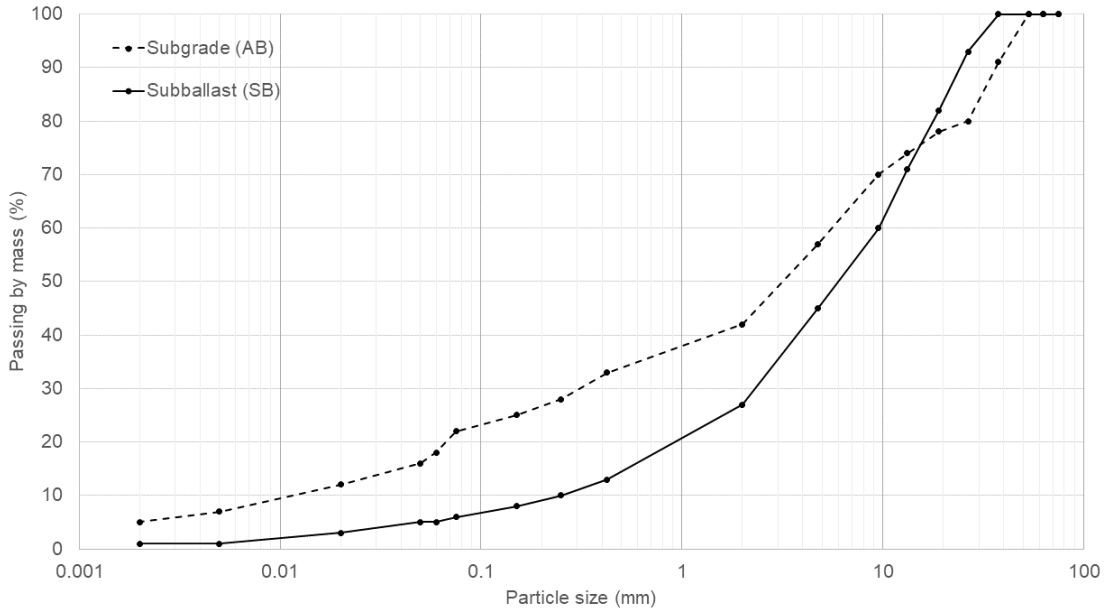

Figure 3.12: Particle size distribution for SB and AB materials

Table 3.3: Material Atterberg limits, maximum dry density (MDD) and optimum moisture content (OMC)

Property	**Material**	
	SB	**AB**
Atterberg limits		
Liquid limit (%)	NP	31
Plastic limit (%)	NP	21
Plasticity index (%)	NP	10
Weighted PI (%)	NP	3.3
Linear shrinkage (%)	0.0	5
Property	**Material**	
	SB	**AB**
MDD & OMC		
Maximum dry density (kg/m^3)	2136	2070
Optimum moisture content (%)	5.6	11.1

Table 3.4: Material grading parameters

Property	**Material**	
	SB	**AB**
Grading		
Gravel (%)	73	58
Sand (%)	22	24
Silt (%)	4	13
Clay (%)	1	5
TRB Classification	A -1 - a	A - 2 - 4
Unified Classification	GW - GM	GC

Table 3.5: Material CBR properties

Property	**Material**	
	SB	**AB**
CBR (Mod AASHTO)		
Swell (%)	0.0	0.0
90%	20	10
93%	30	15
95%	40	19
97%	50	24
98%	60	27
100%	80	33

Additionally, tests were performed at the University of Pretoria Civil laboratory to determine the specific gravity (G_s) of the soils. It was found that the subballast and subgrade had G_s values that equated to soil solid particle densities of 2736 kg/m^3 and 2660 kg/m^3 respectively.

3.3.2 Soil Water Retention Curve

To establish the expected range of suctions in the materials, as well as relationships between matric suction and moisture content, tests were done to determine the soil water retention curves (SWRCs) of both the SB and AB materials. This test was done in 2 stages. In the first stage, tensiometers were used to continuously measure the suction change as the moisture leaves the sample and the degree of saturation (S_r) decreases. Once the air entry suction of the ceramic was reached, cavitation would occur and the tensiometer would cease providing representative suction values. This drying test therefore provides an incomplete SWRC as the tensiometer is incapable of recording data of the suctions in the dry soil states. The second stage aims to complete this curve by using the filter paper method to measure data points in the dry range.

The soils were sieved to obtain the fraction smaller than 2 mm This soil was dried at 105 °C. Approximately 250 g of material were used for each test. Once the sample was compacted, the mass of the dry soil and bowl was measured as an initial condition. Water could then be added for saturation.

For the SWRC test, it was important that a soil dry from a saturated state to a drier state. To ensure that the soil was saturated in the initial condition, the G_s was obtained and used to calculate the volume of voids in the sample in a compacted state. A volume of de-aired water approximately 1.5 times that of the volume of voids was added to the sample. The bowl with sample and water were then covered and left in a cool place for 2 hours to ensure that the water penetrated into all the voids. The mass of the bowl, sample, and water was recorded to confirm how much water was added before drying.

Once the sample had been saturated, the tensiometers could be easily pressed into the middle of the soil layer. Once sufficient contact between the ceramic and soil was achieved, the tensiometer was covered with surrounding soil and placed on the laboratory scale. Figure 3.13 shows an example of a saturated compacted SB material with tensiometers. The scale and tensiometers were continuously logged at 20 Hz and 1 Hz respectively.

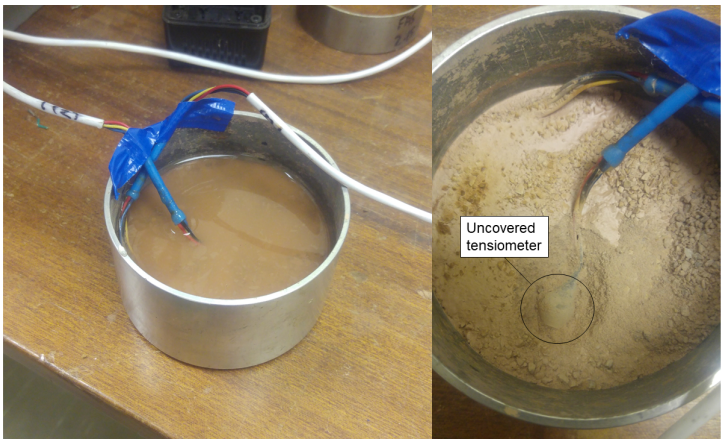

Figure 3.13: Saturated SB sample with tensiometers installed (left) and dried sample with tensiometers uncovered (right)

The test was given 48 hours to complete. It was assumed that the soil would dry enough in this time to cause cavitation in the tensiometer. Once the test was complete, the tensiometers were removed while making an effort to disturb as little soil as possible. The remaining soil mass was recorded and the sample was then left in a drying oven overnight to perform a moisture content test.

To complete the SWRC, Whatman #42 filter paper was used to measure the suction in the soil. For the filter paper test, the method described by ASTM (2003) was used as a guideline for sample preparation. Samples were made from the <2 mm fraction of the formation soil. To provide a complete range of suction data points to populate the SWRC, 8 samples were prepared at the same density in steel rings. These samples were then wetted to saturation and then allowed to dry under ambient conditions until certain degree of saturation goals were reached. Once a specified degree of saturation goal was reached, 2 filter papers were placed on the surface of the sample and the sample was sealed. The samples were sealed with a first layer of cling wrap, then a layer of aluminium foil and a final layer of cling wrap as recommended by Heymann and Clayton (1999).

The samples were left to equilibrate for 14 days before being measured for soil mass (wet and dry) and filter paper mass (wet and dry). The filter paper moisture content was related to matric suction using the calibration graph presented by Hamblin (1981). A reproduction of this graph is shown in Figure 3.14.

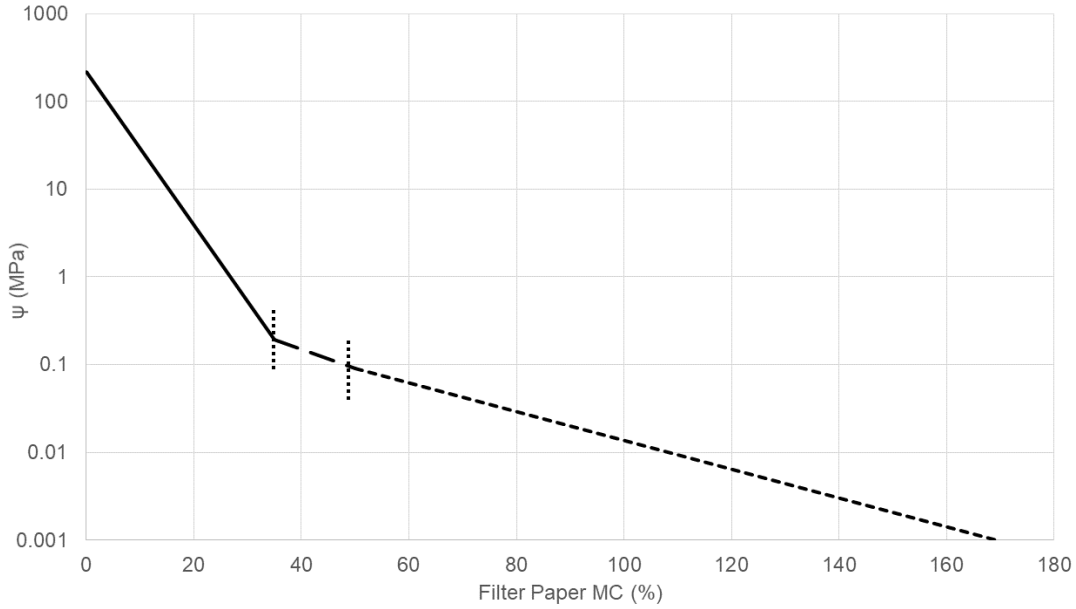

Figure 3.14: Piecewise filter paper calibration graph adapted from Hamblin (1981)

The wetting curve of the SWRC was determined in a similar manner to the drying curve, although an initial dry condition was required. The 8 samples were therefore dried out at 105 °C. Once they were completely dry, the samples were wetted to the correct water content and sealed with 2 filter papers in the ring. It was important that both wetting and drying curves were established, as these curves define the envelope of possible suction-moisture relationships. It is unlikely that suction values found in testing would occur on either of these curves, but rather on a scanning curve falling between the primary wetting and primary drying curve.

It is useful to present SWRCs in terms of the gravimetric moisture content (MC) and degree of saturation (S_r). Figure 3.15(a) and 3.15(b) presents the SWRC of the AB and SB materials respectively as fitted to the data by the Fredlund and Xing method (Fredlund and Xing, 1994).

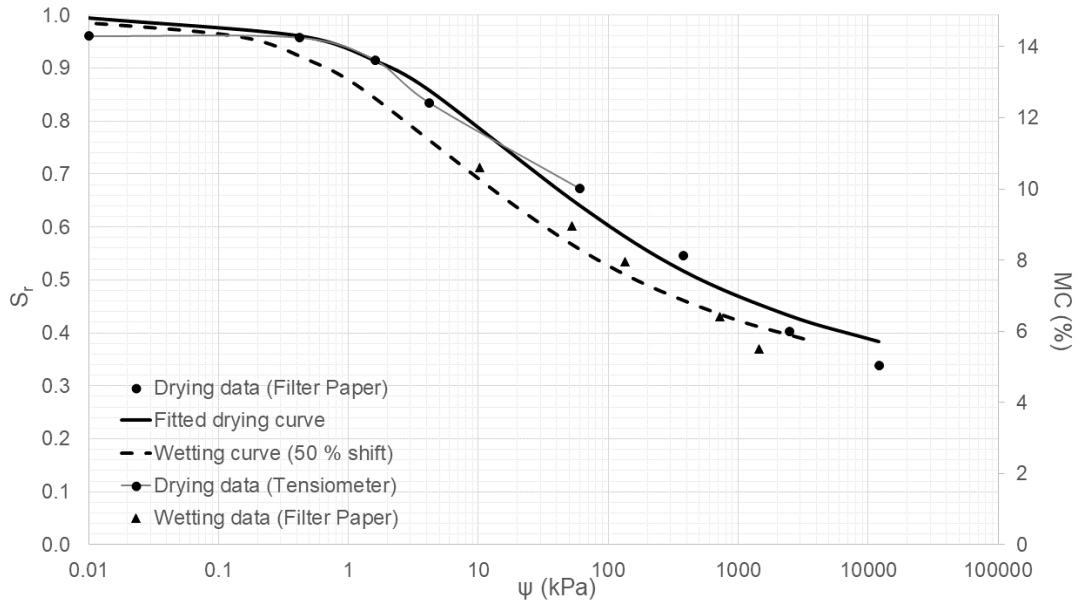

(a)

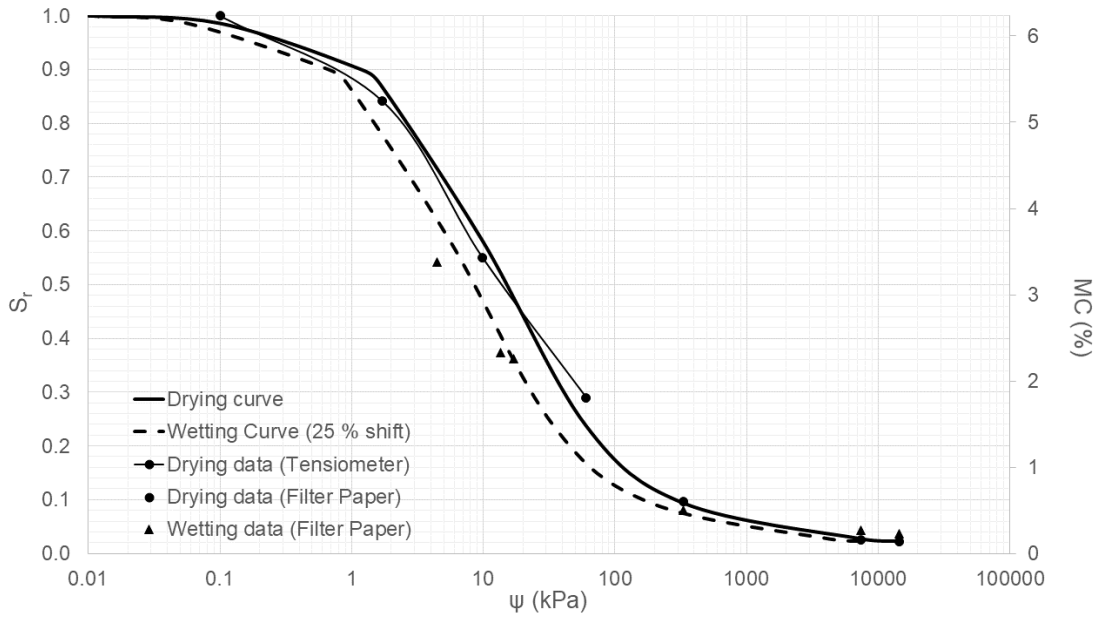

(b)

Figure 3.15: SWRCs of **(a)** subgrade (AB) and **(b)** subballast (SB) materials in terms of S_r and MC

While the drying curves in Figures 3.15(a) and 3.15(b) were determined with the Fredlund and Xing method based on tensiometer and filter paper data, only filter paper data was used to plot the low moisture content part of the wetting curve. The method of shifting the drying curve by a defined

percentage of a log cycle to approximate the wetting curve (Fredlund et al., 2011) was then applied to match the filter paper data of the wetting curve and thereby complete the wetting curve. The required percentage shift was determined by calculating the lateral distance between wetting and drying curve points, and comparing the resultant log shift with an expected percentage shift for different soil types as found in Fredlund et al. (2011). Shift values of 50 % for the AB material and 25 % for the SB material were found to be in agreement with the data points and the values in literature.

3.4 TENSIOMETER DEVELOPMENT

As described earlier, tensiometers constructed with UV hardening glue were found to be affected by the total stress imposed by the soil sample on the tensiometer casing. To mitigate this effect and ensure a tensiometer response which is representative of the matric suction in the soil, it was necessary to evaluate the cause and effect in response to loading on the tensiometer casings. This cause and effect testing would allow total stress responses of the tensiometer to be separated from matric suction stress changes. Shielded and modified-shielded tensiometers were constructed in an attempt to eliminate the total stress effect. Once built, it was necessary to test these shielded models to ensure that only the change in pore water pressure was being measured.

A simple test was planned whereby the tensiometers were tested inside a large bowl of water. The pore water pressure in this bowl remains constant. The test works on the premise of a null type test where no observed change in the measured pore water pressure should be observed if the total stress response has been nullified. G-clamps were used to exert a force on the tensiometer so that the response could be observed.

G-clamps were seated on the casing of the tensiometer being tested, and then tightened by rotating the clamp through 30° (Figure 3.16). The tensiometer response was logged throughout the clamp tightening. A response in tensiometers was indicative of total stress dependency.

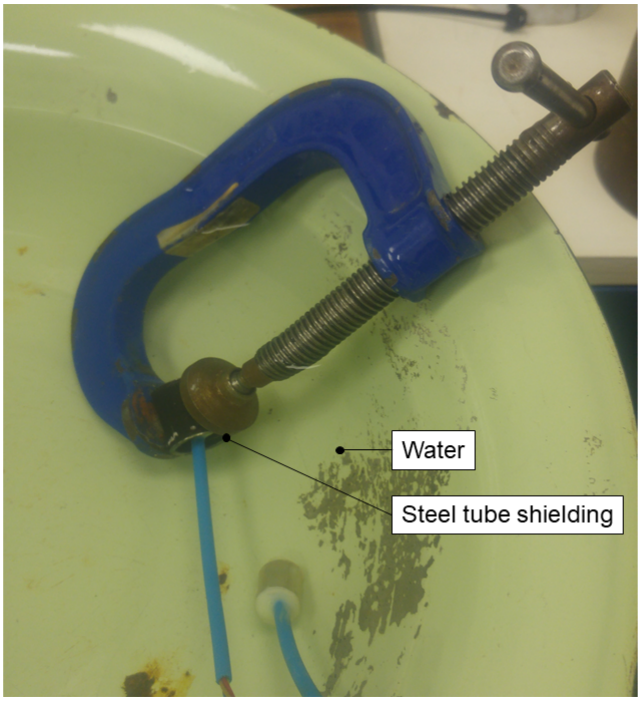

Figure 3.16: Total stress dependency test on tensiometers

In testing the unshielded tensiometers, it was found that applying and maintaining a constant force on the casing would result in a large positive spike, followed by a muted negative spike, before the reading would once again stabilise at the same value before load application. This total stress response would not be of concern in a static loading scenario, as a constant surcharge load can be applied to drive a change in pore pressures and the unshielded tensiometer reading will quickly stabilise to the pre-load reading, thereby continuing to measure pore pressure change until another change in loading condition. However, in dynamic conditions, the constant application and removal of loads does not allow the tensiometer time to return to the pre-load reading before the load is removed and then applied again. This would not allow one to distinguish between a total stress response and a pore water pressure response.

The shielded tensiometers showed a dampened response to the application of a load to the casing. While a muted response was considered an improvement, the ultimate goal was to have no load effect on the readings. This was achieved by the modified shielded tensiometers. When subjected to the same loading conditions as the unshielded and the shielded tensiometers, the modified shielded tensiometers did not show any response. Table 3.6 presents the average responses of different tensiometer models

calibrated to the resistance reading. A higher average response indicates that that tensiometer model would have proportionally larger noise under test conditions given the same loading.

Table 3.6: Average response of tensiometer models to loading on the casing

Tensiometer model	Average response (kPa)
Unshielded	447
Shielded	56
Modified shielded	<1

The shielded and modified shielded tensiometers also proved to be more resilient to repeated tests and drying/saturation cycles. A typical unshielded tensiometer was found to produce acceptable results for the first 2 – 3 drying/saturation cycles before reduced performance was observed. In contrast, the shielded and modified shielded tensiometers were found to perform satisfactorily for at least 4 – 5 drying/saturation cycles, and would not crack in high load conditions, extending their life further.

Finally, it was useful to establish the noise in tensiometer readings under ambient conditions. In conjunction with the previously mentioned tensiometer behaviour, quantifying the instrument noise provided a better framework for interpreting the data. Noise was measured by submerging tensiometers in de-aired water and recording the small-scale fluctuation of pressures while the tensiometer remains undisturbed. Table 3.7 provides an overview of average noise levels for each tensiometer. Noise falls within the range of 0.20 – 0.35 kPa.

Table 3.7: Average noise in tensiometers

Tensiometer	Mean noise amplitude (kPa)
1	0.214
2	0.240
3	0.210
4	0.220
5	0.323
6	0.292

3.5 DATA PROCESSING

This section describes the processes used to extract workable data from the raw data as recorded by the instruments. Both deformation and tensiometer data were processed using Matlab R2017a software, allowing raw data with thousands of data points to be manipulated as required. Examples of raw data and processed data are included in this section to explain methodology and present outcomes.

3.5.1 Deformation Data Processing

Deformation data was collected from 4 LVDTs placed at points in the strongbox as shown in Figure 3.1. LVDT A was used to monitor deformation of the material beneath the loading block, LVDTs B and C were used to measure the heave or sag behaviour of the material beside the loading block, and LVDT D was placed on the strongbox itself to monitor any vertical strongbox movement. Table 3.8 presents the sampling frequencies used to capture LVDT data. A minimum of 15 points per cycle were used so that the shape of the entire cycle could be captured.

Table 3.8: LVDT sampling frequency by test stage

Test stage	Loading frequency (Hz)	Sampling frequency (Hz)
1	0.25	10
2	1	20
3	2	50
4	10	150

The raw LVDT data from LVDTs A, B and C required correction for strongbox movement during loading. To achieve this, the deformation values from LVDT D (positioned on the strongbox) were subtracted from LVDTs A, B and C (positioned at various points on the formation) to yield only formation displacement. Figure 3.17a presents an example of uncorrected LVDT data and Figure 3.17b presents an example of corrected LVDT data to demonstrate the process used in isolating formation deformation.

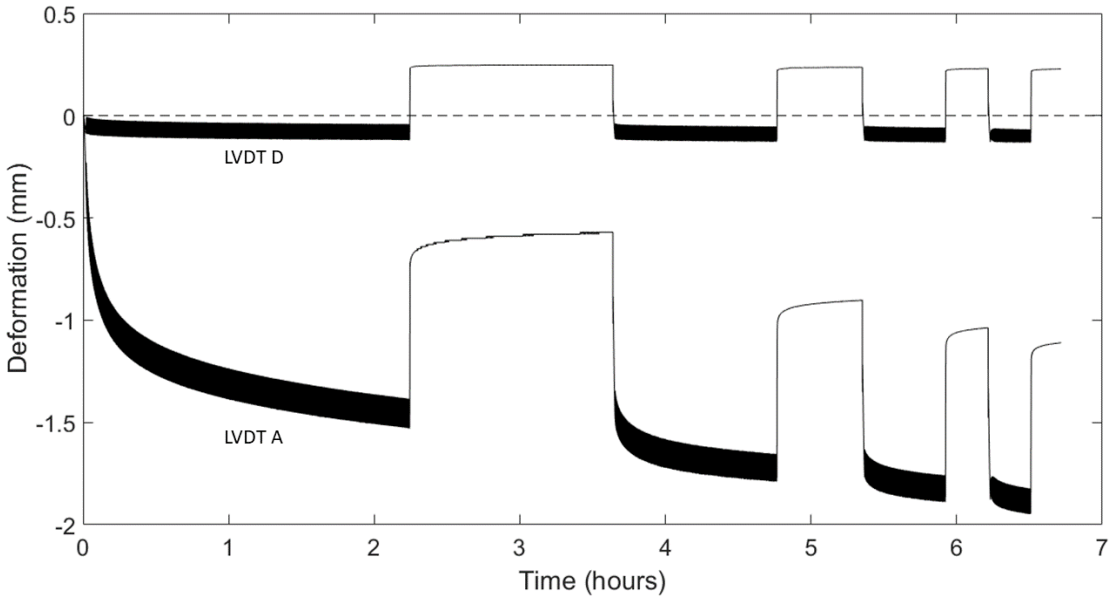

(a) Subgrade (AB) 9 % MC LVDT A and LVDT D deformation data

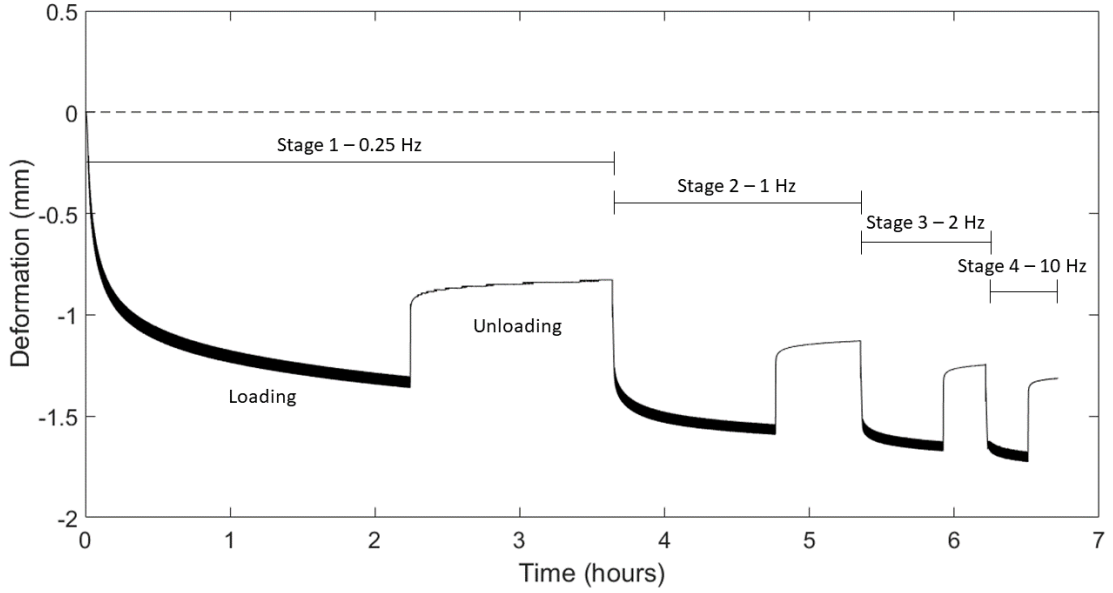

(b) Subgrade (AB) 9 % MC LVDT A corrected with LVDT D deformation data

Figure 3.17: Deformation data processing example

For the purposes of analysis, data points were sampled from each stage of testing from representative points on the deformation curve. Figure 3.18 shows these points on an example curve.

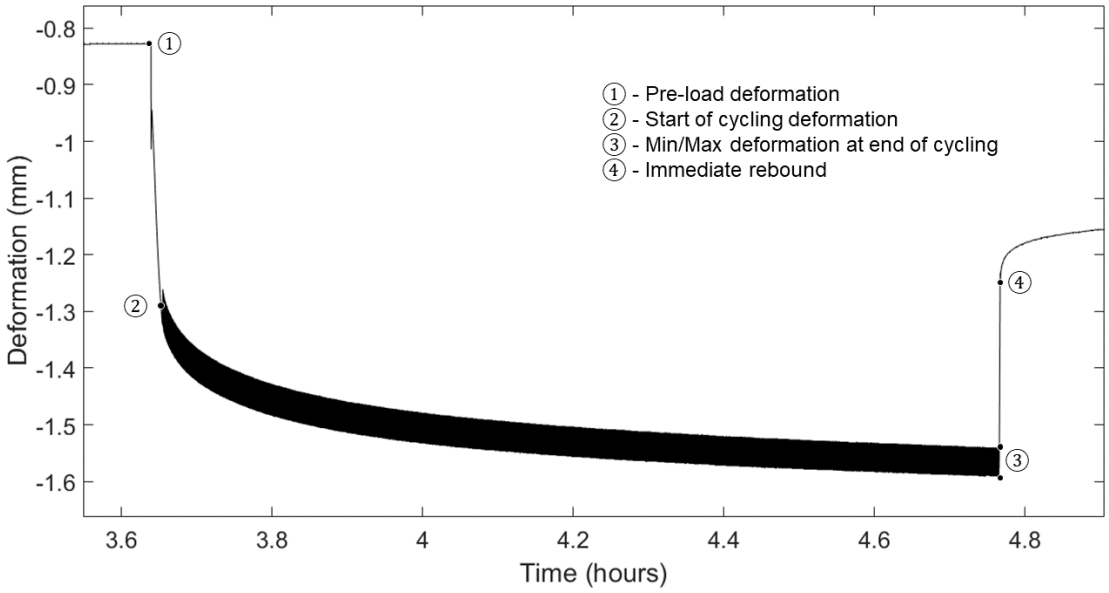

Figure 3.18: Representative points taken from deformation measurements

3.5.2 Tensiometer Data Processing

Tensiometer data was recorded for each stage of each test at a variety of different frequencies depending on the cyclic loading rate. Table 3.9 presents the data sampling frequencies for each stage of testing. The data sampling rate was always recorded a minimum of 10 times greater than the the loading frequency.

Table 3.9: Tensiometer sampling frequency by test stage

Test stage	Loading frequency (Hz)	Sampling frequency (Hz)
1	0.25	5
2	1	10
3	2	20
4	10	100
Overnight	-	1

To effectively process the mass of data, it was necessary to write an algorithm to obtain workable data. Tensiometer data was simplified by creating an envelope of measured data. This data envelope

reduced the data to a 'High' boundary and a 'Low' boundary, containing maximum and minimum values obtained during cycling. A Hampel function (Matlab, 2017) was used to identify unexpected peaks in data, and then remove them. Finally, a Savitsky-Golay filter (Matlab, 2017) was used to smooth the data. Figure 3.19 shows an example of a typical envelope plotted over raw data after being processed with a Hampel function and a Savitsky-Golay filter to remove outliers and smooth data. Data points were sampled at the beginning and end of each testing stage so that the filtered data could be charted against other test data at representative times and MCs.

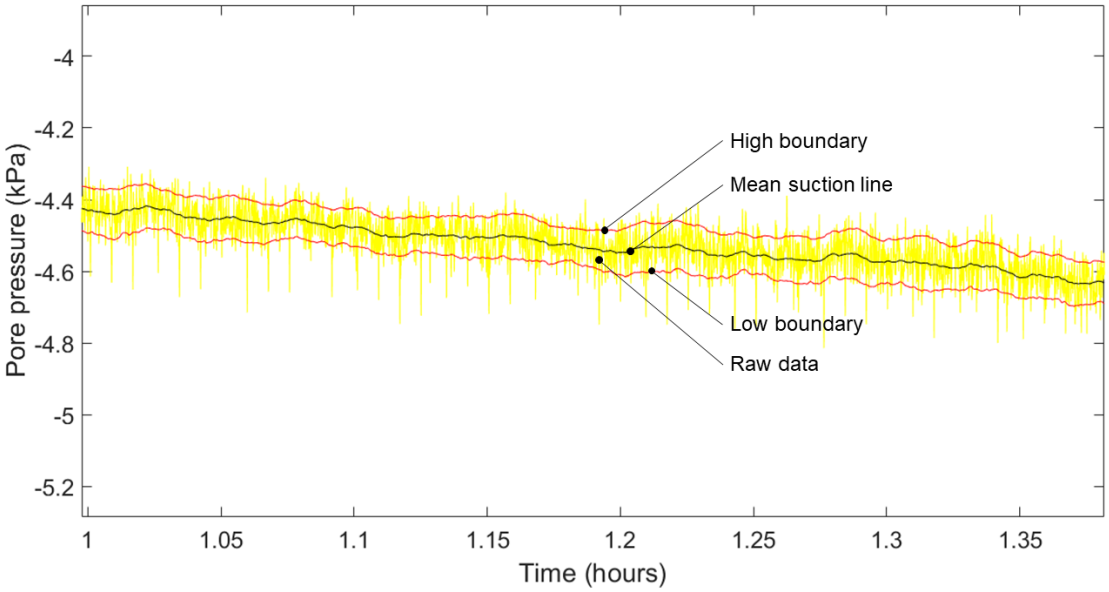

Figure 3.19: Detail of data envelope for raw tensiometer data

Once determined from the algorithm, the mean suction curves were used as the primary source of suction values. From these mean suction lines, points were sampled at the start and end of each loading stage for analysis. Figure 3.20 presents an example of a mean suction line from Position 4 in the AB 9 % MC material.

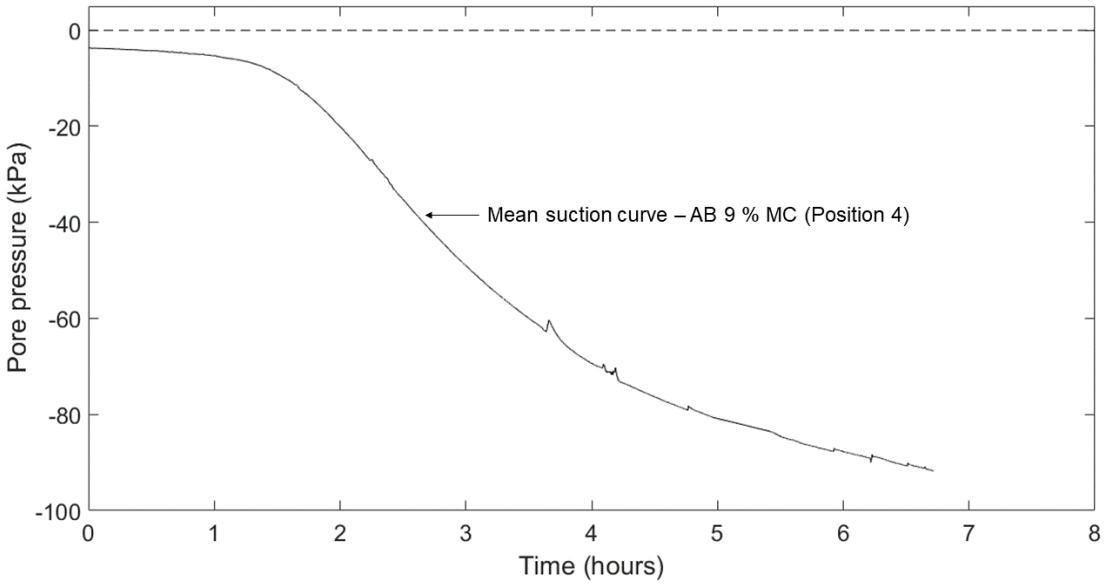

Figure 3.20: Tensiometer mean suction line example

3.6 SUMMARY

This section presented the details of the testing methodology, as well as the assumptions and theoretical considerations which informed that methodology. A 500 x 500 x 350 mm strongbox was decided upon to allow construction of a 200 mm formation to allow modelling of deformations without the need for scaling the depth of material. The loading block inside the strongbox was sized to provide a 100 kPa surface pressure on the material, at a loading of 10 kN. Initial testing found that the MTS machine did not function reliably at high frequencies and low loads. Due to this it was considered more important to have a larger loading block footprint to ensure reliable operation of the machine at the required surface pressure. This is in contrast to using a lower load on a smaller loading block which would minimise the effect of confinement. The eventual width of the loading block (200 mm) was decided on as it allowed a comfortable operating force for the machine (10 kN), while simultaneously allowing space beside the loading block for LVDT instrumentation. Tensiometers were distributed evenly throughout the depth of the soil to permit measurement of the suctions at various locations throughout the formation. This would allow the difference in suction responses as a function of location to be analysed.

Standard laboratory tests were conducted to establish a range of material parameters. Soil parameters such as OMC and MDD were required in planning densities, masses, and moisture states of the final

formations used in testing. In terms of soil behaviour: material grading, fines content, moisture state and SWRCs were identified in literature as crucial to understanding the deformation and suction behaviour of the materials. In addition to the material parameters, testing parameters such as loading magnitude, loading frequency were also identified as having an effect on deformation and suction behaviour of the material.

Initial testing of the tensiometers in the materials showed clear evidence of total stress interference in the tensiometer readings. Development was therefore started on a new tensiometer model that would eliminate the total stress interference on tensiometer readings. A new tensiometer model named the 'Modified Shielded Tensiometer' was developed. This model consisted of a foam sleeve wedged between the rigid tensiometer casing and a rigid steel cylinder that eliminated interference in the tensiometer.

However, these results were to be supplemented by discrete suction measurements as provided by the filter paper method. Literature provided evidence of differences in measured suctions between tensiometers and the filter paper method. Therefore, it was decided to compare these two commonly used methods in their applicability to railway formation suction measurement.

The data processing algorithm was described as a method to extract workable data out of the large dataset comprising both suction and deformation measurements. The majority of the tensiometer showed some cyclic behaviour while undergoing cyclic loading. It was not possible to separate possible small-scale pore pressure cyclic fluctuation from possible small-scale total stress interference given the limitations of the tensiometers. Therefore tensiometer data was processed to find the mean suction line that occurred between the high and low boundaries of the raw data. Deformation data was corrected by subtracting the deflection of the strongbox from the total deformation measured. This allowed the deformation of the material to be isolated.

The experimental procedure was therefore planned as a robust means of testing deformation and suction response in the material under differing moisture and loading conditions that may be encountered in an unsaturated railway formation. An emphasis was placed on providing ways to compare methods MC, suction and deformation measurements to verify their magnitudes and effects on the soil.

CHAPTER 4 ANALYSIS

This chapter presents the interpretation of the experimental results. Attention is given both to the deformation behaviour of the soils, as well as to the soil suctions and tensiometer performance. This will allow suction results from the strongbox tests to be contextualised. Data is presented to evaluate the effect of material type, loading frequency and moisture state on the pore pressure behaviour and the associated performance of the formation material. To directly compare the behaviour of the subgrade (AB) and suballast (SB), one aspect of material behaviour will be discussed in each subsection, allowing the differences between the materials to be made clear.

In sections of the analysis, the impact of soil suctions on formation strength are discussed. Formation strength was not explicitly dealt with in this study as a numerical value. Rather, the deformation and deformability of the formation materials in the box test were seen as indicative of the general trends of strength gain and loss as a function of the soil suctions that may be present in a railway formation.

For the sake of brevity, the different formation tests are referred to by their material type and their gravimetric moisture content (MC), e.g. AB 9 % MC denotes the subgrade material with a moisture content of 9 %. All results discussed were recorded during the primary testing stage, unless otherwise stated. This means that data were recorded while the formation was cyclically loaded between 0 and 10 kN at a pre-determined loading frequency. Loading frequencies were referred to by their chronological stages in the test where applicable (Stage 1 = 0.25 Hz, Stage 2 = 1 Hz, Stage 3 = 2 Hz, Stage 4 = 10 Hz). Table 4.1 and Table 4.2 present the different physical formation models tested, as well as the schedule of testing.

Table 4.1: Summary of tests

Tests					
Material	Moisture content (%)	Key	Material	Moisture content (%)	Key
Subgrade (AB)	9	AB 9 % MC	Subballast (SB)	2	SB 2 % MC
	11	AB 11 % MC		4	SB 4 % MC
	13	AB 13 % MC		6	SB 6 % MC

Table 4.2: Summary of testing procedure for each test

For each test:					
Testing phase	Stage	Frequency (Hz)	Cycles	Time (min)	Time (h)
Primary	Stage 1	0.25	2000	133	2.22
		Rest period		5	0.08
	Stage 2	1	3000	50	0.83
		Rest period		5	0.08
	Stage 3	2	3000	25	0.42
		Rest period		5	0.08
	Stage 4	10	10000	17	0.28
		Rest period		5	0.08

4.1 DEFORMATION BEHAVIOUR

This section discusses the permanent deformation characteristics of the tested materials. Aspects of deformation behaviour such as total deformation, rate of deformation and side heave/settlement behaviour are analysed for both AB and SB materials concurrently. The analysis focuses on interpreting deformation behaviour as a function of different materials, frequencies and MCs.

4.1.1 Material Deformation Overview

The deformation data of material AB at different MCs are presented in Figure 4.1. Two figures are presented, Figure 4.1(a) presents the deformation as a function of the time the material was loaded, while Figure 4.1(b) presents the deformation as a function of loading cycles. The Li and Selig (1998) method of granular layer thickness determination states that formation failure has occurred once permanent deflection has exceeded 2 % strain. In a 200 mm deep formation, a permanent deformation of 4 mm corresponds to 2 % strain. In the AB 13 % MC material this limit was exceeded during the Stage 1 loading at 0.25 Hz. Both the AB 9 % MC and AB 11 % MC materials did not exceed this failure criterion.

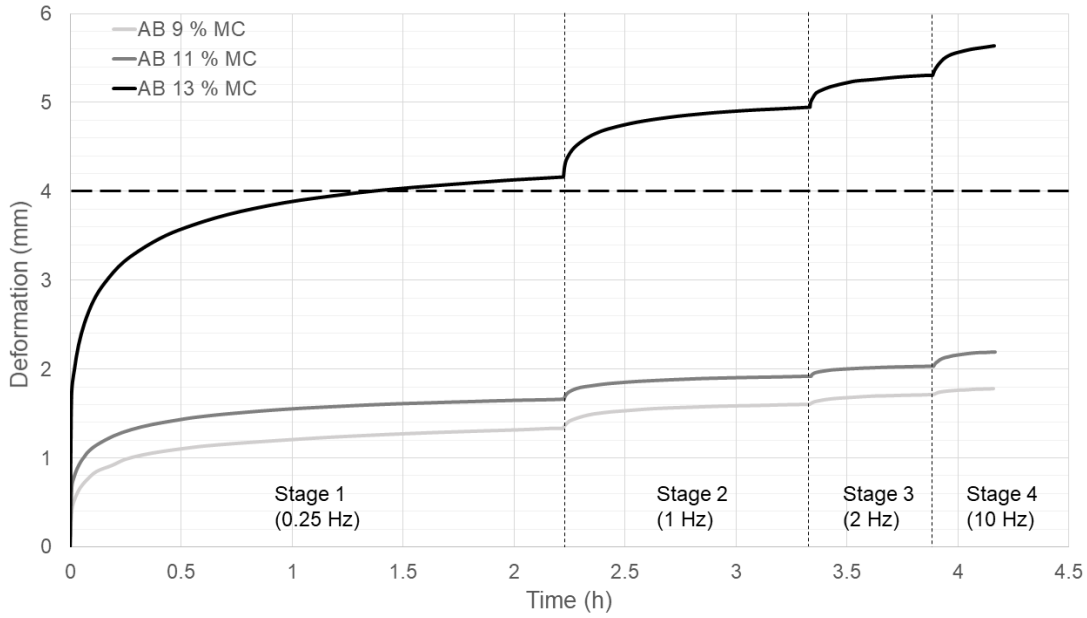

(a)

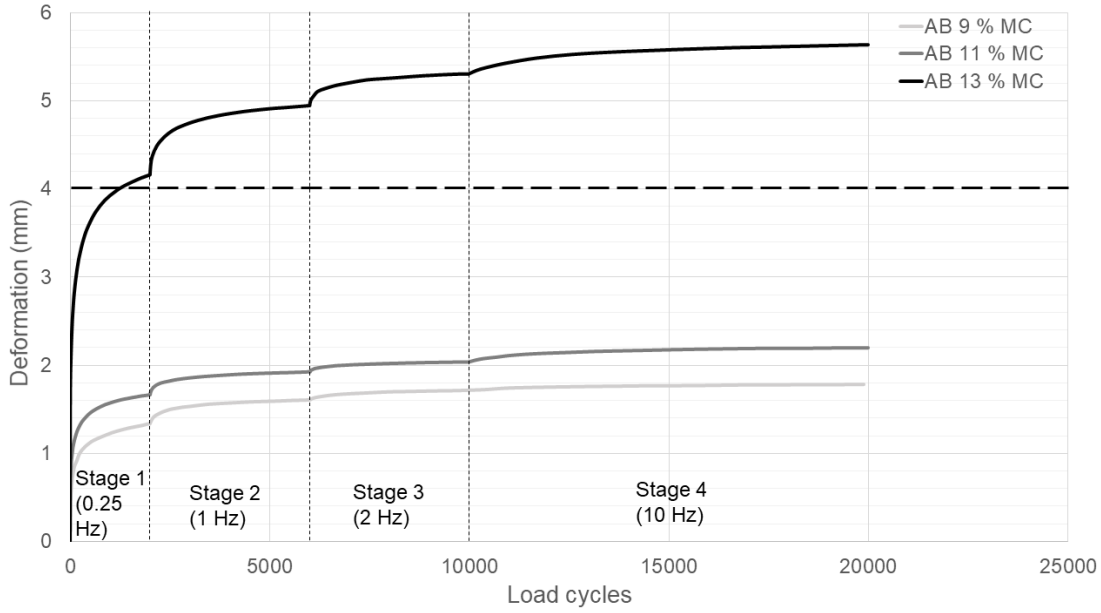

(b)

Figure 4.1: Subgrade (AB) material deformation during testing

It is clear from Figure 4.1 that increasing MC was associated with an increase in deformation throughout all phases of the test. However, the increase in deformation between the AB 11 % MC formation and the AB 13 % MC material was far greater than the increase in deformation between the AB 9 % MC

material and AB 11 % MC material. Deformation behaviour in the AB material is therefore non-linear in relation to the MC. This is in agreement with findings from Vorster (2016), where it was found that an increase in MC caused an incremental increase in the deformation, until a certain MC was exceeded. Large deformations will occur past this critical moisture condition given the same material and loading conditions. The difference in incremental deformation response is summarised in Figure 4.2.

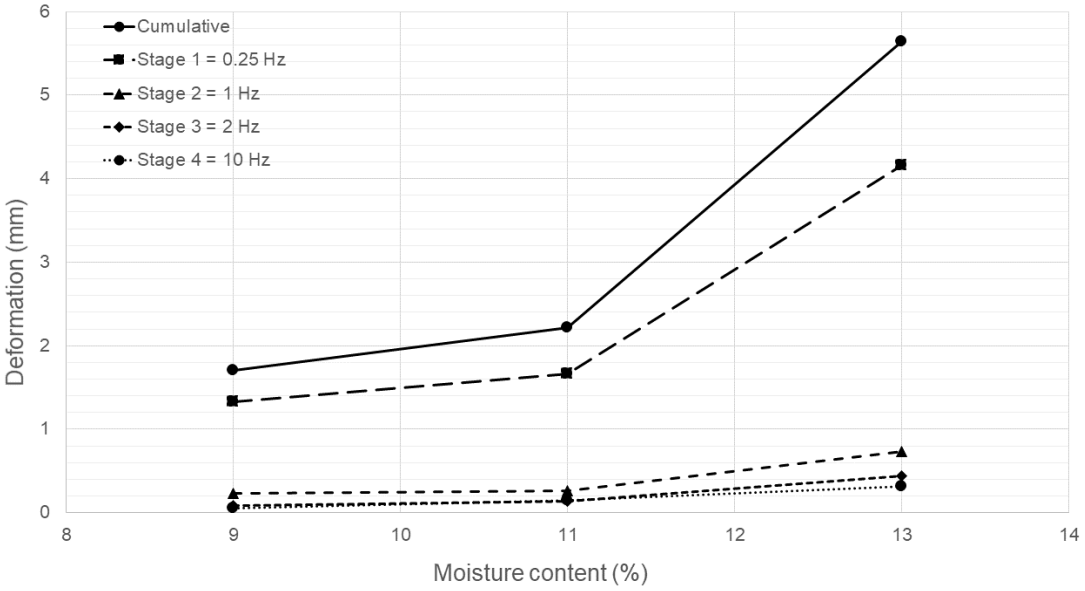

Figure 4.2: Permanent deformation of subgrade (AB) material as a function of moisture content (MC) for the different testing stages

Figure 4.3 presents the permanent deformation of the SB material, as well as the Li and Selig (1998) failure criterion of 4 mm. Firstly, it is notable that the deformation does not exceed 3 mm, and therefore is not considered to have failed. This was expected, as the SB material is designed to be stronger than the underlying AB material layer in order to dissipate loads from trains to the weaker underlying layers. Secondly, the SB material also shows a higher deformation at higher MCs. However, the difference in deformation as a result of an increase in MC is less than the more pronounced difference in the permanent deformation of material AB as a result of an increase in MC, as shown in Figure 4.1.

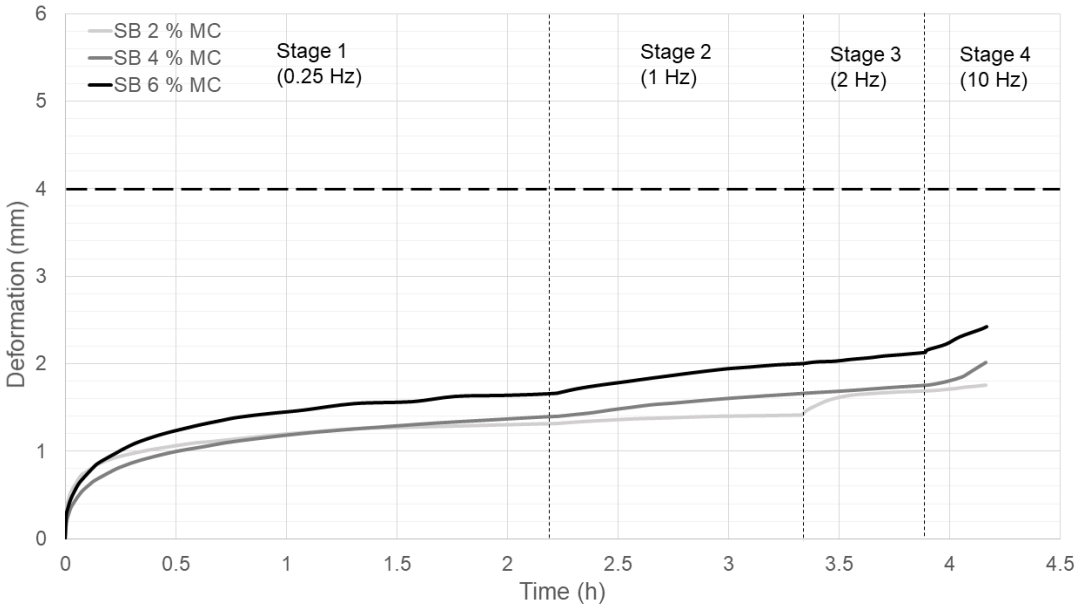

(a)

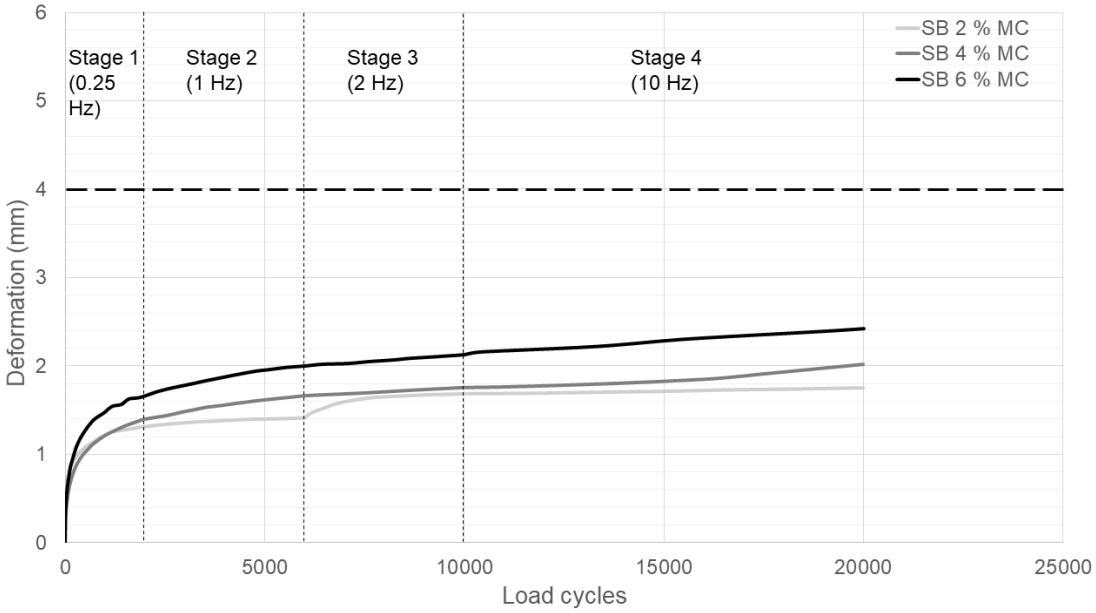

(b)

Figure 4.3: Subballast (SB) material deformation during testing

Figure 4.4 demonstrates that the increase in deformation with increased MC was approximately linear in the SB material. As with the AB material, Stage 1 was responsible for the majority of the deformation across all tested values of MC.

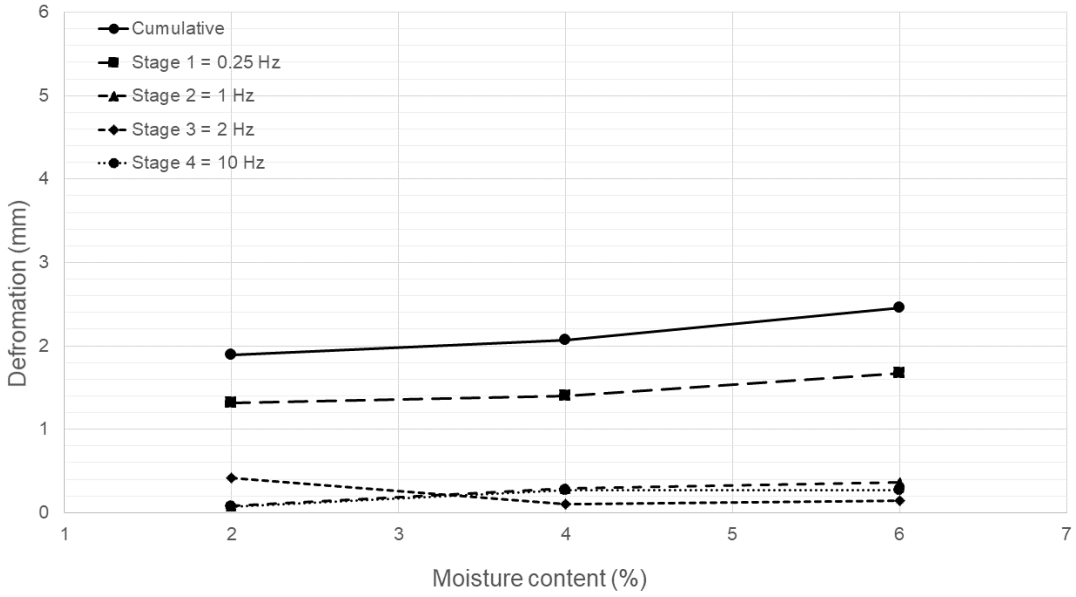

Figure 4.4: Permanent deformation of subballast (SB) material as a function of moisture content (MC) for the different testing stages

The overview of deformations in the AB and SB materials presented in this section revealed that the effect of MC change on deformation was fundamentally different for both materials. The presence of significant fines in the AB material caused a non-linear increase in deformation with increase in MC (Figure 4.2). In comparison, the change in deformation with MC is approximately linear for the SB material (Figure 4.4). The implication of this is twofold. Firstly, it is important that AB materials are protected against moisture changes by providing working fin drains and a free-draining SB layer constructed above the AB layer. These steps prevent an accumulation of moisture that could lead to wetting collapse. Secondly, the SB material is only differentiated from the AB material by its relative lack of fines. Should the SB material accumulate clayey and silty fines from material breakage and contamination from outside sources, the SB material could also experience larger deformations.

The cumulative deformation of the AB and SB materials as presented in Figures 4.2 and 4.4 are summarised in Figure 4.5 as total deformations of the respective materials. It was important to compare the change in deformations in the 2 materials as a function of MC change. The MC values are therefore normalised by converting the MC values into values of degree of saturation (S_r). This normalisation allowed both the AB and SB deformations to be directly comparable on the same axis.

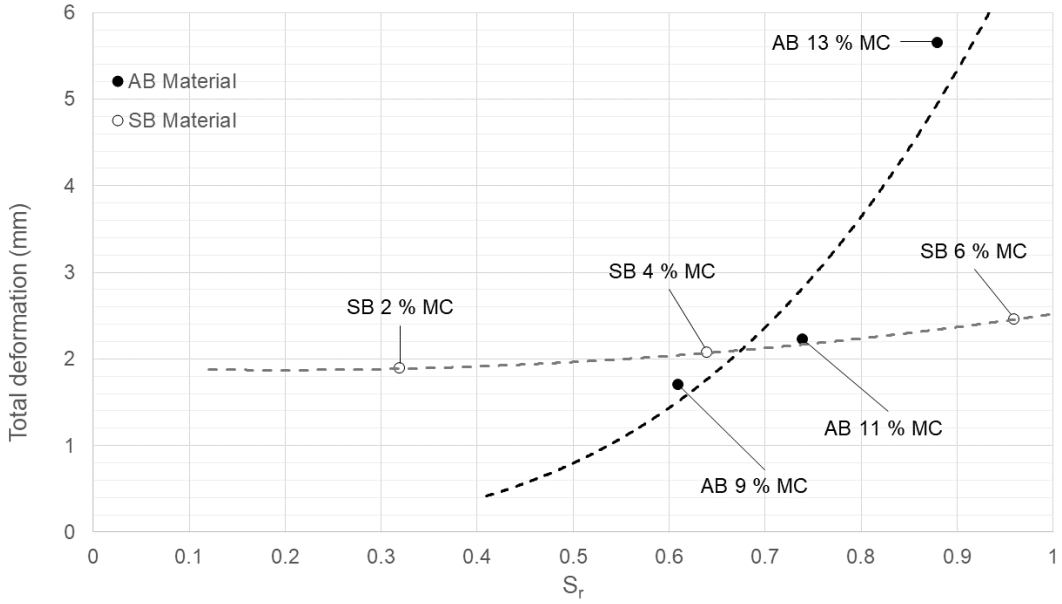

Figure 4.5: Comparison of total deformation of the subgrade (AB) and subballast (SB) materials against degree of saturation (S_r)

Figure 4.5 clearly illustrates the difference in deformation potential between the AB and SB materials as a result of changing moisture states. This difference in deformation is caused by the strengthening effect of significant suctions present in the AB material at 9 and 11 % MC.

4.1.2 Material Failure Mode

Analysis of heave and settlement behaviour beside the loading block provides information on the type of deformation a material undergoes, as the deformation beside the loading block gives an indication of the manner in which material was displaced. Heave/settlement behaviour was monitored by LVDTs B and C as shown in Figure 3.1. To remain consistent with the deformation convention used for LVDT A, settlement is taken as positive while heave is taken as negative.

The deformation of the formation next to the loading block at the location of LVDT B showed that for all values of MC the AB material settles with loading, for all frequencies tested. Figure 4.6 presents the settlement/heave behaviour of the AB material in terms of permanent deformation in each stage. Material AB 9 % MC showed the greatest settlement in Stage 1, with a maximum of 0.09 mm

settlement. In subsequent stages this magnitude of settlement decreased to values comparable to those of the AB 11 % MC and AB 13 % MC materials. The settlement behaviour of materials AB 11 % MC and AB 13 % MC were present, but negligible (0.01 – 0.04 mm).

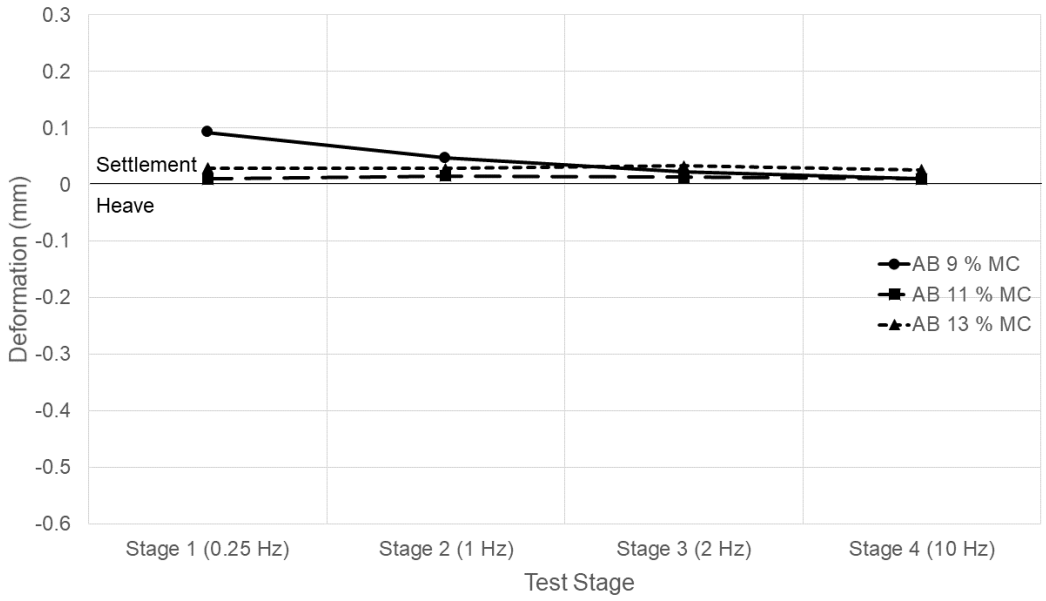

Figure 4.6: Subgrade (AB) material deformation 50 mm from loading block (LVDT Position B)

The heave and settlement behaviour of the SB material was more complicated than the AB material. The behaviour appeared to be a mix of heave and settlement of various magnitudes as shown in Figure 4.7. The consistent patterns across all the SB materials was that the highest heave deformation occurred in Stage 1 at low frequency, and then decreased in the later stages. In both materials tested (AB and SB), Stage 1 was shown to induce the highest proportion of permanent deformation under the loading block as shown by Figure 4.2 for the AB material and Figure 4.4 for the SB material. It therefore stands to reason that the period of greatest heave or settlement would also be in Stage 1 due to the large deformations occurring in the adjacent soil material. In that regard the SB material behaves as would be expected.. Notably, the SB 2 % MC material showed the most heave in Stage 1, whilst the SB 6 % MC material showed the least, despite the SB 6 % MC material experiencing more permanent deformation than the SB 2 % MC material. From Stages 2 – 4 this behaviour was reversed, with the SB 2 % MC settlement the most, and material SB 6 % MC settlement the least. This consistent pattern showed that the SB 2 % MC material was most influenced by deformation changes in adjacent soil. Furthermore, it showed that there was a consistent pattern of heaving behaviour in Stage 1 across all SB materials, and settlement or reduced heave in the subsequent stages.

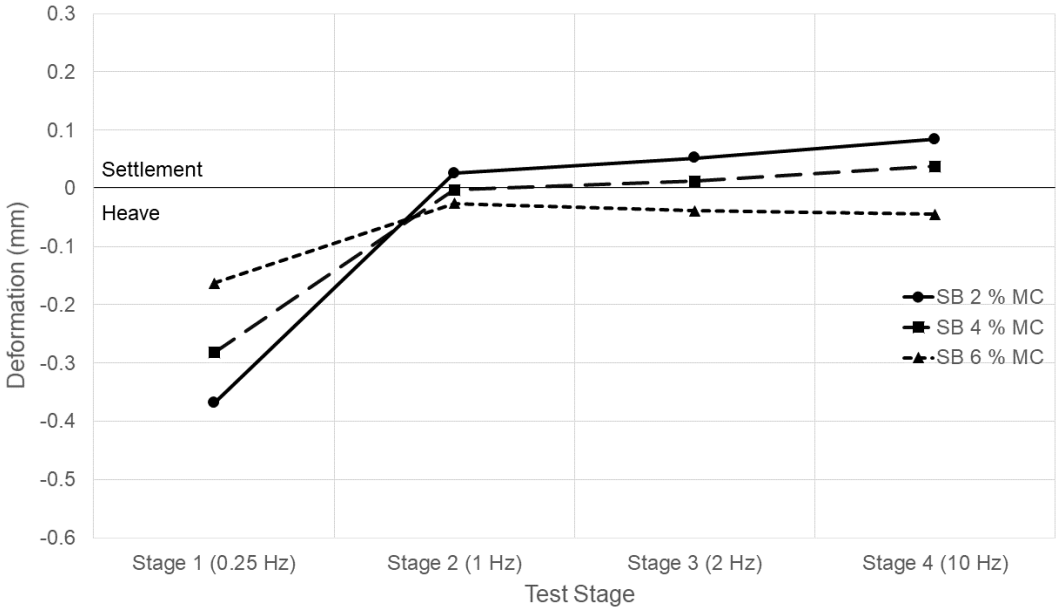

Figure 4.7: Subballast (SB) material deformation 50 mm from loading block (LVDT Position B)

The reason for the variable heave and settlement behaviour in the SB material is uncertain. However, it was clear that the difference in heave and settlement is a function of different formation MCs and independent of the loading frequency. This was evidenced by the fact that deformation did not change greatly in Stages 2 – 4 despite the progressive increase in frequencies. The AB material was similarly not affected by loading frequency, and was furthermore not affected by changes in MC, as evidenced by the minimal change in settlement between frequencies and MC values as shown in Figure 4.2.

If the loading block placed on the material is regarded as a shallow foundation problem, then it is possible to describe the failure modes of the 2 materials in geotechnical terms. The deformation behaviour of the AB material is consistent with the description of 'punching shear failure' by Knappett and Craig (2012). This source describes punching shear failure as: 'high compression of the soil under the footing, accompanied by shearing in the vertical direction around the edges of the footing. There is no heaving of the ground surface away from the edges … relatively large settlements are also characteristic of this mode'. The lack of significant heave shown in Figure 4.6 and the large deformations that given high values of MC as shown in Figure 4.2 are consistent with this description. It is important to note that the deformations described above would likely not occur in a properly designed railway formation, as the AB layer should be protected by the SB layer. This aspect of the

experiment underlined the need for a properly designed SB layer due to the compressibility of the AB layer under high stresses.

The deformation behaviour of the SB material has more in common with 'general shear failure' as described in Knappett and Craig (2012): 'heave of the surface occurs on both sides of the footing … this mode of failure is typical of soils of low compressibility (i.e. dense coarse grained soils)'. This description however has limitations in terms of the observed deformation performance. Firstly, it does not explain the initial side settlement seen in Stage 1 of all SB materials, and secondly it is unclear how the presence of aggregates change the deformation behaviour.

4.1.3 Material Stage Deformation Behaviour

This section discusses the deformation behaviour demonstrated during the different stages in the different materials. The effect of increasing loading frequency on the material is discussed, both as a function of the material type and the MC. The cumultive deformation of each stage was shown in Figures 4.2 and 4.4 as a function of MC. To provide a clearer trend of deformation behaviour during different loading stages, Figure 4.8(a) presents the permanent deformation during individual stages, and Figure 4.8(b) presents the cumulative deformation at the end of each stage. Both charts in Figure 4.8 show the diminishing contribution of each successive stage to cumulative deformation. The AB 9 % MC and AB 11 % MC materials show similar rates of deformation and a relatively small change in deformation between the two. However, the AB 13 % MC material shows an increased rate of deformation between stages and a greatly increased overall deformation in relation to the AB 9 % MC and AB 11 % MC materials.

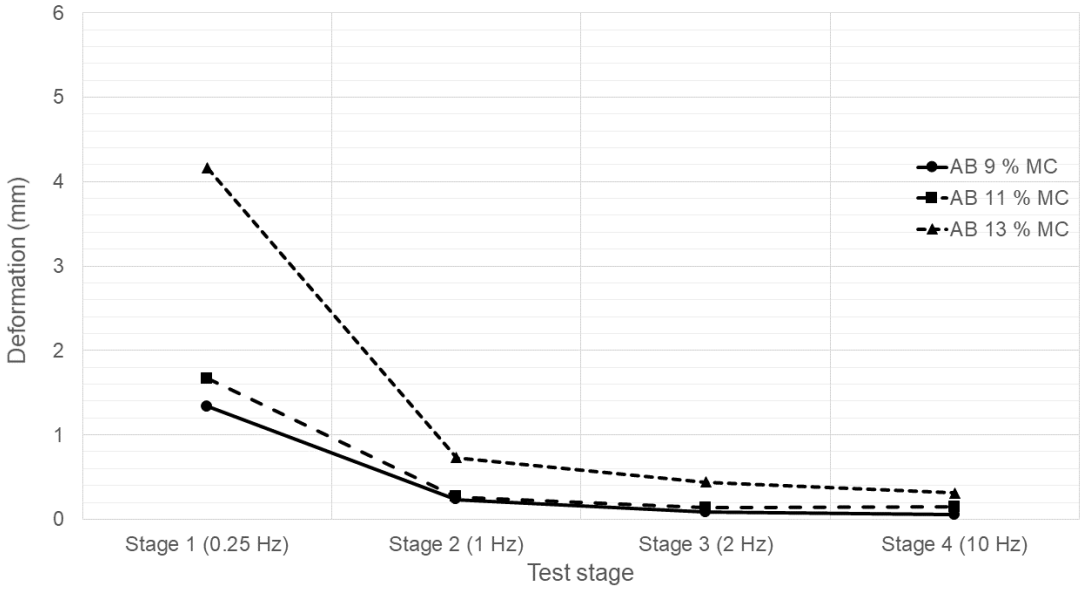

(a)

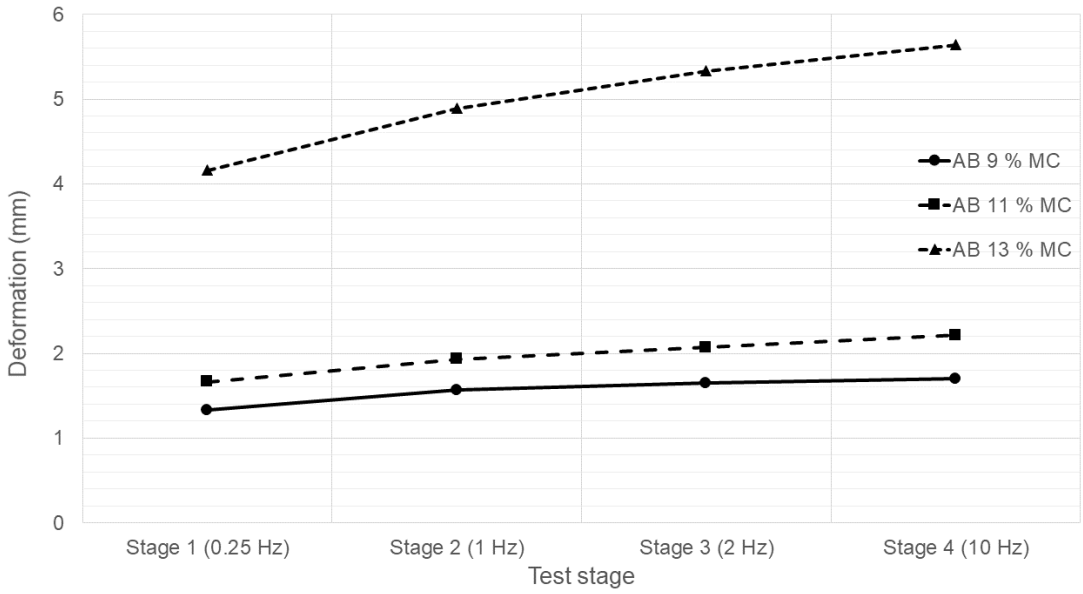

(b)

Figure 4.8: Subgrade (AB) **(a)** permanent deformation behaviour and **(b)** cumulative permanent deformation during loading stages

The deformation due to cyclic loading in the SB material falls in a narrow range as shown in Figure 4.9(a). An unexpectedly high cyclic deformation in the SB 2 % MC material during the Stage 3

loading phase was found. The possible causes of the deviation in Stage 3 of the SB 2 % MC material are explored in further detail later in the section. Figure 4.9(b) shows that the cumulative deformation increased in each stage in a linear manner. Due to the fact that the stage loading frequency increases were non-linear (0.25 Hz, 1 Hz, 2 Hz, 10 Hz), it is clear that the cumulative deformation was not linearly related to the loading frequency.

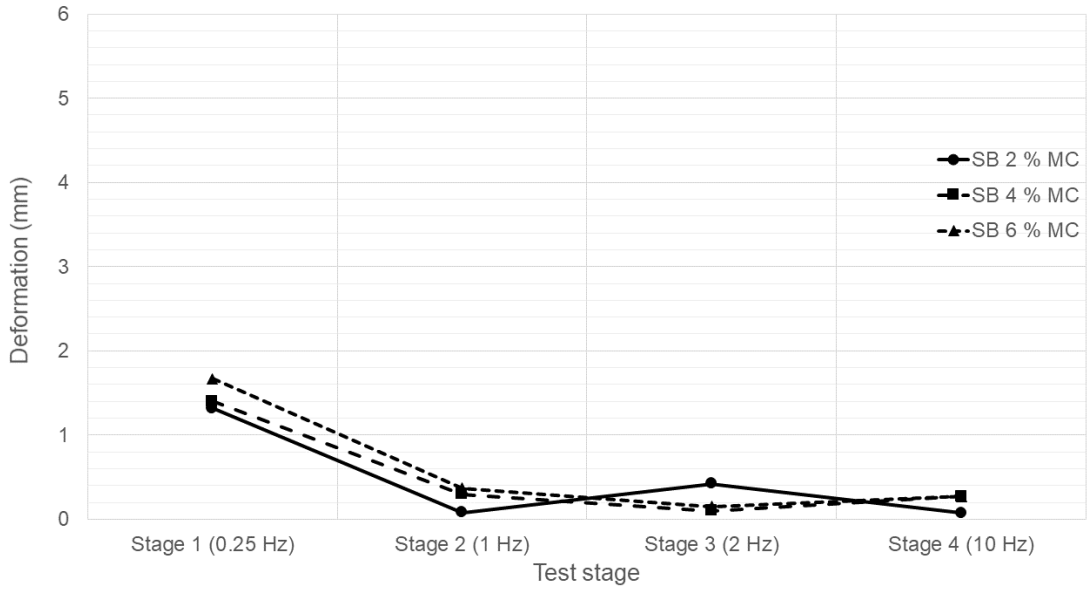

(a)

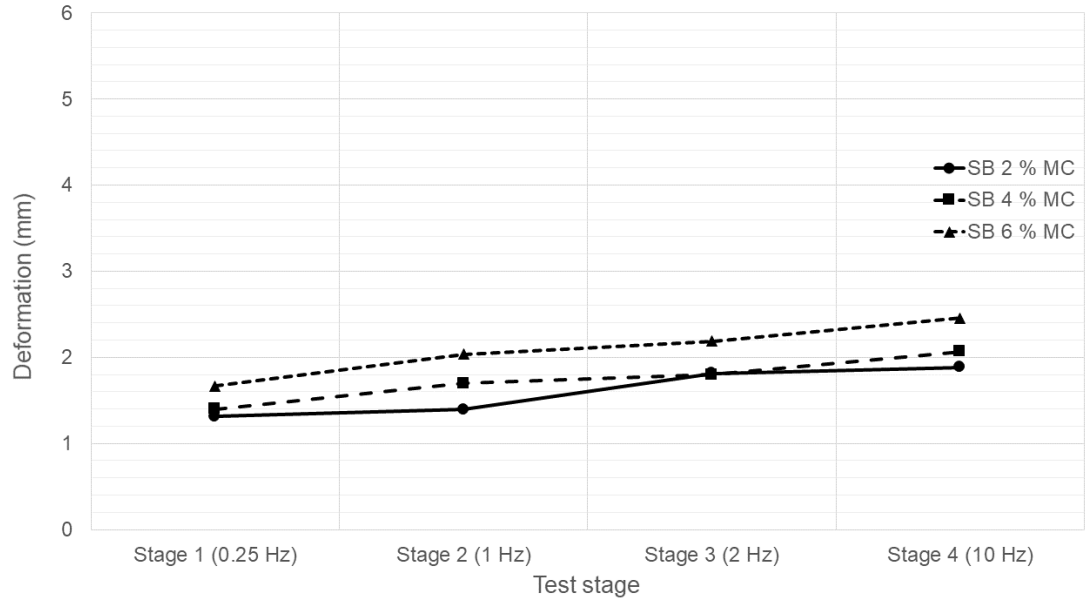

(b)

Figure 4.9: Subballast (SB) **(a)** permanent deformation behaviour and **(b)** cumulative permanent deformation during loading stages

Figures 4.8 and 4.9 are summarised in Figure 4.10. This figure presents a stacked bar graph with a side-by-side comparison of total deformation between the AB and SB material at different values of

MC. This figure clearly illustrates the difference in deformations possible in a material due to MC, as well as the absolute difference between the AB and SB materials in deformation potential.

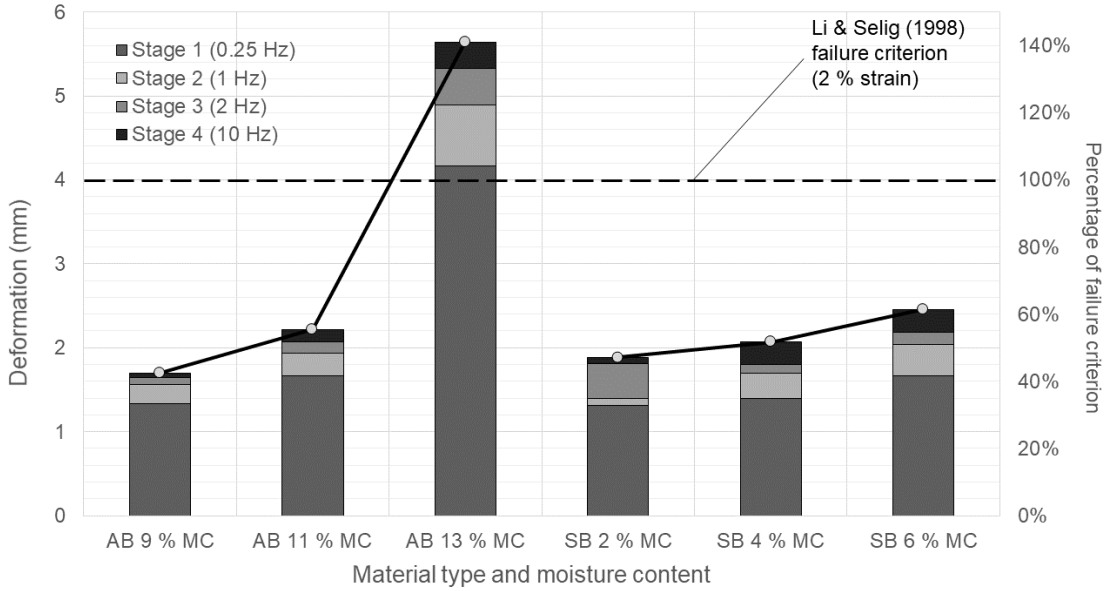

Figure 4.10: Summary of total deformations of tested materials at different moisture contents

Figure 4.10 shows that in both materials, the majority of the cumulative deformation occurred in the first stage (0.25 Hz). Stage 1 loading was responsible for 73–78 % (AB material) and 68–70 % (SB material) of the cumulative deformation. Table 4.3 presents the percentage contribution of each loading stage to the cumulative deformation, demonstrating the diminishing contribution of further loading stages to the cumulative deformation. This table shows that trends for deformation contribution in each stage was different between the AB and the SB materials.

Table 4.3: Deformation in each loading stage as a percentage of cumulative material deformation

Material	Moisture content (%)	Stage 1 (0.25 Hz)	Stage 2 (1 Hz)	Stage 3 (2 Hz)	Stage 4 (10 Hz)
AB	9	78%	14%	5%	3%
	11	75%	12%	6%	7%
	13	74%	13%	8%	6%
SB	2	70%	4%	22%	4%
	4	68%	14%	5%	13%
	6	68%	15%	6%	11%

The diminishing deformation proportion in consecutive stages of the AB material presented in Table 4.3 shows a consistent deformation proportion pattern for each stage. A graphical representation of the data in Table 4.3 is presented in Figure 4.11(a) for the AB material and Figure 4.11(b) for the SB material. In the AB material (Figure 4.11(a)) a tight distribution of deformation proportion values can be seen. Fitting a power function to the material AB deformation proportion data for all MCs provides a regression value of $R^2 = 0.94$. This indicates both numerically and visually that each loading frequency essentially contributed the same proportion of deformation to the total deformation, regardless of MC. While the AB material shows the diminishing response across all 3 MC tests (9 % MC, 11 % MC, 13 % MC), the SB material showed typical large proportions of deformation in Stage 1, but with other significant deformations (> 10 %) taking place either in Stages 2, 3 or 4. The deformation behaviour of the SB material appears erratic, as materials SB 4 % MC and SB 6 % MC show good agreement in their deformation proportions (Figure 4.11(b)). In contrast, the SB 2 % MC material behaves differently, with lower deformations in Stage 2 and 4 but higher deformation in Stage 3.

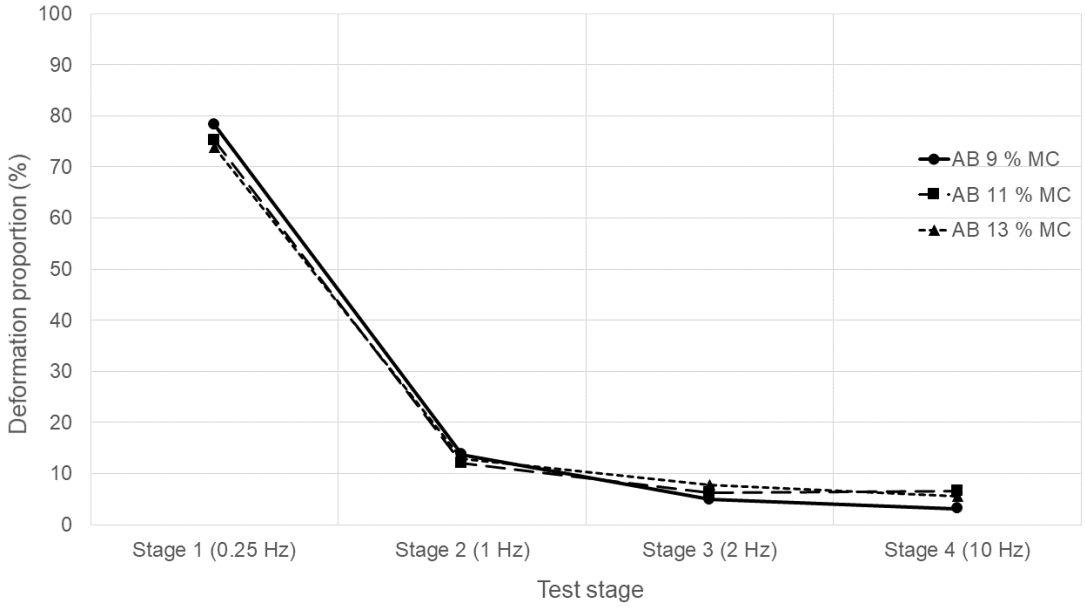

(a)

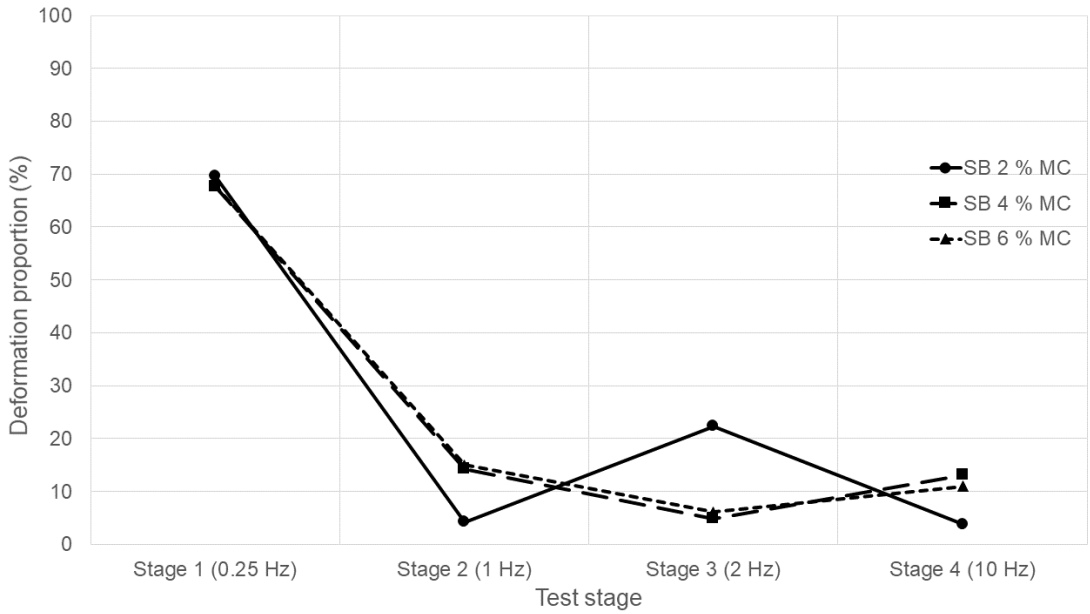

(b)

Figure 4.11: Distribution of deformation proportions across loading stages for **(a)** subgrade (AB) and **(b)** subballast (SB) materials

It is believed that this difference in behaviour is the result of 2 different modes of deformation: moisture state dependent deformation and vibratory compaction deformation. The moisture state dependent

deformation refers to the previously described behaviour of materials deforming more under higher values of MC than lower values through the strengthening effect of suctions present at lower moisture contents. The vibratory compaction deformation occurs due to vibrations in the material at higher loading frequencies being high enough that the material re-arranges and compacts. The interplay of these 2 behaviours explains why there was a difference in deformation performance between the SB 2 % MC material on the one side, and the SB 4 % MC and SB 6 % MC materials on the other.

The caveat is that while the analysis of proportions of deformations suggested that the AB material did not undergo vibratory compaction, plotting the rate of deformation (RoD) against load cycles suggested that the vibratory compaction in the AB material was not negligible. Figure 4.12(a) shows that while Stages 1, 2 and 3 required 500 – 1500 loading cycles to reach a RoD that approached 0 mm/s, Stage 4 required 1000 – 4000 loading cycles to reach similar values. This points to the fact that on a cycle to cycle basis, the Stage 4 loading frequency (10 Hz) was able to sustain non-negligible RoDs that were greater than the previous stages. This is despite the fact that significant densification had already occurred by the time Stage 4 had started. A possible additional factor in the increased RoD in the AB material at high frequencies is the presence of excess pore pressures. The high loading frequency in the latter stage caused excess pore pressures to be maintained, weakening the material and leading to further deformation. This mechanism is discussed in greater detail in Section 4.2.1.

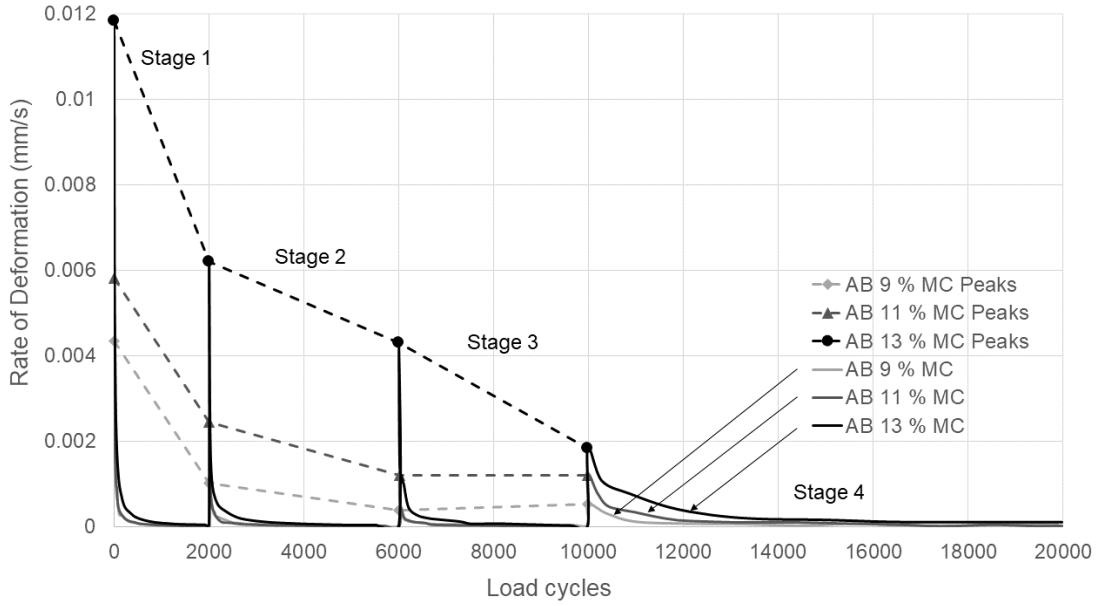

(a)

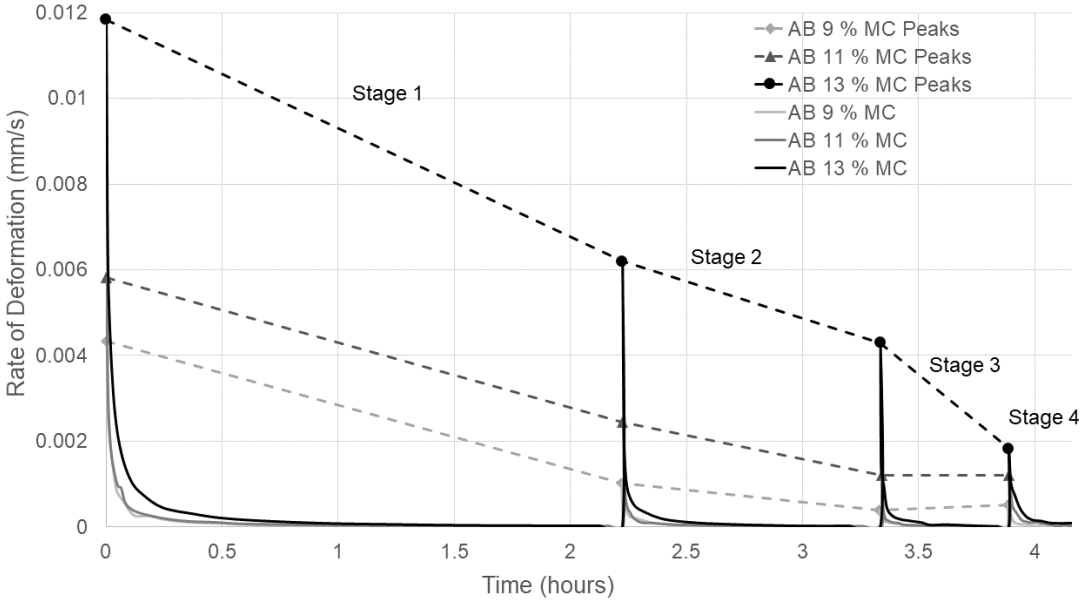

(b)

Figure 4.12: Rate of deformation of subgrade (AB) across all loading stages as a function of **(a)** loading cycles and **(b)** time

These findings have implications for laboratory testing on formation materials. In railway engineering it is common to test deformation characteristics of ballast layers at high frequencies (≥ 10 Hz) in

laboratory testing (du Plooy, 2015). This 'accelerated testing' allows the ballast to undergo enough loading cycles to model a year or more worth of loading cycles in a matter of hours or days. The results presented above suggest that when testing formation materials, accelerated testing may lead to unrealistic deformation patterns if the frequency at which the material will begin to undergo vibratory compaction is not considered. The finer AB material was less prone to this vibratory compaction behaviour as evidenced by the consistency of deformation proportions across moisture contents in Figure 4.11(a). This view is supported by industry, whereby it is recommended that vibratory compaction methods are 'not suited to materials with high silt and/or clay content' (Franki, 1995). The SB material has 5 % total clay and silt content while the AB material contains 18 %, and therefore AB material is less susceptible to this behaviour. However as Figure 4.12 showed, vibratory compaction in materials with higher fines contents may still occur at higher frequencies, providing further justification not to perform accelerated testing at high frequencies on any formation materials.

4.2 SUCTION BEHAVIOUR

Suction behaviour formed the largest section of novel work in this research project. Suction measurements were taken both by tensiometers during cyclic loading, as well as by filter paper after the conclusion of the test. The intention was to primarily use the tensiometers to record suctions in the formation before, during, and after testing. In addition, the filter paper suction measurements were carried out to supplement and validate the magnitudes of suctions with an alternative suction measurement method. These suction measurement techniques are seldom applied to granular soils. Therefore a secondary objective was to assess under which conditions the measurement techniques functioned optimally.

In this section the terms pore pressure and suction may appear to be used interchangeably. To be clear on the terminology used: pore pressure may be positive or negative depending on the conditions, while positive suction refers to the negative range of pore pressures only. The term suction has been used as far as possible, as the negative range of pore pressure is of greatest interest to the analysis. However, positive pore pressures are discussed in Section 4.2.1 in a soil where no suctions are present.

4.2.1 Material Suction Overview

This section presents and discusses the general trends observed during tensiometer suction testing. These include observations on the magnitude of the suctions present in the different materials, as well as the magnitude of those present at different MCs. Tensiometer data is presented as examples of typical behaviour observed in different materials, and how the behaviour may be the result of soil-tensiometer interaction.

All 3 SB material tests had tensiometers installed in the same 4 locations. An example of tensiometer data from Position 1 is presented in Figure 4.13. In this figure the start and end of loading stages are denoted by symbols. When interpreting the tensiometer data, it was important to consider the start and end values as the absolute change in suction over the course of the test. However, it is also important to observe the effect on the pore pressure during the test. The behaviour of the tensiometer during the test was an indication of how well it performed in the given conditions. Sudden deviations in the suction measurements were treated as possible indications of total stress effects during loading.

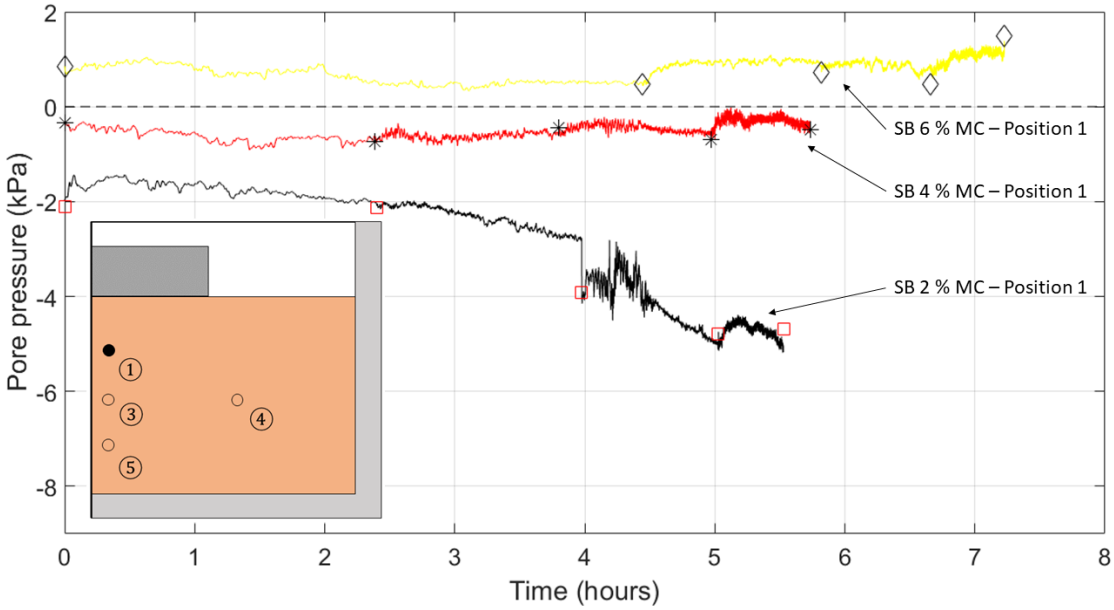

Figure 4.13: Suballast (SB) suctions at Position 1 with tensiometer locations in formation (inset) with symbols showing start and end of stages

The conditions in the SB 6 % MC material remained effectively saturated in all tests. In all 4 positions,

the SB 6 % MC material showed positive (albeit small) pore pressures. Therefore, at SB 6 % MC suctions were not present to contribute to formation strength. Conversely, pore pressures in the SB 4 % MC test were shown to be just slightly negative indicating some suctions were present. The SB 2 % MC test showed negative pore pressures in the range of - 1.4 kPa to - 2.4 kPa before loading, and had a gradual decrease as testing continued.

In terms of the behaviour of pore pressures in specific locations, final pore pressure values in SB 2 % MC correspond in some respects to MC data presented in Figure 4.19(a). The higher MC zone around Position 5 resulted in a higher pore pressure and no gradual decrease, and the drier conditions at Position 4 resulted in the lowest final pore pressures. There is, however, a discrepancy between pore pressures measured at Positions 1 and 4 (- 4.7 and - 8.1 kPa respectively) despite those two positions both containing MCs of around 2.2 %. This discrepancy is thought to be due to redistribution of pore water and drying in the time between the end of the test and the moisture samples being taken.

Although general increase/decrease trends are found in the data, the causes of erratic tensiometer data require investigation. Sudden increases and decreases and general erratic behaviour were associated with the application or removal of load. The erratic behaviour of SB 2 % MC in Stage 3 as shown in Figure 4.13 coincides with the period of rapid deformation as shown in Figure 4.11(b). Two possible mechanisms may be responsible for the erratic readings under loading:

1. Total stress interference with the tensiometer upon loading
2. Movement of soil at the face of the tensiometer

With regard to the former point, despite the extensive effort to shield tensiometers from total stress effects, it remains possible for these stresses to influence the reading. This could be due to improper bedding of the tensiometer casing and face, or as a result of material rearranging in such a way as to apply a force to a sensitive position on the tensiometer. The latter point is compelling as it is described in Lourenço et al. (2009) as the reason for sudden drops in readings when undergoing dynamic tests. This drop occurs when soil in contact with the ceramic face of the tensiometer shifts and breaks the water-phase link between the soil water and the tensiometer ceramic water. The severing of this link creates a sudden disconnect between the pressure experienced by the tensiometer and the actual pressure in the soil. This is a limitation of the tensiometer, as the problem may occur in any dynamic test or under any sudden local deformations.

As with the SB material, the AB material showed suction behaviour dependent on the MC. A variety of behaviours were seen, which reveal the pore pressure response of the material as well as the manner that the tensiometer interacts with the soil around it. These themes will be addressed throughout the section. Figure 4.14 presents typical trends of the pore pressures present at the different MCs. The AB 13 % MC formation maintains a positive pore pressure slightly above zero, while AB 11 % MC has a negative pore pressure slightly below zero. The measured pore pressures in the AB 9 % MC material were markedly different from the other two materials in that the AB 9 % MC material started at a low negative pore pressure and subsequently decreased to a higher negative pore pressures (between -20 – -90 kPa).

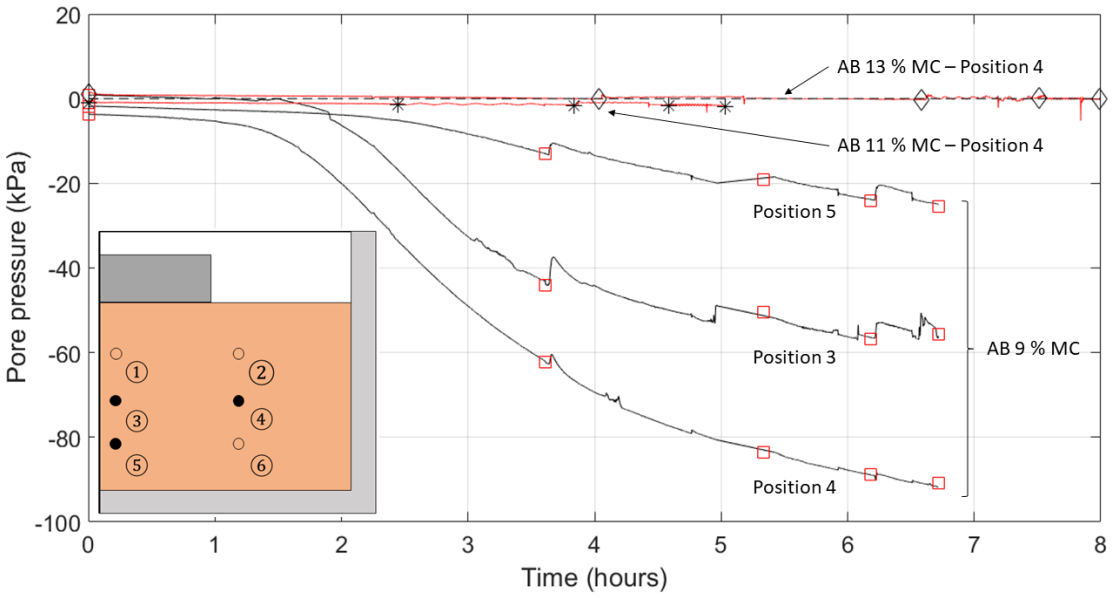

Figure 4.14: Subgrade (AB) suctions at Positions 3,4 and 5 with tensiometer locations in formation (inset)

The decrease in pore pressure shown in the AB 9 % formation (Figure 4.14) is similar to the previously discussed pore pressure behaviour in the SB as it starts at a higher than expected pore pressure, and only stabilises at a lower pore pressure over time. Guan and Fredlund (1997) described the behaviour of tensiometers installed in a glacial till. It was found that equalisation of pressures between the tensiometer and the soil could take between 1 – 18 hours, with longer equalisation times associated with lower values of degree of saturation (S_r). It is believed that this equalisation time is responsible for the initially high pore pressures in the dry material.

Pore pressure build-up and dissipation were recorded in the AB 13 % MC material at Positions 1 and 5 (below the loading block and above the centre of the box floor, respectively). As noted previously, pore pressures in the AB 13 % MC formation were typically slightly above zero in the positive range. In the two described positions, pore pressure build-up was recorded coinciding with the initial stages of cyclic loading as shown in Figure 4.15. The fact that pore pressures were recorded by the tensiometers at a higher S_r is due to the response time for tensiometers in wetter formations being significantly higher than those installed in dry formations.

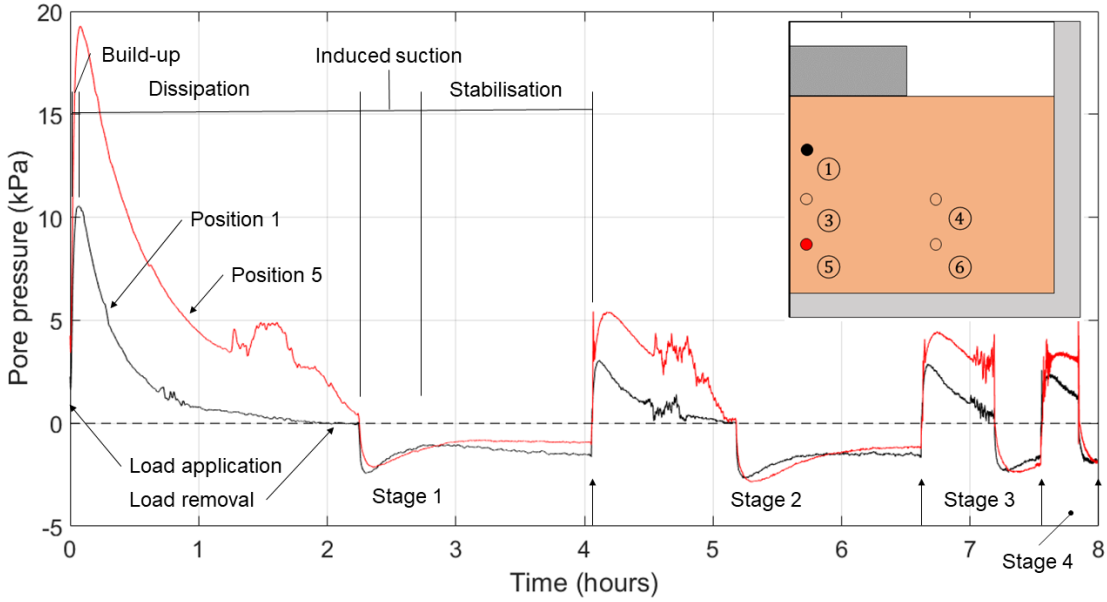

Figure 4.15: Pore pressure build-up in subgrade (AB) for test AB 13 % MC

A comparison of pore pressure build-up against the deformation showed that the build-up occurs during the periods of rapid deformation at the beginning of a loading stage. This behaviour observed is in line with the findings of Mamou et al. (2017). In that study, excess pore pressures were found to be associated with volumetric instability and the ensuing rapid deformation or failure of a formation. The study suggested that the volumetric change caused the pore pressure build-up, rather than pore pressure build-up governing volumetric change. In accordance with this, literature suggests that when the clay content is increased, the pore pressures do not increase to the same degree, as the inclusion of finer particles stabilise the material.

Some apparent pore pressure build-up was recorded in material AB 9 % MC as shown in Figure 4.14. However, the build-up occurs before the tesniometer has fully equalised, so it is unlikely that these

values are a reflection of the true excess pore pressures present in that material. The presence of build-up of excess pore pressures in an unsaturated formation material such as the AB 9 % MC material is in agreement with the work done by Cary and Zapata (2016), and suggests that the tensiometers used in this study were capable of measuring these build-ups.

Figure 4.16 presents a summary of the suctions measured in both AB and SB materials as a function of S_r. This summary graphically shows the increase in suction associated with the desaturation of the material. This increase in suctions was clearly demonstrated to be more rapid in material AB than material SB. The large difference in possible suctions in the AB material (1 – 95 kPa) over a relatively small range of S_r values (0.61 – 0.88) is related to the difference in the total deformation observed in the AB material as summarised in Figure 4.10. This is due to the strengthening influence of increasing soil suction stress with increasing soil suction as described in Section 2.2.3.

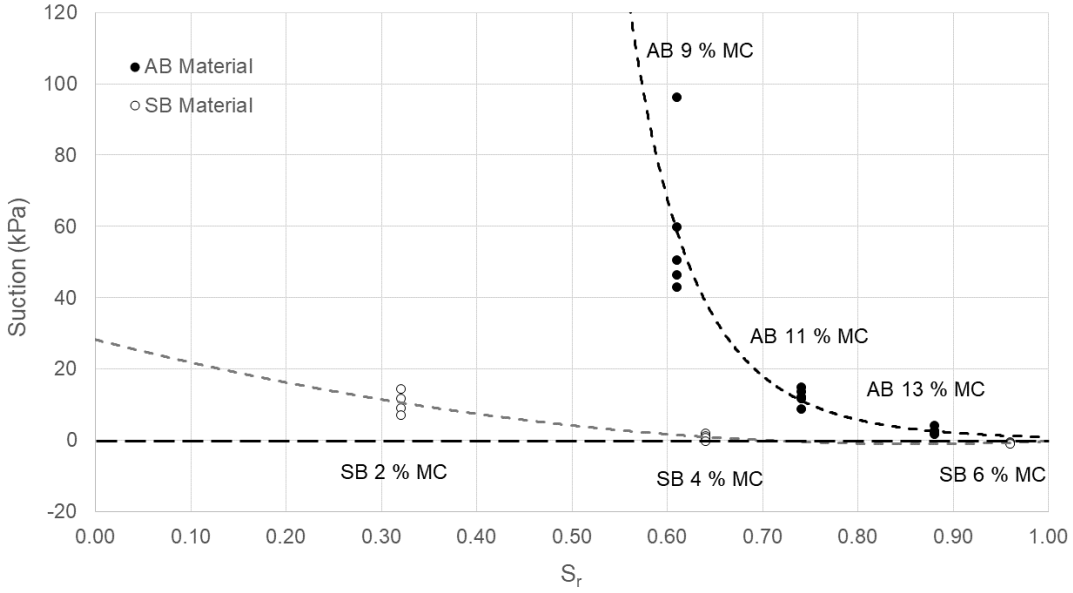

Figure 4.16: Summary of soil suctions in subgrade (AB) and subballast (SB) materials as a function of degree of saturation (S_r)

Figure 4.16 may be seen as the counterpart to Figure 4.5. Taken together, these figures show how material deformability and soil suctions are inversely related.

4.2.2 Suction Equalisation and Agreement with the Soil-Water Retention Curve

To demonstrate the difference in tensiometer performance between the 2 materials, Figure 4.17 shows the change in pore pressure readings from commencement of the test to the formation being deconstructed the following day for both AB (Figure 4.17(a)) and SB (Figure 4.17(b)) materials. These figures consist of tensiometer readings from the start of testing (denoted by grey circles) connected to readings from the tensiometers before the model was deconstructed, after being left to monitor the suctions with no superimposed load overnight (denoted by black triangles). These suction readings were plotted on the soil-water retention curves (SWRC) of the AB and SB materials described in Section 3.3.2. The suction values at the start of the test are assumed to occur at the targeted MC for that test (i.e. 9 % MC for the AB 9 % MC test), because it was not possible to take in-situ MC readings before the start of the test without disturbing the model significantly. However, for the overnight suction readings the corresponding values of MC plotted are not assumed, but are the actual values of MC measured after the model was deconstructed (as shown in Figures 4.19 and 4.20). It is clear from Figure 4.17(a) that the suction readings in AB reached values of suction and MC that could be realistically expected in the soil, as all final suction values were within the boundaries of the SWRC.

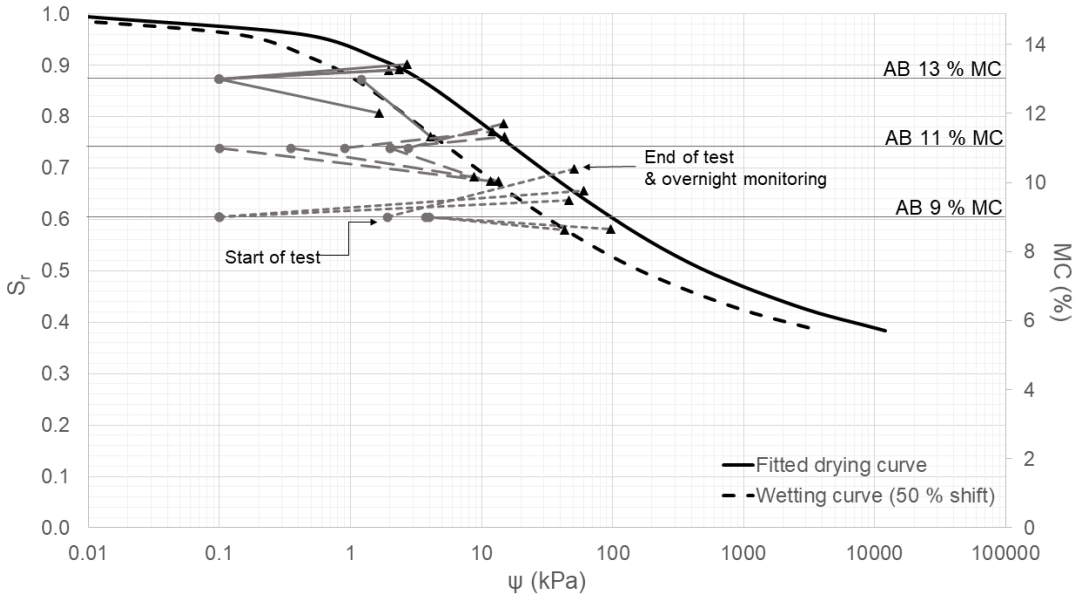

(a)

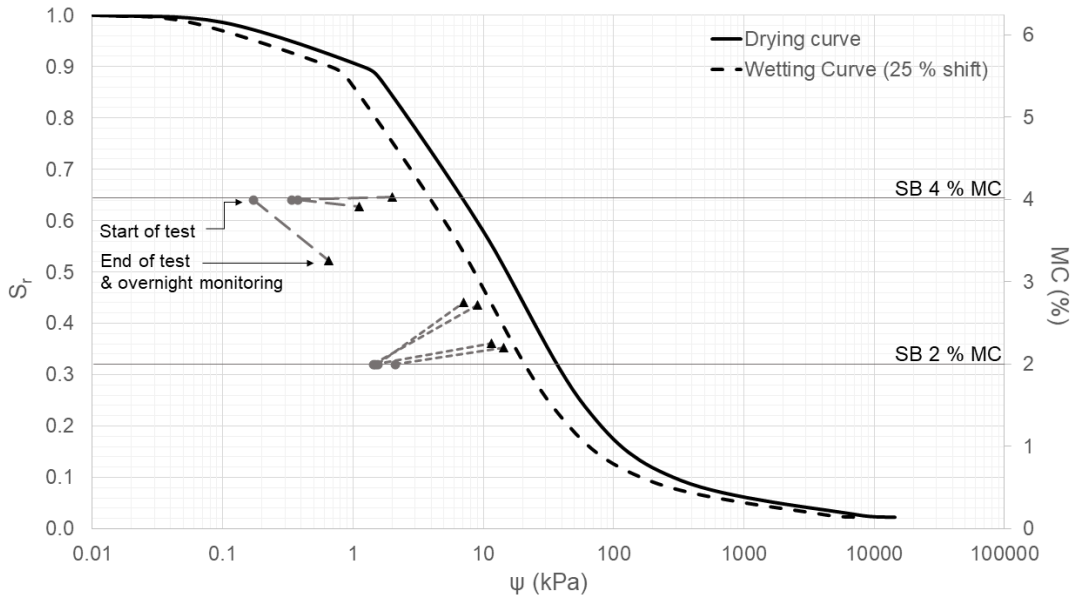

(b)

Figure 4.17: Change in negative pore pressures from the start of the test (•) to the end of the test and overnight monitoring (▲) for **(a)** subgrade (AB) and **(b)** subballast (SB) materials

Conversely, the measured suctions in the SB material did not fully agree with the calculated SWRC for that material. Figure 4.17(b) shows that the suctions measured were below those predicted by the

SWRC. The SB 2 % MC material approached the wetting curve of the SWRC, but the SB 4 % MC suctions did not reach the SWRC curve even given prolonged equalisation time (± 10 hours). The SB 6 % MC pore pressures were not included in Figure 4.17(b) because all pore pressures recorded in that test were positive, and therefore no suction was present.

To explain the apparent discrepancy in SB material suctions it is necessary to consider the interaction of the tensiometers and the material, as well as the nature of the SWRC itself. Due to the granular particle size distribution of the SB material, every effort was made to select finer in-situ material (roughly < 2 mm) to pack around the tensiometer ceramic. Without a matrix of finer material around the ceramic face, the tensiometer would have difficulty forming a hydraulic connection with the surrounding soil. Without this connection, suctions cannot be measured. Additionally, it was noted in Section 4.2.1 that abrupt changes in suction readings were recorded during material deformation, as material moves past the tensiometer face and disrupts the hydraulic connection. It is possible that these shifts in measured suction value shifted the final suction value away from the 'true' suction value in-situ.

Some error may also be present in the SWRC that contributes to the discrepancy. The SWRC drying curves are curve fits calculated according to the Fredlund and Xing (1994) method, and with wetting curves calculated by the log-shifting of the drying curve (Fredlund et al., 2011) as detailed in Section 3.3.2. The SWRCs for the 2 materials shown in Figure 4.17 were produced from a combination of tensiometer data and filter paper measurements. Finally, the SWRC has been noted to be dependent on the compaction condition present when the SWRC data is captured. It is likely that compaction conditions differ somewhat between the small-scale SWRC test and the larger scale formation test described in this section. Due to these factors, some systematic error is unavoidable in the SWRCs. Careful planning can minimise this error but cannot eliminate it. For this reason it is wiser to use the SWRC as a guide that allows comparison of suction measurements taken in the material during testing to expected suctions established by the careful preparation of the SWRC.

4.2.3 Filter Paper Results

The filter paper tests performed during model deconstruction were intended for comparison with the final tensiometer readings from the overnight monitoring to supplement the understanding of the materials' suction behaviour. The results from these tests were different from the final tensiometer readings in that they showed greatly increased suctions for the same values of MC. Figure 4.18 presents

the SWRC of the AB and SB materials respectively, with final tensiometer values plotted alongside the data obtained from the filter paper tests.

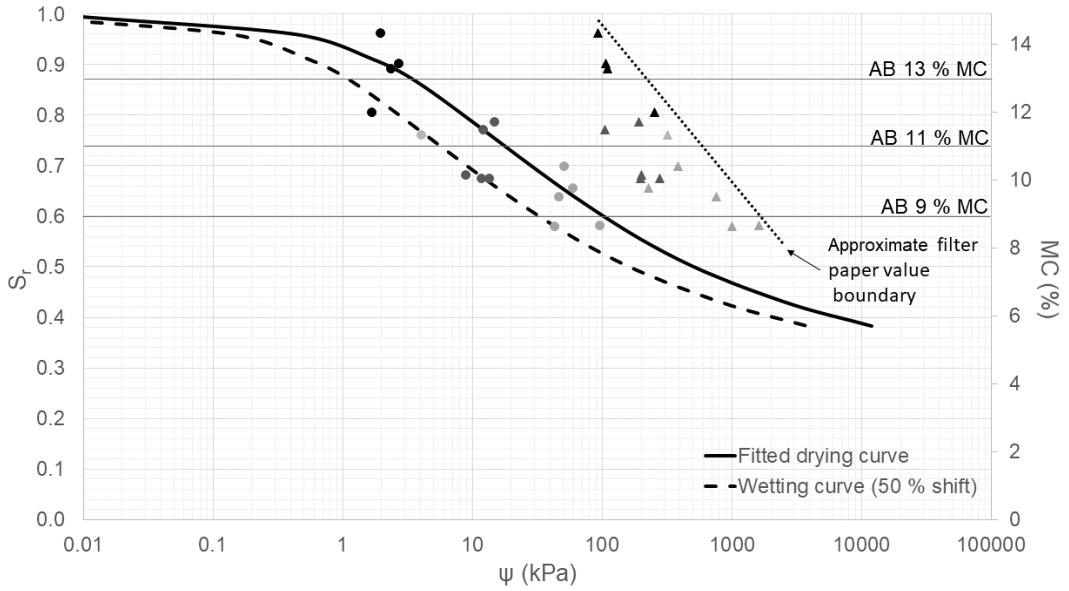

(a)

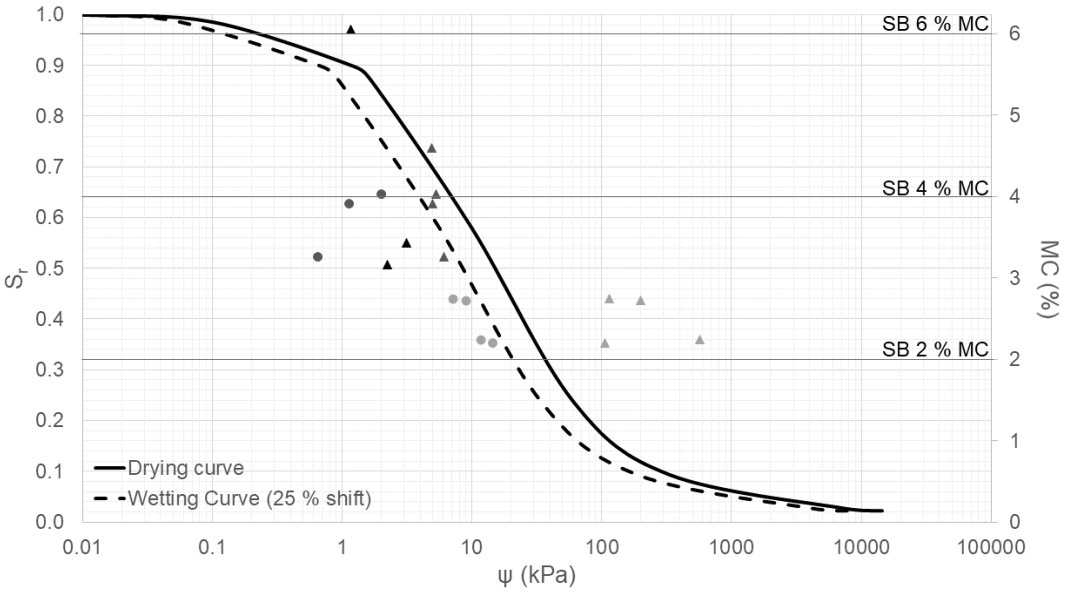

(b)

Figure 4.18: Difference in final tensiometer (●) and filter paper (▲) suction values for **(a)** subgrade (AB) and **(b)** subballast (SB) materials

The AB material suctions in Figure 4.18(a) show a clear discrepancy between the suctions as measured by the tensiometers and the filter paper method. The filter paper suction values are shifted between 1.5 - 2.5 log-cycles to the right of those of the tensiometers. The maximum suctions from the filter paper suction values form an apparent boundary that is offset from the drying curve of the SWRC by approximately 2 log-cycles. This consistent shift suggests that the difference in suction values between the two methods was due to a systematic error. Work done by Marinho and da Silva Gomes (2011) found that the performance of the filter paper suction measurement method is dependent on the moisture state of the soil, particle size distribution and above all, the contact conditions between filter paper and soil. Given poor contact between the filter paper and the soil, it was found that the filter paper test would measure a suction value consisting of an undefined combination of matric and osmotic suction. This suction would be greater than the matric suction (represented by the SWRC) and less than the total suction (the sum of the matric and osmotic suctions). Furthermore, it was noted that it was unlikely to achieve good contact between filter paper and soil in a granular material, as the roughness and unevenness of the surface on which the filter paper was placed led to lower overall contact. Therefore, one would inevitably measure a combination of matric and osmotic suction to some degree.

The SB material filter paper suctions in Figure 4.18(b) did not show the same consistent shift in suction values as the AB material did. Ultimately, the filter paper suctions as well as the tensiometer suctions for the SB material were shown to be more erratic, as evidenced by the right shift in SB 2 % MC filter paper suctions away from the SWRC and the left shift of SB 4 % MC tensiometer suction values. Figure 4.18(b), along with the pre-test values of suction shown in Figure 4.17(b), therefore indicates the uncertainties with measuring suction in granular materials. In these low-fines materials, tensiometers may require a great amount of time to couple with the soil water, or may not couple at all, while filter paper methods may have problems with sufficient contact as previously mentioned. Fredlund et al. (1995) found that variability of suction readings below 100 kPa were present in all contemporary suction measurement techniques. In addition to this, Marinho and da Silva Gomes (2011) asserted that the steep slope of the funicular regime in granular materials means that slight errors in either suction reading or MC can result in values that do not agree with the SWRC. For these two reasons it is especially important in granular materials that great care is taken in establishing an accurate SWRC to allow comparison of suction values and outliers to be discarded.

4.2.4 Suction and Moisture Content Comparison

While the composition of a soil in terms of fractions of sand, silt and clay determine the possible suctions in a soil, it is primarily the S_r for a fixed combination of these fractions that governs the suction in the soil at any given time. This section seeks to investigate the moisture state in the model formations. The values of MC were obtained using the method described in Section 3.2.3.

Contour plots of MC for the AB and SB materials are shown in Figures 4.19 and 4.20 where black circles denote sampling locations. The measured MCs were more consistent and continuous for the SB material as compared to the AB material. Figure 4.19(a, b, c) shows that the MC of the SB formation approximately increased diagonally from the top right to bottom left. This is due to the top right of the figure being the part of the formation open to atmosphere, and the left of the figure situated along the wall of the strongbox. Figure 4.20(a, b, c) show the MC distributions in the AB materials. Despite the charts for the AB material being more irregular, the trend described in the SB material holds true for material AB as well. The highest MC is found at the bottom of the formation in the centre (y-axis on Figures), where the longest drainage path exists.

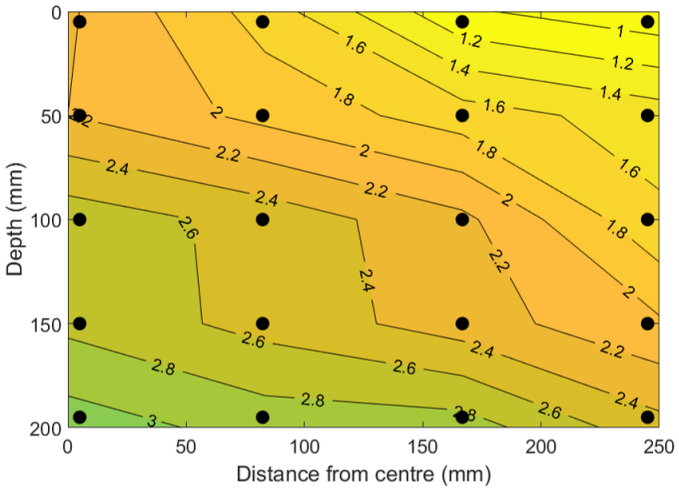

(a)

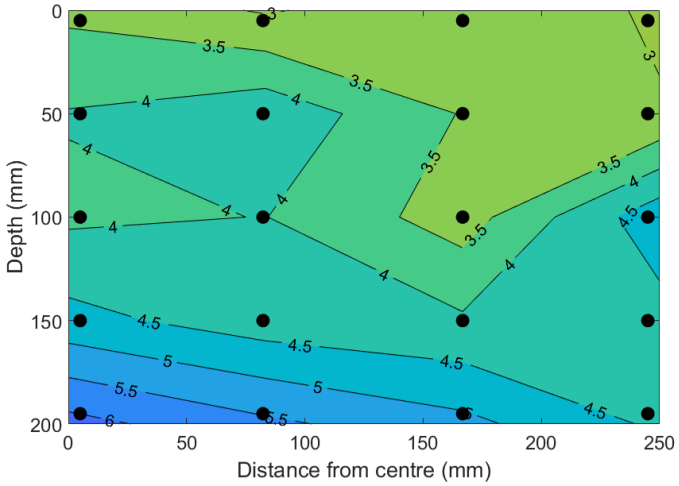

(b)

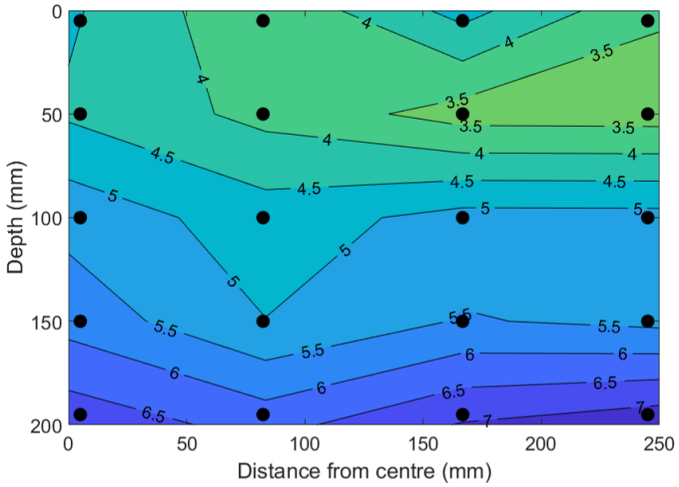

(c)

Figure 4.19: Moisture content contours and sampling locations (•) for subballast (SB) materials **(a)** SB 2 % MC, **(b)** SB 4 % MC, **(c)** SB 6 % MC after testing

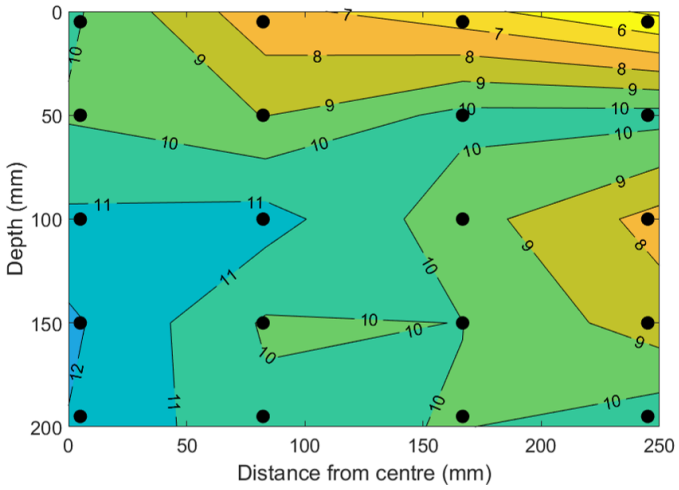

(a)

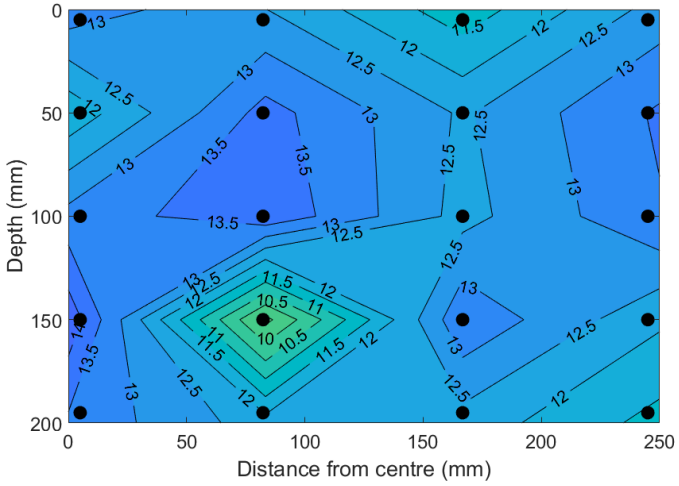

(b)

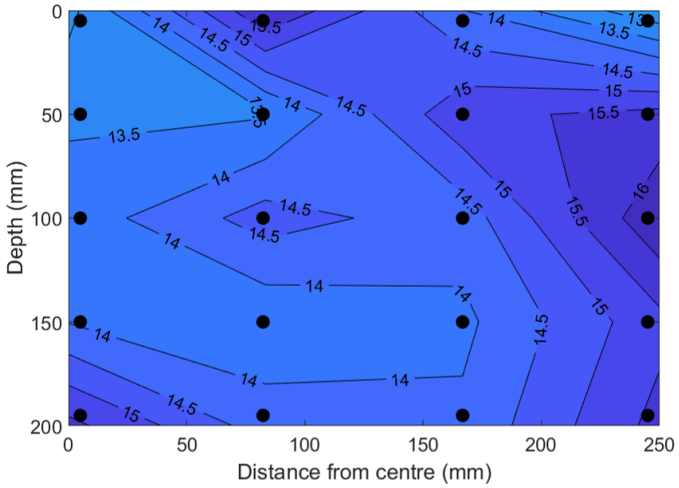

(c)

Figure 4.20: Moisture content contours and sampling locations (•) for subgrade (AB) materials **(a)** AB 9 % MC, **(b)** AB 11 % MC, **(c)** AB 13 % MC after testing

Table 4.4 presents the average recorded MC throughout the formation in comparison to the targeted MC for each formation. The MCs appear to be approximately between 0.1 – 1.5 % higher than the targeted MCs for each formation. Only the SB 6 % MC formation showed a lower average MC than the target MC at the end of the test.

Table 4.4: Comparison of target versus average moisture contents after testing

Material	Target MC (%)	Average MC (%)	Difference (%)
AB	9	9.56	0.56
	11	12.62	1.62
	13	14.45	1.45
SB	2	2.17	0.17
	4	4.11	0.11
	6	5.05	-0.95

The lower average MC than targeted in the SB 6 % MC material can be explained by the fact that there was leakage of soil water from the formation around the base of the strongbox as testing progressed. While the formation at this MC was well below its theoretical saturation value, the soil did not have the capacity to retain the moisture due to its low fines content. Shedding water is one of the primary functions of subballast (Li et al., 2016), and this behaviour was therefore not unexpected.

It should be noted that the process of acquiring MC readings for this experiment was limited as particle size may have affected calculated MC values. Due to the coarse nature of the material, small soil samples taken for purposes of MC calculation may produce erratic results because of the difference between fine and coarse particles in their ability to retain water. In a material composed mostly of fines, the mass of any one particle is a small fraction of the total soil mass. In a granular material, a single large aggregate may contribute a significant fraction of the mass in a small sample. Furthermore, the finer material can retain more water per unit of dry mass than is possible for an aggregate. The implication of this is that a single large aggregate that is removed or included in a small sample of soil may have a significant effect on the value of MC calculated. This may lead to calculation errors that manifest in erratic contour plots as shown in Figures 4.20(a, b, c).

The solution to this problem is, of course, to take larger samples, causing any individual aggregate particle to contribute a smaller fraction to the overall sample mass. Unfortunately this solution could not be implemented in the experiment due to space limitations. The MC readings were intentionally recorded at representative points to illustrate the distribution of the moisture in the model. If larger samples had been taken, the soil sample would partially include adjacent sampling areas. A solution to this would be take samples further apart. However, this would lead to fewer sampling locations, and therefore less data for a contour plot.

To assess the validity of the measured MC values, it is interesting to compare the suction values in both materials AB and SB when using the MC values from the samples taken post-test against the suctions plotted using the 'targeted' MC (e.g. 9 % MC was targeted for the AB 9 % MC test). Figure 4.21 shows suction against measured and targeted MC plotted on the SWRC for the respective materials. Each individual line plots the difference in suctions between tests at the same position. In Figure 4.21(a) the targeted values of MC are plotted, while in Figure 4.21(b) the measured values of MC are plotted. Figure 4.21(a) shows that there is internal consistency in how the different positions plot when the targeted MC is used, as well as agreement with the drying and wetting boundary curves predicted by the SWRC. Conversely, the plot of the measured MC in Figure 4.21(b) is more erratic. This evidence suggests that the in-situ moisture state of the AB material did not deviate significantly from the targeted moisture state even after the test and overnight monitoring period had passed.

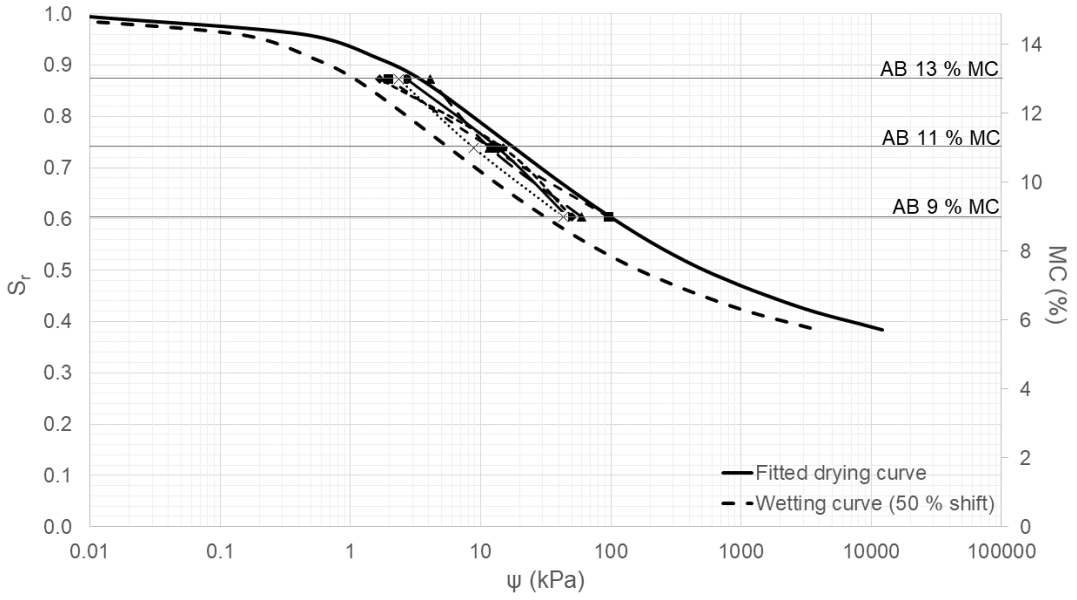

(a)

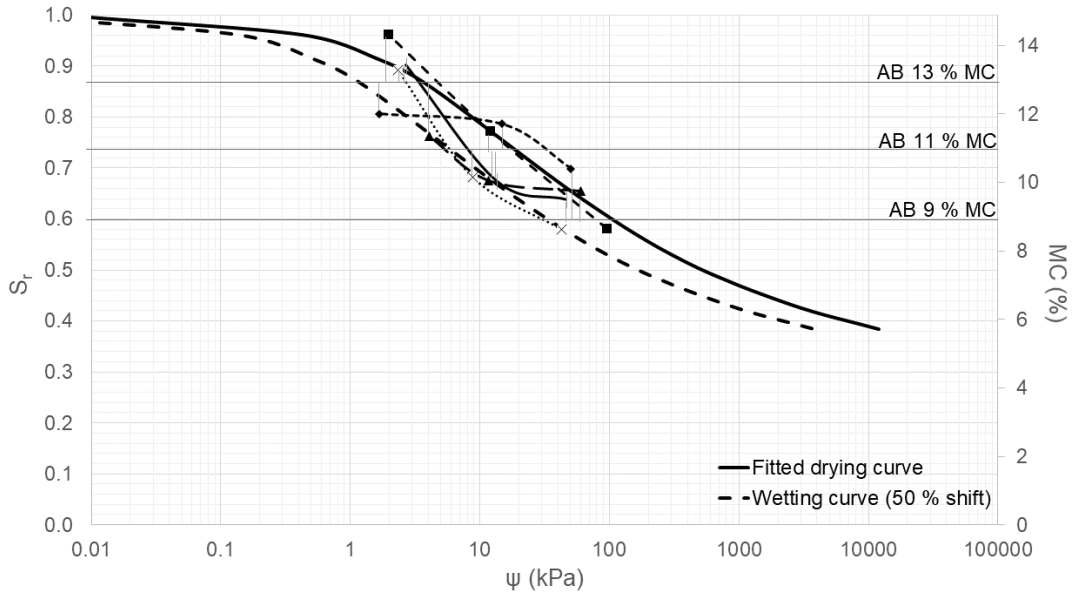

(b)

Figure 4.21: Overnight suctions in relation to the **(a)** targeted and **(b)** measured moisture contents (MC) in the subgrade (AB) material

An identical comparison is presented in Figures 4.22(a) and 4.22(b) for the SB material. The suction values of the SB material do not plot as well over the SB material SWRC as their AB material

counterparts do. The SB 2 % MC and the SB 6 % MC suctions show the closest match to suctions predicted by the SWRC. The SB 4 % MC material departs from this trend by having suctions that appear significantly lower. However, comparing the targeted MC plot in Figure 4.22(a) and the measured MC plot in Figure 4.22(b) supports the point that the suctions follow a more predictable pattern when the targeted MC was used.

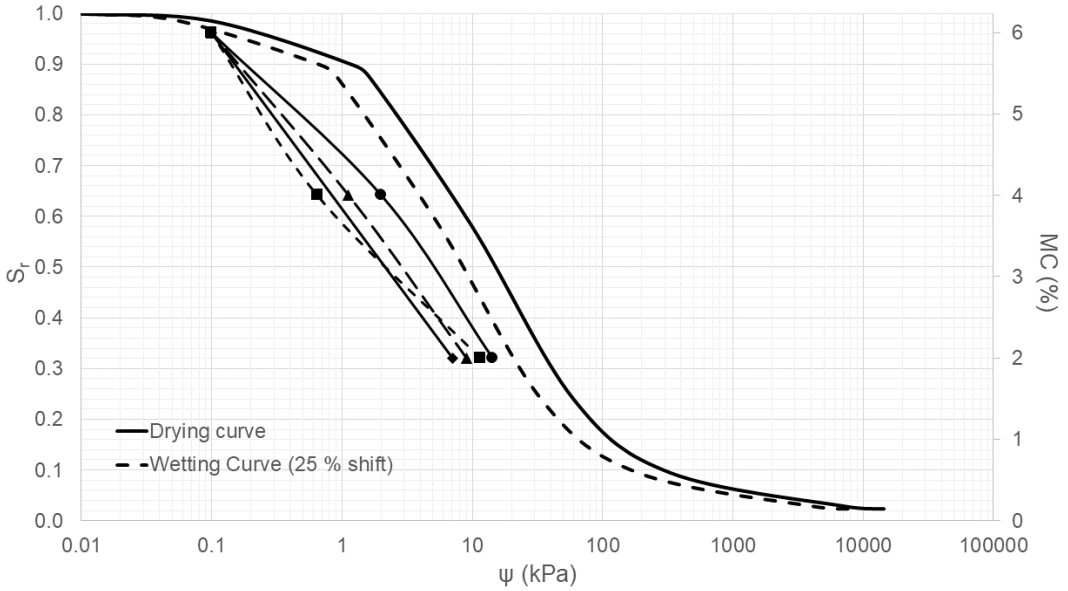

(a)

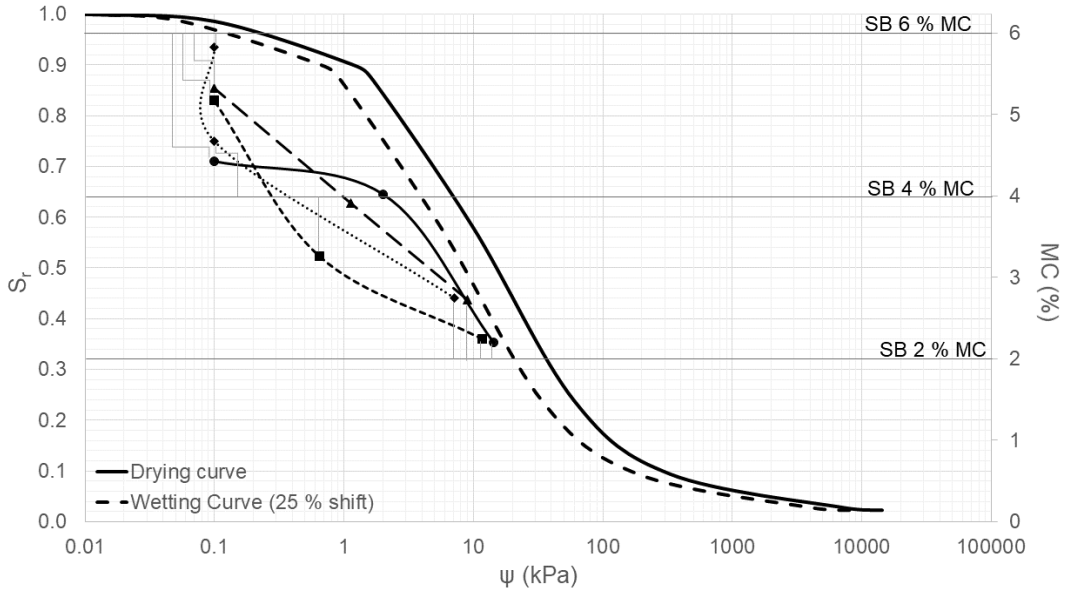

(b)

Figure 4.22: Overnight suctions in relation to the **(a)** targeted and **(b)** measured moisture contents (MC) in the and subballast (SB) material

4.3 DISCUSSION

This section focused on analysing and presenting the cyclic loading behaviour of two typical South African railway materials by investigating the material deformation and suction behaviour to understand the factors that govern deformation and ultimately failure of railway materials. The deformation behaviour as presented in Section 4.1 showed that the AB and SB materials behaved fundamentally differently under the same loading conditions. Increased MC was associated with increased deformation in both AB and SB materials, but to different degrees. As a comparison of Figures 4.2 and 4.4 showed, an increase in MC in the SB material caused an almost linear increase in deformation, while an increase in MC in the AB material showed a proportionally larger deformation at higher values of MC as plastic collapse occurred.

An analysis of soil movement beside the loading block concluded that the AB material experienced punching shear, while the SB material experienced a mixed deformation pattern. The mixed deformation pattern of the SB material shares some aspects of a general shear failure, but was not found to be in complete agreement with that failure mode.

The effect of loading frequency on deformation was analysed to find the applicability of accelerated testing to formation materials. It was found that accelerated testing was unsuitable for both AB and SB materials for different reasons. In both materials, higher frequencies were found to coincide with sustained high rates of deformation due to the effect of vibratory compaction (in the case of the SB material) and the inability of excess pore pressures to dissipate with repeated loading (for the AB material). The implication of this was that accelerated testing on railway formation materials would lead to deformations exceeding those experienced by railway formations in-situ and would therefore be an unreliable indicator of possible deformations in a proposed railway line.

The suction analysis presented in Section 4.2 primarily focused on the magnitude of suctions present in the materials, as well as the interaction of the soil material and suction measurement techniques. Both the AB and SB materials showed a range of positive and negative pore pressures (suctions). The magnitude of the maximum suctions were however higher in the AB material due to the presence of fines. These higher suctions indicate that the AB material has a greater capacity for strength gain at lower values of S_r than the SB material does. In addition to this, the presence of fines in the AB material also caused build-up of excess pore pressures under repeated loading. This build-up of pore

pressures was as a result of the high S_r and large deformations occurring in the formation. It seemed that the tensiometers did record some excess pore pressure build-up in drier AB materials.

Figure 4.23 shows a direct comparison of the chart presented in Figure 4.10 with a clustered bar chart of suctions found in the respective materials. This comparison illustrates the strengthening effect of the AB material suctions, as well as the difference in suction and deformation behaviour between the AB and SB materials, as discussed.

The AB material showed deformations that were 141 % of the Li and Selig (1998) failure criterion of 2 % strain under low suction (3 – 5 kPa) conditions. A slight increase in suctions up to 10 – 15 kPa however resulted in a marked decrease in deformation to 55 % of the failure criterion. Further desaturation showed that the AB material could generate higher suctions to the magnitude of 40 – 100 kPa, these suctions caused a further strengthening of the material to 43 % of the failure criterion. The greatest increase in performance was noted between 5 and 15 kPa, wherein the deformation decreased by 90 % of the failure criterion.

The SB material reached a maximum deformation of 61 % of the failure criterion in effectively saturated conditions (all pore pressures measured were positive). When desaturated, suctions in the range of 7 – 14 kPa were generated, leading to a decreased deformation of 47 % of the failure criterion. The SB material showed a low suction generation potential when compared to the AB material, leading to comparatively little strength gain between the wettest and driest moisture states tested. The AB material at its driest state (AB 9 % MC or S_r = 0.61) was sufficiently strengthened by high suctions to deform less than the driest SB material (SB 2 % MC or S_r = 0.32).

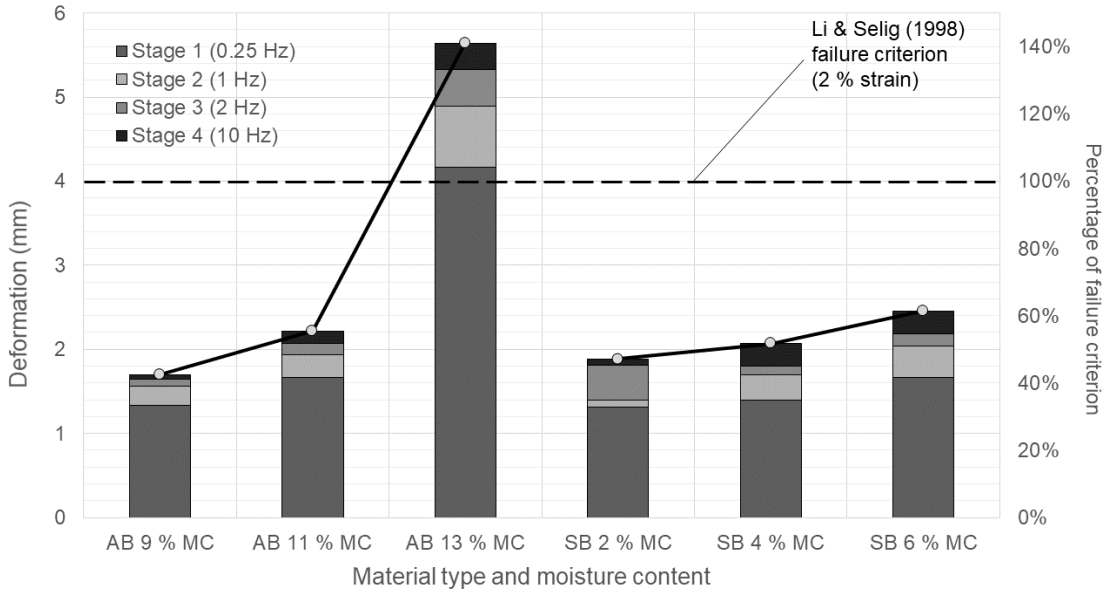

(a)

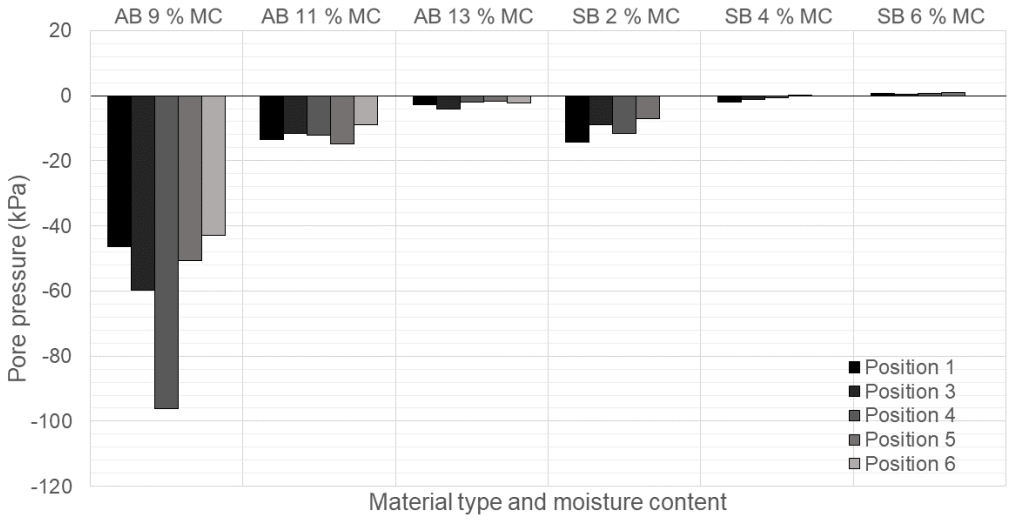

(b)

Figure 4.23: Comparison of **(a)** total deformations with **(b)** soil suctions of tested materials

A comparison of the tensiometer results from the start and end of testing with the SWRC for the material revealed that a significant amount of time was required for equalisation of suctions between the tensiometer and the soil. It was during this equalisation time that the systematic increases in pore

pressure occurred, and therefore their values may not accurately reflect their magnitudes. However, this does suggest that measurement of pore pressure build up in drier materials is possible with current instrumentation, given enough equalisation time.

This leads to the question of how to best utilise tensiometers and filter paper as methods to measure suctions in granular formation materials. The comparison of SWRC to final tensiometer readings show that equalisation of suctions is attainable in granular material. However, the equalisation time is lengthened for more granular materials such as the SB. It is believed that this increased equalisation time is a function of the lower value of S_r.

As a guideline, it was found that tensiometers could produce good results in terms of pore pressure build-up and equalisation time (both requiring good response time) in materials with high values of S_r and fines present. If a material contained significant fines, but a mid to low value of S_r, then equalisation would occur (albeit over a longer period), but it is uncertain whether small incremental changes could be measured. In the case of coarse granular material such as the SB, the nature of the soil-tensiometer interface meant that equalisation was hampered.

Filter paper and MC tests were similarly found to have limitations when applied to granular materials. In the case of filter paper tests, the contact area between soil and filter paper was found to produce a mixed result consisting of matric and osmotic suction. This issue was aggravated with increasingly granular soils as the contact area was reduced.

When plotting the suctions at the end of the test on the SWRC for the sample using 'targeted' MC values and measured MC values, it was found that the suctions plotted more favourably when using the targeted values of MC. It is believed that this was caused by error induced when sampling material when large aggregates in relatively small samples may cause large changes in the calculated value of MC either by their inclusion or exclusion.

When regarded in relation to each other, the findings point to the fact that suction and deformation testing on the AB material yields the most potential for improvement in current design methods. Given a certain budget and time limit, it would be wisest to test the AB material for possible pore pressure build up and accelerated deformation at higher MC values. In the AB material both extremes of the suction range have implications for the deformation properties of AB materials. High S_r values lead to

accelerated deformation, while low S_r values lead to significantly higher suctions than found in the SB material, thereby strengthening the material through suction stress. The granular SB materials pose a greater challenge to measure suctions and MC accurately, and provide less valuable information even if measured properly. The relatively small magnitude of suctions present in the SB material means that they have a small impact on soil strength when compared to the possible suctions generated in the AB material. This view is supported by the linear increase in SB material deformation with an increase in MC as opposed to the non-linear increase in AB material deformation with MC.

CHAPTER 5 CONCLUSIONS AND RECOMMENDATIONS

This chapter provides a summary of the outcomes of the investigation presented in previous sections, as well as recommendations for further investigation in the area of unsaturated railway formations.

5.1 CONCLUSIONS

Two related lines of inquiry were followed in the course of testing and analysis. These were as follows:

- The deformation behaviour of the subgrade (AB) and subballast (SB) materials at different values of moisture content (MC) and different frequencies were established.
- The suction behaviour of the AB and SB materials at different values of MC, as well as the performance of suction measurement techniques in granular material.

Finally, the main conclusions are discussed in terms of:

- The impact of soil suctions on the on the strength of the AB and SB railway formation materials.

The conclusions for these investigations are detailed in separate subsections.

5.1.1 Deformation Behaviour

- Deformation does not increase linearly with increasing MC in AB material. Once a critical value of MC is exceeded rapid deformation ensue. This is supported by findings in Vorster (2016) that showed rapid deformation past a critical MC value in railway embankment materials.
- For the granular SB material tested, deformation was found to increase approximately linearly with MC. No rapid deformation of the SB occurred at higher MC values.
- The majority of deformation in both materials occurred in the first loading stage (0.25 Hz loading frequency) as material densified. This large deformation occurred despite the fact that the cyclic loading stages were preceded by a 10 minute period of static loading at the same load (10 kN). This is in line with findings by Vorster (2016) showing that formations that are stable under static loading will deform under cyclic loading at an equivalent load.

5.1.2 Suction Behaviour and Measurement

Material Suction Overview

- Suctions measured in the SB material tended to be of a low magnitude and could behave erratically during periods of increased deformation, while the AB material showed a greater range of both positive and negative pore pressures (suctions).
- There were 3 factors identified as possible causes of this erratic behaviour in the SB material:
  - Total stress interference of aggregate particles on the tensiometer casing.
  - Movement of the material at the tensiometer ceramic face, thus disturbing the hydraulic coupling between soil and tensiometer required for suction measurement (Lourenço et al., 2009).
  - Improper seating of the tensiometer in the soil matrix, leading to an insufficient level of hydraulic coupling.

Suction Equalisation and Agreement with the Soil-water retention Curve

- Comparison with the soil water retention curve (SWRC) show that by the end of testing, all AB material suctions had equalised as the tensiometer readings plotted within the bounds of

expected suctions as presented by the SWRC. The suctions in material SB had equalised in the higher MC material (SB 6 % MC), but were still approaching the SWCC by the end of testing in the lower MC materials. This suggests that granularity as well as low values of S_r can inhibit hydraulic coupling.

- The build-up of pore pressure in material AB 13 % MC coincided with a period of rapid and large deformations (> 4 mm). Work done by Mamou et al. (2017) suggests that this may be due to compression of the soil matrix, squeezing pore water and causing excess pore pressure. In the latter stages of testing at higher frequencies, there were sustained periods of excess pore pressure as the time between loading cycles did not allow for dissipation of pressure.

Filter Paper Results

- The filter paper method of suction determination was found to be ill-suited measuring suctions in granular formation materials due to the decreased contact area between the filter paper and the soil. Decreased contact was found to cause a combination of matric and osmotic suction to be measured, causing the measured suctions to be offset from the expected suctions shown by the SWRC and tensiometers.

Suction and Moisture Content Comparison

- Measured values of MC tended to deviate from the targeted MC in the AB materials. It is thought that this was due to the possible inclusion or exclusion of large aggregates affecting the value of MC when measured along with the finer soil particles.
  - The view that the actual MC present in the formation did not differ greatly from the targeted MC was supported by the fact that the suction results at the end of the test compared more favourably to the SWRC when plotted using the targeted MC than when using measured the MC.

5.1.3 Effect of Suction on Deformation

- The AB material experienced a maximum deformation of 141 % of the Li and Selig (1998) failure criterion with suctions of 3 – 5 kPa present.

  - A slight increase of suctions to 10 – 15 kPa resulted in a strengthened material that deformed to 55 % of the failure criterion. This slight increase of suction by approximately 10 kPa therefore resulted in a 86 % deformation decrease in relation to the failure criterion.
  - The highest suctions recorded in the AB material were between 40 – 100 kPa and strengthened the material sufficiently to cause a deformation 43 % of the failure criterion. This deformation was lower than the minimum deformation experienced by the granular SB material.
- The deformation of the SB material varied between 47 – 61 % of the failure criterion depending on the moisture state of the material.
  - A low suction generation capacity was noted in the SB material, at the driest moisture state suctions between 7 – 14 kPa were measured. These suctions only caused a 14 % decrease in deformations as opposed to effectively saturated conditions.

5.2 RECOMMENDATIONS

This section identifies further areas of study and improvement as identified in the course of the project. Attention is given to possible future studies into further suction testing and recommended improvements to the suction instrumentation used.

- An accurate SWRC is important to allow comparison of suction values during testing to suctions measured in controlled conditions. The most effective methods for measuring suction during a SWRC test in granular materials should be explored.
- Efforts should be made to develop testing procedures for determining the suction-stress characteristic curve (SSCC) of granular materials. The suction stress results obtained from the SSCC would be invaluable in quantifying strength gain in drying formation materials.
- A climate chamber should be developed to provide controlled MC change during testing. This would allow the effect of controlled MC change on the material deformation to be quantified given the same loading stress and frequency. A climate chamber would allow a single test set-up to investigate the characteristic deformation change in a specific formation material as a function of the MC, rather than requiring a number of test set-ups at various targeted values of MC.
- Once the methods of determining both SWRCs and SSCCs are established for granular soils, efforts should be made to incorporate soil suction and stress theory into existing formation design methods. This would allow for the prediction of the effects of changing climate patterns

on railway formation materials. Understanding the weakening and strengthening behaviour of a proposed railway formation material with likely changes in MC will allow for better decision making on the suitability of a material.

- Tensiometer design, construction and saturation at the University of Pretoria should be formalised along the lines of tensiometer technology described in contemporary literature. The following steps are recommended:
  - Design of a machined housing for the pressure sensor.
  - Manufacturing of a soft sleeve and steel outer shield to minimise total stress interference.
  - Modification of the saturation apparatus to allow individual tensiometers to be isolated and removed while others continue to undergo saturation.
- Filter paper tests should be dispensed of as a method of suction measurement in granular formation materials for reasons described in this study. If suction comparisons to tensiometer readings are required, alternative methods should be considered.
- Alternative methods of MC determination such as frequency domain/capacitance moisture probes should be investigated for suitability in granular formation materials. This method would allow continuous MC measurement, and may prove to be more accurate than traditional lab tests for MC.

REFERENCES

ASTM (2003), D5298-03 Standard Test Method for Measurement of Soil Potential (Suction) Using Filter Paper, Technical report, West Conshohocken, United States.

Azam, A. M., Cameron, D. A., Gabr, A. G. and Rahman, M. M. (2014), Matric Suction in Recycled Unbound Granular Materials, *in* 'Geo-Congress 2014 Technical Papers', pp. 1367–1376.

Azam, A. M., Cameron, D. A. and Rahman, M. M. (2013), 'Model for prediction of resilient modulus incorporating matric suction for recycled unbound granular materials', *Canadian Geotechnical Journal* **50**, 1143–1158.

Bishop, A. (1959), 'The principle of effective stress', *Teknisk Ukeblad* **39**, 859–863.

Brown, S. and Selig, E. (1991), 'The design of pavement and rail track foundations', *Cyclic loading of soils* pp. 249–305.

Cary, C. E. and Zapata, C. E. (2011), 'Resilient modulus for unsaturated unbound materials', *Road Materials and Pavement Design* **12**(3), 615–638.

Cary, C. E. and Zapata, C. E. (2016), 'Pore Water Pressure Response of Soil Subjected to Dynamic Loading under Saturated and Unsaturated Conditions', *International Journal of Geomechanics* **16**(6), 1–9.

du Plooy, R. (2015), Characterisation of rigid polyurthane foam reinforced ballast through cyclic loading box tests, Masters dissertation, University of Pretoria.

Franki (1995), *A Guide to Practical Geotechnical Engineering in South Africa*, 3rd edn.

Fredlund, D. (1987), Non-linearity of strength envelope for unsaturated soils, *in* 'Proceedings of the 6th International Conference on Expansive Soils', Rotterdam:Balkema, New Dehli, pp. 49–54.

Fredlund, D. G., Gan, J. K. M. and Gallen, P. (1995), 'Suction measurements on compacted till specimens and indirect filter paper calibration technique', *Transportation Research Record* (1481), 3–9.

Fredlund, D. G., Sheng, D. and Zhao, J. (2011), 'Estimation of soil suction from the soil-water characteristic curve', *Canadian Geotechnical Journal* **48**(2), 186–198.

Fredlund, D., Morgenstern, N. and Widger, R. (1978), 'The shear strength of unsaturated soils', *Canadian Geotechnical Journal* **15**(3), 313–321.

Fredlund, D. and Xing, A. (1994), 'Equations for the soil-water characteristic curve', *Canadian Geotechnical Journal* **31**(3), 521–532.

Gräbe, P. J. and Clayton, C. R. I. (2009), 'Effects of Principal Stress Rotation on Permanent Deformation in Rail Track Foundations', *Journal of Geotechnical and Geoenvironmental Engineering* **135**(4), 555–565.

Gräbe, P. J. and Clayton, C. R. I. (2014), 'Effects of Principal Stress Rotation on Resilient Behavior in Rail Track Foundations', *Journal of Geotechnical and Geoenvironmental Engineering* **140**(2), 1–10.

Gräbe, P. J., Clayton, C. R. I. and Shaw, F. J. (2005), Deformation measurement on a heavy haul track formation, *in* 'Proceedings of the 8th International Heavy Haul Conference', number January, pp. 287–295.

Guan, Y. and Fredlund, D. G. (1997), 'Use of the tensile strength of water for the direct measurement of high soil suction', *Canadian Geotechnical Journal* **34**(4), 604–614.

Gupta, S., Kang, D. and Ranaivoson, A. (2009), Hydraulic and mechanical properties of recycled materials, Technical report, Minnesota Department of Transportation.

Hamblin, A. (1981), 'Filter-paper method for routine measurement of field water potential', *Journal of Hydrology* **53**, 355–360.

Han, Z. and Vanapalli, S. K. (2016), 'Stiffness and shear strength of unsaturated soils in relation to soil-water characteristic curve', *Géotechnique* **66**(8), 627–647.

Heymann, G. and Clayton, C. (1999), Block sampling of soil: Some practical considerations, *in* 'Geotechnics for Developing Africa', Balkema, Rotterdam, The Netherlands, pp. 331–339.

Hosseini, S., Naeini, S. and Hassanlourad, M. (2017), 'Monotonic , cyclic and post-cyclic behaviour of an unsaturated clayey soil', *International Journal of Geotechnical Engineering* **11**(3), 225–235.

Huat, B. B., Toll, D. G. and Prasad, A. (2012), *Handbook of Tropical Residual Soils Engineering*, CRC Press/Balkema, Boca Raton.

Jones, H. and Kohnke, H. (1952), 'The influence of soil moisture tension on vapor movement of soil water', *Soil Science Society of America Journal* **16**(3), 245–248.

Knappett, J. and Craig, R. (2012), *Craig's soil mechanics*, 8th edn edn, Spon Press, New York.

Lekarp, F., Isacsson, U. and Dawson, A. (2000), 'State of the art. I: Resilient response of unbound aggregates', *Journal of Transportation Engineering* **126**(1), 66–75.

Li, D., Hyslip, J., Sussman, T. and Chrismer, S. (2016), *Railway Geotechnics*, 1st edn, CRC Press/Taylor&Francis, Boca Raton.

Li, D. and Selig, E. (1998), 'Method for railroad track foundation design I: Development', *Journal of Geotechnical and Geoenvironmental Engineering* **124**(4), 316–322.

Lourenço, S. D. N., Gallipoli, D., Toll, D. G., Augarde, C. E., Evans, F. D. and Medero, G. M. (2008), 'Calibrations of a high-suction tensiometer', *Géotechnique* **58**(8), 659–668.

Lourenço, S. D. N., Gallipoli, D., Toll, D. G. and Evans, F. D. (2009), 'On the measurement of water pressure in soils with high suction tensiometers', *Geotechnical Testing Journal* **32**(6), 565–571.

Lu, N., Godt, J. W. and Wu, D. T. (2010), 'A closed-form equation for effective stress in unsaturated soil', *Water Resources Research* **46**(5), 1–14.

Lu, N., Kaya, M. and Godt, J. W. (2014), 'Interrelations among the Soil-Water Retention , Hydraulic Conductivity , and Suction-Stress Characteristic Curves', *Journal of Geotechnical and Geoenvironmental Engineering* **140**(5), 1–10.

Lu, N. and Likos, W. J. (2004), *Unsaturated soil mechanics*, Vol. 106, Wiley.

Lu, N. and Likos, W. J. (2006), 'Suction Stress Characteristic Curve for Unsaturated Soil', *Journal of Geotechnical and Geoenvironmental Engineering* **132**(2), 131–142.

Mamou, A., Powrie, W., Priest, J. A. and Clayton, C. (2017), 'The effects of drainage on the behaviour of railway track foundation materials during cyclic loading', *Géotechnique* **67**(10), 845–854.

Marinho, F. A. M. and Oliveira, O. M. (2006), 'The Filter Paper Method Revisited', **29**(3), 250–258.

Marinho, F. and da Silva Gomes, J. (2011), 'The Effect of Contact on the Filter Paper Method for Measuring Soil Suction', *Geotechnical Testing Journal* **35**(1), 172–181.

Matlab (2017), 'Signal Processing Toolbox Documentation'.

McQueen, I. and Miller, R. (1974), 'Approximating soil moisture characteristics from limited data: Empirical evidence and a tentative model', *Water Resources Research* **10**(3), 521–527.

Nokkaew, K., Tinjum, J. and Benson, C. (2012), Hydraulic properties of recycled asphalt pavement and recycled concrete aggregate, *in* 'GeoCongress 2012: State of the Art and Practice in Geotechnical

Engineering', pp. 1476–1485.

Oliveira, O. M. and Marinho, F. A. M. (2008), 'Suction equilibration time for a high capacity tensiometer', *Geotechnical Testing Journal* **31**(1), 101–105.

Otter, L., Clayton, C. R. I., Priest, J. A. and Gräbe, P. J. (2016), 'The stiffness of unsaturated railway formations', *Proceedings of the Institution of Mechanical Engineers Part F-Journal of Rail and Rapid Transit* **230**(4), 1040–1052.

Rahardjo, H. (2010), 'Water characteristic curves of recycled materials', *Geotechnical Testing Journal* **34**(1), 89–96.

Rorke, L. (2016), Some factors affecting the cyclic stiffness of railway formation material, Doctoral dissertation, University of Southampton.

Saad, B. (2014), 'Analysis of excess water impact on the structural performance of flexible pavements', *International Journal of Pavement Engineering* **15**(5), 409–426.

Take, W. A. and Bolton, M. D. (2003), 'Tensiometer saturation and the reliable measurement of soil suction', *Géotechnique* **53**(2), 159–172.

Tandon, V., Picornell, M. and Nazarian, S. (1996), Evaluation and Guidelines for Drainable Bases, Technical Report December, Center for Highway Materials Research, University of Texas at El Paso.

Terzaghi, K. (1943), *Theoretical Soil Mechanics*, John Wiley & Sons, Inc, New York.

Thom, N. and Brown, S. (1987), Effect of moisture on the structural performance of a crushed-limestone road base, *in* '66th Annual Meeting of the Transportation Board', Washington D.C., pp. 50–56.

Toll, D., Ali Rahman, Z. and Gallipoli, D. (2008), Critical State conditions for an unsaturated artificially bonded soil, *in* 'Unsaturated Soils: Advances in Geo-Engineering', Taylor&Francis Group, London, pp. 435–440.

Transnet (2006), S410: Specification for railway earthworks. Transnet Limited, Technical report, Pretoria, South Africa.

van Genuchten, M. T. (1980), 'A Closed-Form Equation for Predicting the Hydraulic Conductivity of Unsaturated Soils', *Soil Science Society of America Journal* **44**(5), 892–898.

Vorster, P. (2016), Centrifuge Modelling of Railway Embankments under Static and Cyclic Loading, Masters dissertation, University of Pretoria.

Walker, P. (1997), 'Measurement of total suction and matric suction in pavement materials at Dandenong ALF site', *Road and transport research* **6**(4), 48–58.

Wilson, N. and Greenwood, J. (1974), 'Pore pressure and strains after repeated loading of saturated clay', *Canadian Geotechnical Journal* **11**, 269–277.